

**EDITORIAL BOARD**

E.O. Paton Electric Welding Institute, Kyiv, Ukraine:

**I.V. Krivtsun** (*Editor-in-Chief*),**V.M. Lipodaev** (*Deputy Editor-in-Chief*),**O.M. Berdnikova, Yu.S. Borisov,****V.V. Knysh, V.M. Korzhyk,****Yu.M. Lankin, L.M. Lobanov, S.Yu. Maksimov,****M.O. Pashchin, V.D. Poznyakov,****I.O. Ryabtsev, K.A. Yushchenko;****V.V. Dmitrik, NTUU**

«Kharkiv Polytechnic Institute», Kharkiv, Ukraine;

**E.P. Chvertko, V.V. Kvasnitsky, NTUU**

«Igor Sikorsky Kyiv Polytechnic Institute»,

Kyiv, Ukraine;

**M.M. Student, Karpenko Physico-Mechanical**

Institute, Lviv, Ukraine;

**M. Zinigrad, Ariel University, Israel;****Ya. Pilarczyk, Welding Institute, Gliwice, Poland;****U. Reisgen, Welding and Joining Institute,**

Aachen, Germany

**Founders**

E.O. Paton Electric Welding Institute

International Association «Welding»

**Publisher**

International Association «Welding»

**Translators**

A.O. Fomin, I.M. Kutianova

*Editor*

N.G. Khomenko

*Electron galley*

D.I. Sereda, T.Yu. Snegiryova

**Address**

E.O. Paton Electric Welding Institute,

International Association «Welding»

11 Kazymyr Malevych Str. (former Bozhenko),

03150, Kyiv, Ukraine

Tel./Fax: (38044) 200 82 77

E-mail: journal@paton.kiev.ua

www://patonpublishinghouse.com/eng/journals/tpwj

State Registration Certificate

KV 4790 of 09.01.2001

ISSN 0957-798X

DOI: <http://dx.doi.org/10.37434/tpwj>**Subscriptions**

12 issues per year, back issues available.

\$384, subscriptions for the printed (hard copy) version,

air postage and packaging included.

\$312, subscriptions for the electronic version

(sending issues of Journal in pdf format

or providing access to IP addresses).

Institutions with current subscriptions on printed version

can purchase online access to the electronic versions

of any back issues that they have not subscribed to.

Issues of the Journal (more than two years old)

are available at a substantially reduced price.

All rights reserved.

This publication and each of the articles contained

herein are protected by copyright.

Permission to reproduce material contained in this  
journal must be obtained in writing from the Publisher.**CONTENTS**

NEWS .....	2
<b>Plenary Papers for International Conference «State-of-the-Art Technologies for Joining Materials» May 31 – June 2, 2021, Kyiv, E.O. Paton Electric Welding Institute</b>	
<u>Kuchuk-Yatsenko S.I.</u> , Rudenko P.M., Didkovskiy O.V. and Antipin Ye.V. Operational control of the process of flash butt welding of railway rails by the method of pulsating flashing .....	5
Korzhyk V.M., Grynyuk A.A., Khaskin V.Yu., Illiashenko Ye.V., Klochkov I.M., Ganushchak O.V., Yu Xuefen and Liuyi Huang. Improving the efficiency of robotic fabrication of steel truss welded structures .....	12
Adjamskyi S.V., Kononenko G.A. and Podolskyi R.V. Improving the efficiency of the SLM-process by adjusting the focal spot diameter of the laser beam .....	18
Lobanov L.M., Syzonenko O.M., Holovko V.V., Tashev P., Lypian Ye.V., Prystash M.S., Torpakov A.S., Pashchin M.O., Mikhodui O.L. and Shcheretskyi V.O. Pulsed-discharge treatment of the Al-Ti-C system modifier .....	24
Akhonin S.V., Bilous V.Yu., Selin R.V., Petrychenko I.K. and Radchenko L.M. Argon-arc welding of high-strength sparsely-doped pseudo-β-titanium alloy Ti-2.8Al-5.1Mo-4.9Fe .....	30
Nesterenkov V.M., Skryabinskyi V.V. and Rusynuk M.O. Effect of thermal cycles in electron beam welding of aluminium 1570 alloy on mechanical properties of welded joints .....	35
Sahul Mir., Sahul Mar., Čaplovič L., Marônek M., Klochkov I. and Motrunich S. Analysis of the properties of electron beam welded joints of aluminium lithium alloy latest generation .....	41
Senchenkov I.K., Ryabtsev I.O., Chervinko O.P. and Babinets A.A. Calculation of residual stress-strain state of deposited steel sheet plates .....	46
Tyurin Yu. M., Kolisnichenko O.V., Korzhyk V.M., Gos I.D., Ganushchak O.V., Jin Ying and Zhong Fengping. Pulse-plasma modification of surface of steel hot drawing dies of titanium alloy products .....	51
Kostin V.A., Zhukov V.V., Berdnikova O.M., Holovko V.V. and Kushnaryova O.S. Effect of modification of weld metal of high-strength low-alloy steels on their structure and properties .....	57
Shtofel O.O., Holovko V.V. and Chyzhska T.G. Application of fractal and metallographic analyses for evaluation of quality of weld metal .....	65

## ESTABLISHING BORYS PATON STATE AWARD

On April 15, the Verkhovna Rada of Ukraine adopted Law 5327 «On Amendments to Article 11 of the Law of Ukraine «On State Awards of Ukraine», which establishes the Borys Paton State Award.

Implementation of this Act will have a positive impact on the sphere of scientific and scientific-engineering activity as a whole, as it is aimed at preservation of the memory of Academician B.E. Paton, outstanding Ukrainian scientist and organizer of science, who was characterized by dedication to his calling and tireless creative search that will inspire scientific achievements of the next generations of scientists.

Academician Borys Paton was a state and public figure, President of the National Academy of Sciences of Ukraine from 1962 till 2020, Director of the E.O. Paton Electric Welding Institute of the National Academy of Sciences of Ukraine, Hero of Ukraine. He died on August 19, 2020, at the age of 101.

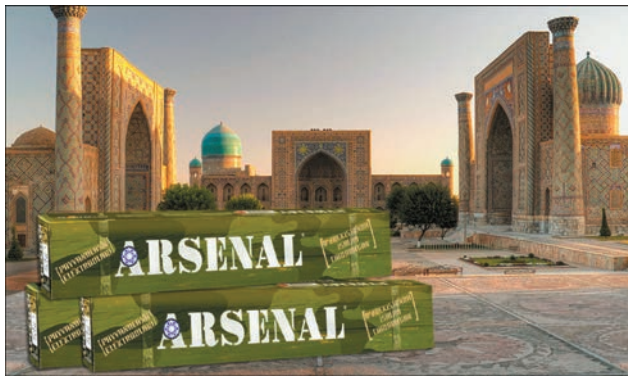
The sum of the State Award is determined every year by an Act of the President of Ukraine according to the established procedure.

The Law was developed by the Ministry of Education and Science at the initiative of the President of Ukraine

on preservation of the memory of Borys Paton, Hero of Ukraine, outstanding Ukrainian scientist and science organizer.



## A NEW ELECTRODE MANUFACTURING PLANT — «MONOLIT ASIA» WAS COMMISSIONED IN UZBEKISTAN



In July, 2020 PJSC «PlasmaTek» Company (Vinnitsa, Ukraine) under the project for expanding its presence in Central Asia countries, commissioned «Monolit Asia» Plant for electrode manufacturing in Tashkent, Uzbekistan.

The capacity of the plant production facilities is 1.5 thou t of electrodes with rutile and basic coating. After the equipment has reached the design parameters, the total capacity of the Group of Companies with plants in Ukraine, Belarus and Uzbekistan will be increased up to 7 thou t electrodes per month.

## ELECTRON BEAM MELTING OF LARGE-SIZED TITANIUM INGOTS

SE «Scientific-Production Center «Titan» of PWI optimized the technology of electron beam melting of large-sized ingots (1080 mm dia, more than 10 t weight) of titanium alloys with specified oxygen content, not containing any high or low density inclusions. This technology allows using titanium scrap and low grade titanium sponge as raw materials. The ingots are produced with glazed or machined surface.

*SPC «Titan» today:*

- main scientific activity — development of titanium-based alloys, technologies and equipment for their production by electron beam melting (EBM);
- main production activity is making titanium alloy ingots and manufacturing equipment for EBM;
- production facilities: six electron units;
- certificate for quality system ISO 9001;

- international deliveries to: Great Britain, China, Germany, USA, France, Sweden, Japan.



## PATON INTERNATIONAL — ONE OF THE LARGEST MANUFACTURERS OF WELDING ELECTRODES IN UKRAINE

PATON INTERNATIONAL Company is the leading manufacturer of welding equipment and consumables in the territory of Ukraine and CIS countries, which are applied with success practically in all sectors of the economy: from housing and communal sector to heavy mechanical engineering and ship-building. The range of PATON™ products includes more than 35 items of welding equipment, as well as more than 10 electrode grades for manual arc welding, which the Company started manufacturing in 2016.

In December, 2019, a new section for welding electrode manufacture was commissioned in the main production site of PATON INTERNATIONAL in Kyiv at 66 Novopyrogivska Str. This section now includes the following areas: charge material preparation and dosing; rod cutting up, electrode moulding, heat treatment, sorting and packing of finished products. Alongside the production areas, the new complex for welding electrode manufacturing also includes laboratory facilities to ensure monitoring of the production process at all the stages: from receiving the raw materials up to acceptance tests of each batch of finished products.

At present the plant has launched production of the most common grades of PATON™ electrodes, which are well-established in the market and are manufactured by the classical coating formulation (ANO-36, ANO-4, UONI-13/55, MR-3); and Elite series electrodes, which are made by an improved coating formulation (Elite ANO-36, Elite ANO-21, 7018 Elite), as well as special purpose electrodes (TsL-11, TsCh-4, T-590).

Two production lines were put into operation in the section, and in the near future it is planned to finish commissioning works in an absolutely new third line, thus increasing the overall production capacity to 1000 t per month. Production is carried out round the clock by several teams with overall number of 50 people.

When a new production site was set up, the main objective was to ensure the highest product quality. In order to reach this objective, the list of raw material component suppliers was revised, and control of raw material quality was enhanced. Only the best Ukrainian suppliers were selected, and direct supplies of high-quality materials from Germany, Slovakia, the Netherlands, India and other countries were organized. Professional training of personnel was conducted with production skill certification for performance of the main manufacturing technology operations. Monitoring raw materials and testing finished products are performed by company laboratory complex, using high-technology equipment: X-ray fluorescence analyzer, carbon and sulphur analyzers, and specialized vibrostand.

The above-mentioned laboratory equipment, together with novel procedures for monitoring the technological production process ensure the high quality and stability of performance of PATON™ welding electrodes, which correspond to all the necessary requirements to this kind of products that is confirmed by certificates from leading Ukrainian and International certification bodies.

Company products are supplied to more than 50 countries all over the world, and welding electrodes take up one of the key positions in the supply structure. Overall scope of export supplies of the electrodes was equal to more than 4000 t just in 2020.

The near-term plans of PATON INTERNATIONAL envisage widening the electrode range and increasing the output volumes by entering new markets. It will allow the Company rising to leading positions in this market segment in the near future, and consolidating its status of a prominent Ukrainian manufacturer of both welding equipment and welding consumables.





## *Dear colleagues,*

*It is with great pleasure that I welcome all the participants and guests of the International Conference and Exhibition devoted to state-of-the-art technologies of material joining.*

*Welding, as before, remains the leading technology in many industries. That is why the range of issues to be discussed at the Conference, information about the results and achievements in the field of welding production, as well as familiarization with samples of welding consumables and equipment presented at the Exhibition, will promote strengthening of the scientific and business contacts, and further development of research and applied work.*

*The traditional fruitful cooperation of science and industry, continuous scientific support, provided by the E.O. Paton Electric Welding Institute of the NAS of Ukraine and active position of manufacturers of welding consumables and equipment allow ensuring their high quality, and satisfying wide demand both in the domestic and foreign markets. As an example, it should be noted that Ukrainian specialists helped establishing a number of welding consumable productions in many countries in the post-Soviet space.*

*Of great interest, in my opinion, are the presentations devoted to plasma-arc and hybrid processes of welding, cutting, material processing and coating deposition; 3D-printing technologies; robotic welding in welded structure fabrication; brazing and surfacing; monitoring flash-butt welding of rails, modern market of welding consumables, etc.*

*On behalf of the Conference Program Committee, I would like to express my sincere gratitude to all the organizations, enterprises, companies and individual specialists, whose active support made it possible to hold the Conference.*

*I believe that consideration of the issues to be addressed by the Conference, exchange of information on the achievements, establishing wider scientific and business contacts will promote development of new priority directions of research in the field of welding and related technologies, and will allow us making our contribution to revival and rise of industrial production in our country.*

*Wishing successful work, great achievements, well-being and good health to all the Conference participants*

*Director of the E.O. Paton Electric  
Welding Institute  
Academician I.V. Krivtsun*

A handwritten signature in blue ink, consisting of a large, stylized initial 'K' followed by a series of connected loops and a long, sweeping tail.

# OPERATIONAL CONTROL OF THE PROCESS OF FLASH BUTT WELDING OF RAILWAY RAILS BY THE METHOD OF PULSATING FLASHING

**S.I. Kuchuk-Yatsenko**, P.M. Rudenko, O.V. Didkovskiy and Ye.V. Antipin

E.O. Paton Electric Welding Institute of the NAS of Ukraine

11 Kazymyr Malevych Str., 03150, Kyiv, Ukraine. E-mail: office@paton.kiev.ua

The article presents a study of the accuracy of reproduction of parameters of operational control of flash butt welding of railway rails in order to increase the reliability of evaluating the compliance of the process to the Technical Specifications (TS) and improve the quality of welded joints. For the statistical analysis of protocols of welding rails at rail-welding enterprises the review of existing indices of accuracy and stability of technological processes was made. For the analysis, the coefficient of variation  $K_v$  was chosen, which is not related to the tolerance of the deviation of the process parameter. Evaluations of  $K_v$  coefficients according to the welding protocols of more than 10 thousand joints and more than 100 specimens of a technological test for the stationary machine K1000 showed that the mode parameters set directly by the control system, are reproduced with an error of not more than 1.5 %. The  $K_v$  coefficients increase sharply for the rate of flashing, transition from flashing to upsetting and particularly upsetting, which are included in the TS for welding rails and an active electric power, that occurred during flashing at the input of the welding transformer. The studies of  $K_v$  coefficients with grouping of welding data by six months showed that the variation of process parameters had no trends and the process was stable over time with a sufficient accuracy. The mean values and the standard deviation of the parameters of the process of welding rails and specimens of a technological test differ within the statistical error, which indicates the possibility of approximating the results of test studies on the rail joints. Evaluation of effect of parameters of the process of rate, tolerance and energy of flashing on the heat-affected zone (HAZ) with the use of linear regression dependence showed an essential dependence of HAZ on variation of electric energy during flashing. For control of active energy, the measuring converter of average active electric power with a pulse output was developed, which is adapted to the control systems of K1000 and K922 machines with input signals of current to 1000 A and voltage to 440 V, a frequency band of these signals to 1 kHz and the resulted error of measurement to 1 %. It is recommended to include active electric power released during flashing at the input of the welding transformer in the list of control parameters to the TS, and to improve the quality of joints not only to control the parameters within tolerance, but to create the conditions of the smallest variation of parameters from obtained data. 7 Ref., 1 Table, 4 Figures.

*Keywords*: flash butt welding, railway rails, statistical control, coefficient of variation, process parameters, quality parameters, heat-affected-zone, active electric power during flashing, quality control

Technical specifications of flash butt welding (FBW) of railway rails [1, 2] regulate the parameters of welding mode, deviation tolerances for them, quality of a welded joint: width of heat-affected-zone (HAZ), hardness of the metal on the rolling surface of the welded joint and indices of periodic process control according to the specimens of a technological test on static mechanical bending: minimum  $L_{fr}$  and fracture load  $P_{fr}$ .

The indices of a joint quality, as well as the results of mechanical tests of specimens depend on the deviations of more than a dozen process parameters from their values, for which the process was adjusted.

Scattering of values of both input parameters and, respectively, output quality indices due to the presence of systematic and random perturbations is usually characterized by a mathematical expectation or the

mean value of  $\bar{x}$  and the variance  $\sigma^2$  or the root mean square (r.m.s.) or a standard deviation  $S = \sqrt{\sigma^2}$  from the average one. If we take into account that the input parameters have different physical properties or differ significantly in values, it is better to use dimensionless values to compare them.

At the statistical control of process indices of accuracy and stability: coefficients of accuracy  $K_{acc}$ , adjustment  $K_{adj}$  and stability  $K_{st}$  are as a rule used:

$$K_{acc} = 6S/\delta, K_{adj} = (\bar{x} - x_\delta)/\delta, K_{st} = S_{t1}/S_{t2}, \quad (1)$$

where  $\delta = x_u - x_l$  is the tolerance field for the parameter;  $x_u$  and  $x_l$  is the upper and lower limit of tolerance for the parameter;  $x_\delta = (x_u + x_l)/2$  is the middle of the tolerance field;  $S_{t1}$  is the r.m.s. at a fixed moment in time  $t_1$ ;  $S_{t2}$  is the r.m.s. at the compared fixed moment of time  $t_2$ .

S.I. Kuchuk-Yatsenko — <https://orcid.org/0000-0002-1166-0253>, P.M. Rudenko — <https://orcid.org/0000-0002-7770-2145>, O.V. Didkovskiy — <https://orcid.org/0000-0001-5268-5599>, Ye.V. Antipin — <https://orcid.org/0000-0003-3297-5382>

© S.I. Kuchuk-Yatsenko, P.M. Rudenko, O.V. Didkovskiy and Ye.V. Antipin, 2021

These evaluations are dimensionless, relative and for their further analysis the physical value of the parameter can be ignored, and for their control the general tolerances can be set, which is convenient for comparing different physical parameters. It is considered, for example, that at  $K_{acc} \leq 0.75$  the technological process is quite accurate, at  $K_{acc} = 0.76-0.98$  the technological process demands careful supervision and at  $K_{acc} > 0.98$  the accuracy is unsatisfactory [3].

Many Japanese enterprises and the US automotive industry use similar evaluations for control — process capability indices:

- process potential for bilateral tolerance limits

$$C_p = (x_u - x_l) / 6S = \delta / 6S,$$

- process efficiency relative to the upper limit of tolerance

$$CPU = (x_u - \bar{x}) / 3S,$$

- process efficiency relative to the lower limit of tolerance

$$CPL = (\bar{x} - x_l) / 3S,$$

- deviation of the average value of the process from the middle of the tolerance field

$$k = 2|x_{\delta} - \bar{x}| / (x_u - x_l) = 2|x_{\delta} - \bar{x}| / \delta,$$

- process efficiency for two-sided tolerance limits

$$C_{pk} = \min \{CPU, CPL\} = C_p(1 - k),$$

which form a group of complementary process capability indices and the indices similar to the coefficients  $K_{acc}$ ,  $K_{adj}$  and  $K_{st}$ , also determine compliance with the process tolerances and adjustment problems. They can be used for one-sided and two-sided tolerances and can be generalized for operation with multidimensional rated values (quality indices) [4].

The mentioned indices refer to the tolerance field  $\delta$ , which determines the probability of a quality product when finding a controlled parameter in it. The control of the FBW process of railway rails in stationary machines K1000 and mobile machines K922 in existing machine control systems includes much more parameters than those included in the TS (Table), and not all of them have tolerances. In addition, the tolerances may not be quite «optimal».

Therefore, to compare the spread of parameters in the future the variation coefficient  $K_v$  (German Variationskoeffizient  $m$ ) was used, which is a relative value to characterize scattering (variability) of a feature and it is used at the moment when it is necessary to compare variability of features of an object, expressed in different measurement units (synonym: unitized risk) [3].

The article presents a study of the accuracy of reproduction of the parameters of operational control of FBW of railway rails in order to increase the reliability of conformity evaluation of the process of TS and improve the quality of welded joints.

Tolerances for parameters of flash butt welding of rails of grades M76 of type R65, K76F of type R65, 60E1 by pulsating flashing for the machine K1000 and K922 (in brackets) according to [1]

Parameter	Tolerance field		Study interval	
	Lower	Upper	Lower	Upper
Welding time $T_w$ , s	60	100	40	275
Flashing rate $V_{fl}$ , mm/s	0.07 (0.065)	0.2	0.03	0.4
Tolerance for flashing $S_{fl}$ , mm	12(9)	18	5	30
Voltage during transition to upsetting $U_u$ , V	355	440	300	500
Flashing voltage $U_f$ , V	250	360	200	500
Rate before upsetting $V_p$ , mm/s	0.7	2.5	0.1	4
Upsetting rate $V_{ups}$ , mm/s	30(20)	80	10	145
Upsetting pressure $P_{ups}$ , atm	12(9)	15(12)-20	5	40
Tolerance for upsetting $S_{ups}$ , mm	11.5	17	5	35
Time of upsetting with current $T_{upsl}$ , s	1-0.49 (0.8)	2(1.8)	0.3	3
Flashing current $I_{fl}$ , A	–	–	80	800
Impedance of the secondary circuit at a sh.-c $Z_{sh-c}$ , $\mu\text{Ohm}$	–	–	25	300
Flashing power $Q_{fl}$ , kW·h	–	–	1.0	5.00

\*Marked parameters that are not included in the TS.

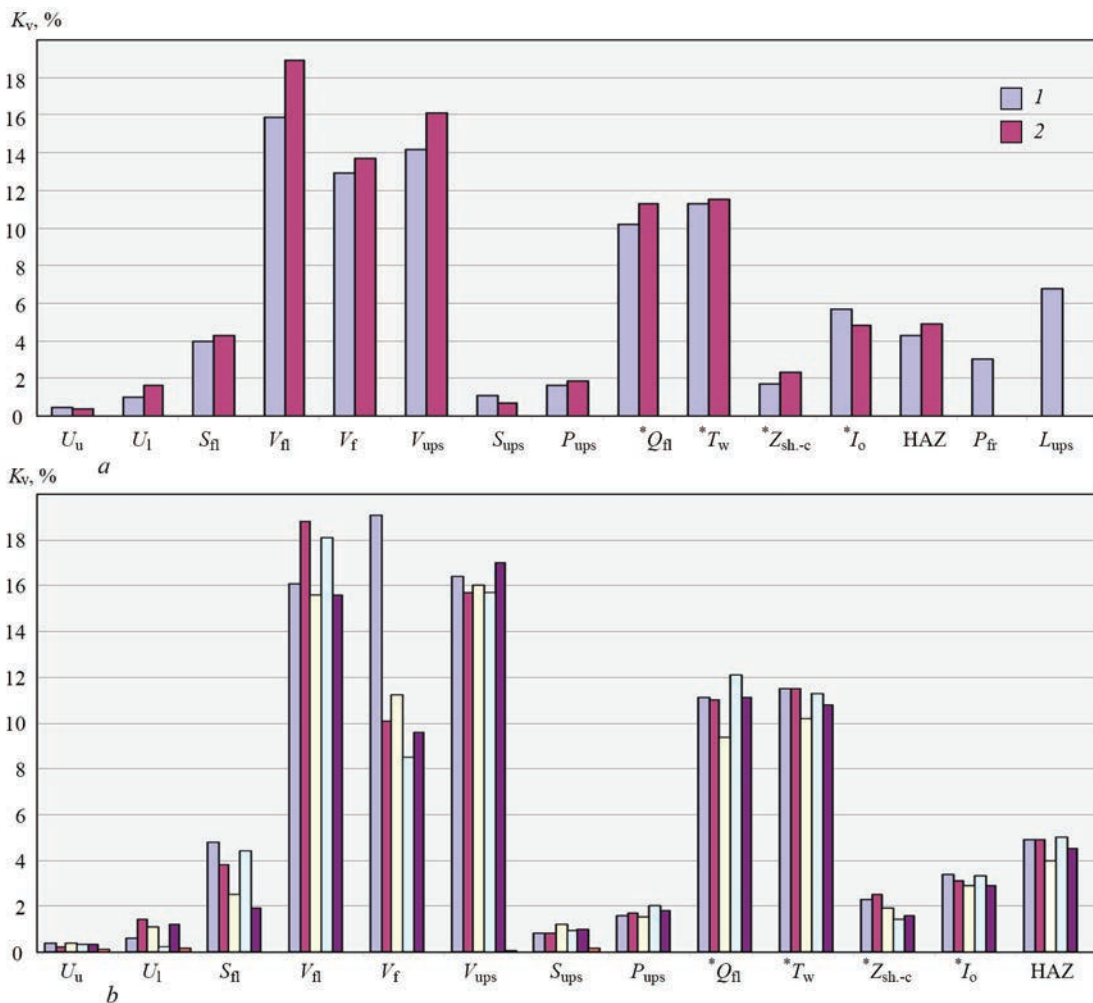


**Figure 1.** Variation coefficients  $K_v$  during welding of R65 rails of grade K76F in the machine K1000 (a): 1 — welding data of specimens of a technological test; 2 — welding data of rail joints (hereinafter HAZ was predicted by regression dependence on  $V_{fl}$ ,  $S_{fl}$ ,  $Q_{fl}$  and  $S_{ups}$  [6] and the change of variation coefficients  $K_v$  over time with a period of six months during welding R65 rails of grade K76F in the machine K1000.  $K_v$  for the same time intervals are shown in the same colour (b)

$K_v$  is the ratio of the mean square deviation to the arithmetic mean and is expressed as a percentage:  $K_v = S/\bar{x} \cdot 100\%$ . Variability is considered to be variable weak if  $K_v < 10\%$ ; average, if  $K_v$  is from 11–25% and significant at  $K_v > 25\%$ .

Evaluation of the accuracy of reproduction of process parameters, or variation of parameters was performed according to the protocols of welding of railway rails during 2015–2020 at rail welding enterprises (RWE) of Ukrzaliznytsia. For example, according to  $K_v$  data of the stationary machine K1000 of the Kyiv RWE, which were calculated by the welding protocols of more than 10 thou joints, the following conclusions may be made (Figure 1).

Among the parameters that determine the compliance of the TS mode, voltage during flashing  $U_l$  and during transition from flashing to upsetting,  $U_u$  tolerance for flashing  $S_{fl}$  and upsetting  $S_{ups}$ , upsetting time under current  $T_{upsl}$  are set directly in the control system, have a fairly small value of the variation coefficient  $K_v$ .  $P_{ups}$  is determined by adjusting the pressure

in the upsetting cylinder and also has a small  $K_v$ . The accuracy of reproduction of these parameters depends entirely on the technical condition of the welding machine, control system and a proper maintenance of external welding conditions, namely, power electricity, pumping station, coolant, etc.

The tolerance for flashing  $S_{fl}$  according to the main algorithm of control of FBW of rails is set in the cyclogram of the mode and its correct operation of the system for control of the machine should be close to the accuracy of the sensor for control of the movement of the moving column of the welding machine. Typically, this sensor is based on an incremental sensor Siemens 6FX2001, it has a measurement discreteness of 0.1 mm and the effect of electromagnetic interference on the measurement accuracy is impossible. In the mentioned data, the variation  $S_{fl}$  is much higher due to the fact that during welding of a new batch of rails, it is possible to adjust the mode, which was usually performed by changing the specified tolerance for flashing. According to  $K_v$  data for eight K1000 machines

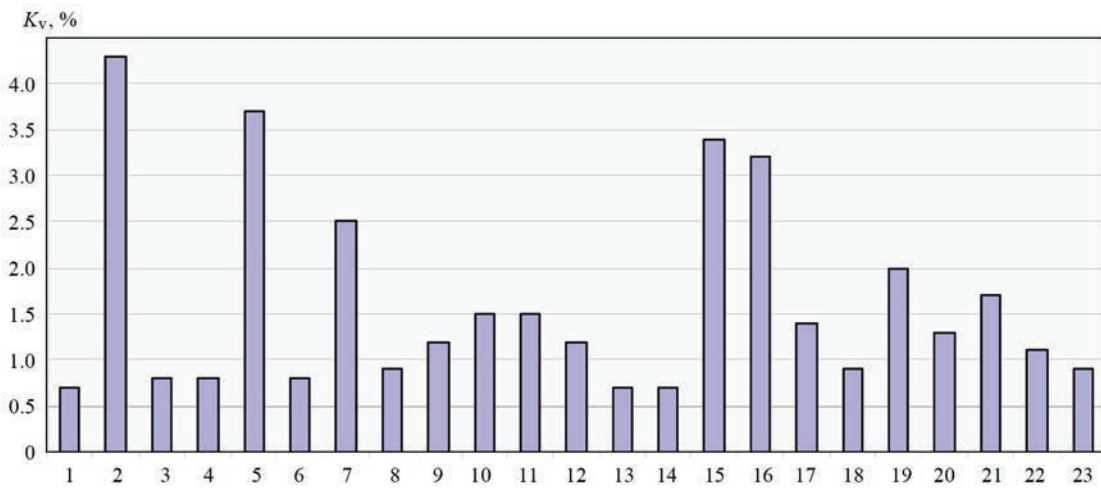


**Figure 2.** Coefficients  $K_v$  for tolerance for flashing  $S_{fl}$  of eight machines K1000 (1–8) and 15 machines K922 (9–23)

and fifteen K922 machines of different RWE it is seen that only in the case of mode resetting, the variation of parameter  $S_{fl}$  is quite large. At the constant set mode,  $K_v$  is lower than 1.0–1.5 % (Figure 2). It is clear that according to other algorithms, for example, the task of time stages, this parameter can have a random distribution with its mean deviation and r.m.s.

The parameters of flashing rate  $V_{fl}$ , transition from flashing to upsetting  $V_f$  and upsetting  $V_{ups}$ , which are included in the TS, shape of current before upsetting (time of probable short circuit  $T_{sh-c}$ ), as well as welding time  $T_w$  and electric flashing power  $Q_{fl}$  are set indirectly and result from the FBW process and, accordingly, from the action of different uncontrolled disturbances.

The rates of flashing  $V_{fl}$  and transition to upsetting  $V_f$

$$V_{fl}, V_f = F(V_u, V_p, I_u, I_o, I_f, I_w), \quad (2)$$

where  $V_u, V_p, I_u, I_o$  are the parameters of the regulator of the feed drive of a mobile column depending on welding current  $I_w$ ;

Welding time

$$T_w = S_c/V_c + S_{fl}/V_{fl} + S_f/V_f + T_{ups} i,$$

where  $S_c, V_c, S_{fl}, V_{fl}, S_f, V_f$  is the tolerance and average speed at the stages of bevel removal, flashing and transition to upsetting.

The upsetting rate  $V_{ups}$  depends on the set upsetting pressure, technical condition of the upsetting drive and the moving column, and the heating of the welding rails before upsetting. Impedance of sh.c of a secondary circuit  $Z_{sh-c}$  characterizes the technical condition of the machine.

From the listed parameters controlled by the control system of machines K1000 and K922, in terms of  $K_v$  the most vulnerable indices are the rates  $V_{fl}, V_f, V_{ups}$  and welding time  $T_w$  and electrical power released at

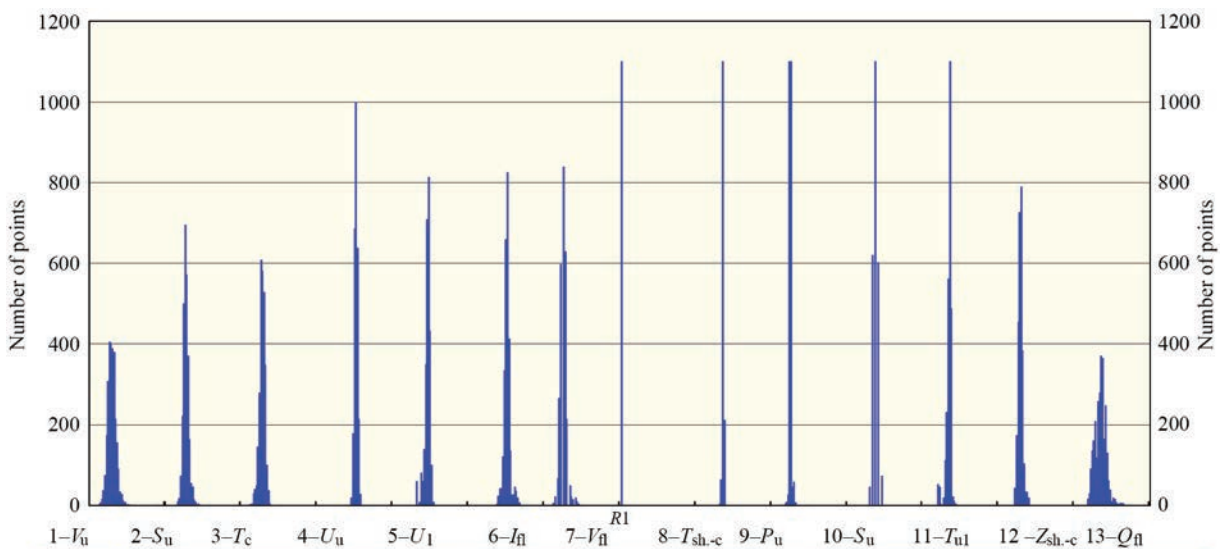


**Figure 3.** Histogram of distribution of process parameters of FBW of 10230 rail joints in the machine K1000, which was calculated on the interval of studies for each parameter (Table), number of intervals for all parameters was 50, step of each parameter is  $\Delta X = (X_{u,f} - X_{l,f})$ , where  $X_{u,f}$  and  $X_{l,f}$  are upper and lower intervals of studies (for example, for  $\Delta S_{fl} = (30-5)/50 = 0.5$  mm)

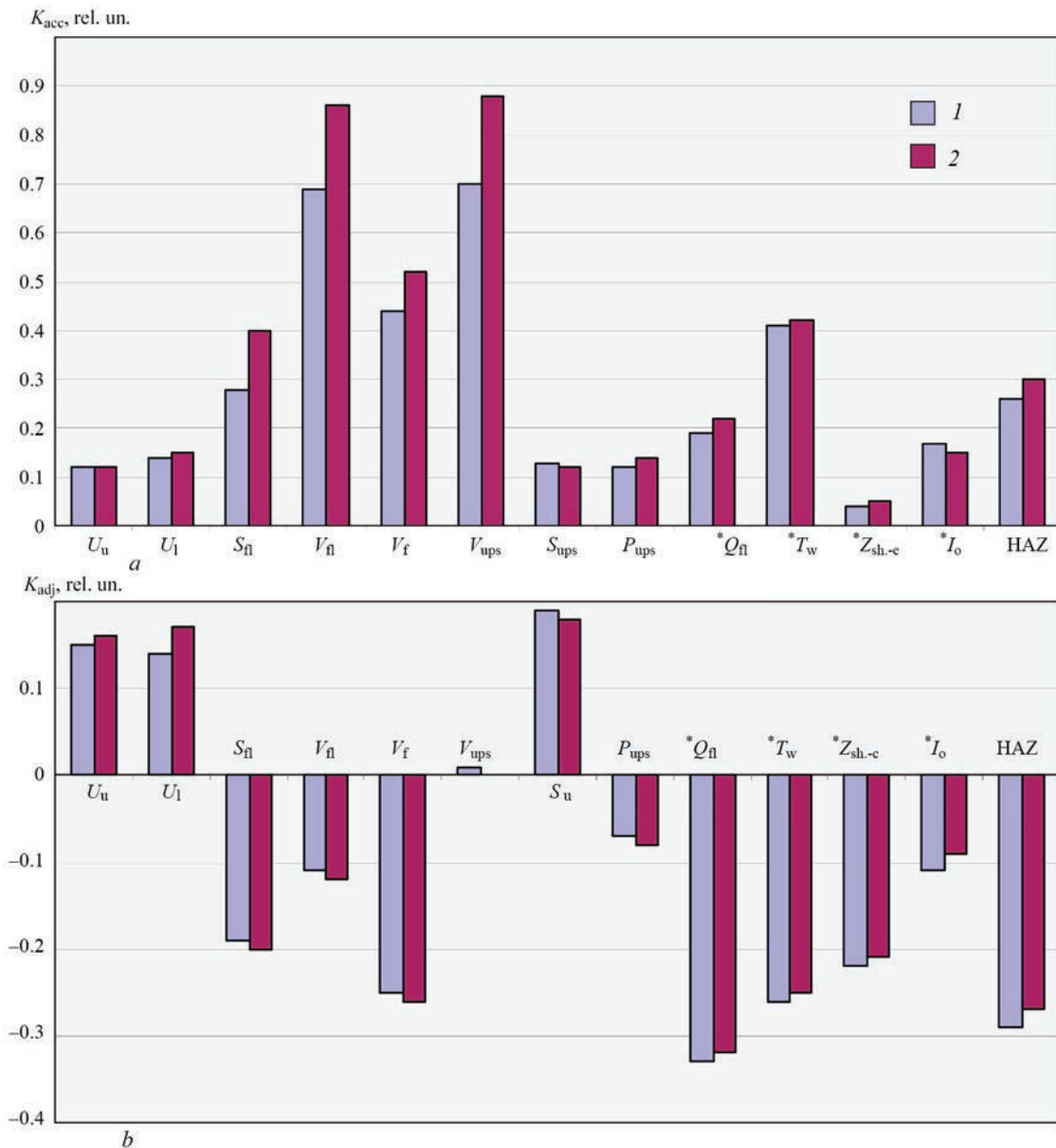


**Figure 4.** Coefficients of accuracy  $K_{acc}$  (a) and adjustment  $K_{adj}$  (b) during welding of R65 rails of grade K76F in the machine K1000 (1 — data on welding of specimens of technological test; 2 — data on welding rails)

the input of the welding transformer at the flashing stage,  $Q_{fl}$  (Figure 1). It should be noted that in addition to the action of perturbations, the r.m.s. of rates  $V_{fl}$  and  $V_f$  is influenced by the fact that the error of their measurement approaches the absolute value of the measured value.

The measurement of rates is performed according to the displacement sensor and the absolute error is  $\Delta V = 0.1 \text{ mm} / T_{meas}$ , where  $T_{meas}$  is the interval between measurements. The measurement discreteness of the control system in time is equal to 0.01 s. Therefore, we have either a very large static error or a large dynamic error for stabilization of these parameters.

According to the data of histograms (Figure 3) reproduction of FBW process parameters, in particular  $V_{fl}$ ,  $V_f$ ,  $V_{ups}$ , it is possible to make an assumption that

the distribution of error of these parameters concerning average value corresponds to the normal law.

The calculation of the accuracy coefficients  $K_{acc}$  (1), which take into account the value of the tolerance field and are accepted for statistical control of technological processes, confirms the general ratio of the accuracy of reproduction of the parameters  $C_v$  (Figure 4). According to the accuracy coefficient  $K_{acc}$ , which takes into account the tolerance for deviation of parameters according to TS (see Table), it is seen that provided that the average value of the rate  $V_{fl}$ ,  $V_f$ ,  $V_{ups}$  is close to the middle of the tolerance field, we have a probability of TS conformity more than 99.7 % of joints. For other parameters, the condition of finding the average value in the middle of the tolerance is already not so rigid.

To identify any trends over time, for example, changes in the technical condition of the welding machine, the coefficients  $K_v$  and  $K_{acc}$  were calculated with an interval of six months (Figures 1, b, 4, b). It is seen that during the control period the welding process was unchanged in terms of variation of FBW parameters and control data of technological test specimens (see Figure 1) for these parameters correspond to the process of welding rails (average values and r.m.s. parameters differ within the statistical errors, see  $K_{adj}$  and  $K_{acc}$  in Figure 4) and testing data of specimens by technological test can be used to evaluate the quality of rail joints.

The influence of output deviation from deviation of input parameters, among other factors, depends on possible interrelationships between inputs. The total variance for multifactor process in the case when the factors are not related to each other consists of the sum of the variances of each factor. In the case of correlated factors, the components of covariance are added to this sum with the corresponding sign — the measure of joint variability of two random variables. The absolute deviation of the output of the function  $Y = f(x_1, x_2 \dots x_n)$  from the deviation of any parameter  $\Delta x_i = S_i$  at the point  $x_i = \bar{x}_i, i = 1 \dots n$ , through  $K_{inp}$  depends on the value of the parameter  $x_i = \bar{x}_i$  and a partial derivative  $\partial Y / \partial x_i$  of the parameter  $x_i = \bar{x}_i$  at this point  $\Delta Y = \partial Y / \partial x_i \bar{x}_i K_{inp}$ . In the same way we can show that the accuracy coefficient is equal to

$$K_{acc} = 6 \bar{x}_i K_{inp} / \delta. \quad (3)$$

The influence of each input factor is a partial derivative  $\partial Y / \partial x_i$  can be evaluated by the mathematical dependence of an output parameter on input parameters. For example, flashing rate  $V_{fl}$ , tolerance for flashing  $S_{fl}$ , electric power during flashing  $Q_{fl}$  determine the temperature field in FBW. Mathematical regression dependences of HAZ on  $V_{fl}, S_{fl},$  and  $Q_{fl}$  were obtained using experimental data and a mathematical model of a temperature field kinetics during continuous flashing, taking into account the multifactorial effect of transient processes of formation and destruction of single contacts on heating intensity, which formed during the technological cycle of flash butt welding of railway rails [5, 6]. To evaluate the effect of parameter deviations on HAZ in the case of using the simplest first-order dependence, we have

$$L_{HAZ} = a_0 + a_1 V_{fl} + a_2 S_{fl} + a_3 Q_{fl} - S_{ups}.$$

The deviation of the HAZ width from the value at the average process parameters has the form:

$$\begin{aligned} \Delta L &= L - L(V_{fl} = \bar{V}_{fl}, S_{fl} = \bar{S}_{fl}, Q_{fl} = \bar{Q}_{fl}) = \\ &= a_1(V_{fl} - \bar{V}_{fl}) + a_2(S_{fl} - \bar{S}_{fl}) + a_3(Q_{fl} - \bar{Q}_{fl}) - (S_{ups} - \bar{S}_{ups}) = \\ &= a_1 \bar{S}_{fl} K_{vS_{fl}} + a_2 \bar{V}_{fl} K_{vV_{fl}} + a_3 \bar{Q}_{fl} K_{vQ_{fl}} + \bar{S}_{ups} K_{vS_u} = \\ &= -23K_{vS_{fl}} + 4K_{vV_{fl}} + 34K_{vQ_{fl}} - \Delta S_{ups}. \end{aligned}$$

Thus, despite the fact that  $K_{vS_{fl}}$  is much lower than  $K_{vV_{fl}}$ , the effect of the deviation of tolerance on quality of the welded joint is almost the same as flashing rate. At the same time, we have a significant influence on flashing electric power  $K_{vQ_{fl}} \approx 3K_{vS_{fl}}$ , and it becomes important to control the electric power during flashing  $Q_{fl}$  and its introduction into the list of parameters of the TS for welding rails (Table).

The complexity of measuring active power is associated with the fact that the harmonic component of active power is determined by those harmonics that are represented in the current signal and in the voltage signal. According to the computer simulation data, the signals of current, voltage and power on frequency spectrum are placed at the input of the power transformer in the range of angles  $\varphi$  (from 0 to 90°) and angles of switching the thyristor contactor  $\alpha$  (from  $\varphi$  to 120°) in the range of up to 1 kHz. These results were confirmed experimentally by recording the welding current and voltage at the input of a power transformer with a frequency of 10 kHz and a subsequent calculation of active power. To control the power  $Q_{fl}$  at the PWI a measuring transducer of average active electric power with a pulse output was designed on the basis of the industrial controller Siemens CPU 314C-2PTP or CPU1512C-1PN with input signals of up to 1000 A current and a voltage of up to 440 V, a frequency band of these signals of up to 1 kHz and a resulting measurement error of up to 1 %, which is adapted to the control systems of machines K1000 and K922.

According to the data of welding specimens of a technological test at RWE, which passed testing on static bending and were recognized as those which meet TS, it is seen that  $K_v$  of a deflection  $L_{fr}$  and a destructive force  $P_{fr}$  is almost 2 times lower than  $K_v$  of parameters of flashing rate, forcing and upsetting (Figure 1, a). The parameters set directly by the control system of the machine, on the contrary, have  $K_v$  almost 2 times lower than that for the indices of a joint quality. Thus, we can very cautiously assume the most significant contribution of these rates to quality. But these parameters are definitely the most vulnerable in terms of the abilities of accuracy of operation of the control system in the reproduction of the desired values of  $V_{fl}, V_{fr}, V_{ups}$ . In addition, taking into account the influence of the parameters on the HAZ width it is necessary that the list of control parameters in the TS (Table) was added by the value of electric power released during flashing.

When choosing the tolerance field, it should be taken into account that while solving any statistical hypothesis, two types of errors are possible:

- the error of the first kind consists in the fact that the hypothesis which is actually true is rejected — in our case the qualitative joint will be recognized as a low-quality one;

• the second kind of error consists in the fact that the hypothesis is accepted, but it is actually incorrect — a poor joint will be recognized as a high quality one.

The boundary between the signs of conformity and nonconformity of the TS is quite blurred and if the probability of errors can be evaluated, it should be chosen taking into account the cost for replacement of a quality joint in the lash (in the first case) and the cost of tolerance of a poor joint in the lash in the other. It is quite natural in this case to choose more rigid tolerances for the control of parameters. According to data on HAZ predicting, it is clear that the most objective evaluations of tolerances can be obtained from the analytical dependences of quality indices on process parameters, which in the case of FBW is currently impossible.

It should be noted that although the control of tolerances is a very common means of preventing rejection, the example of setting the tolerance for flashing for different batches of rails shows that the tolerance  $S_{\Pi}$  in the TS can meet a wide range of quality values, and the variation  $S_{\Pi}$  itself for the set mode is much lower than the tolerance. Thus, the condition of tolerance does not use all the features of welding equipment and technology in general.

According to the method of production management [7], it is considered that compliance with the tolerances of control factors is an insufficient criterion to judge about the quality of products. It is necessary to constantly strive for the rated value, which was obtained when setting the mode, and to reduce the variation of factors, even within the limits set by the project. In this case, the adjustment of the optimal levels of control factors of the process is performed by achieving the optimal ratio «signal/noise», which in our case corresponds to the inverse value of the variation coefficient  $K_v$ .

## Conclusions

1. Statistical studies on the protocols of the FBW process of railway rails at RWE showed that the param-

eters of control of the butt welding process, which are given in the TS and set directly by the control system of the welding machine, do not significantly depend on external perturbations and are reproduced with an accuracy of a control system stabilization.

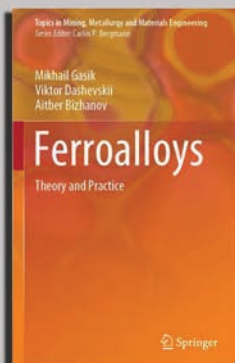
2. The parameters, the values of which are the result of the welding process and the action of uncontrolled perturbations, namely flashing rates, transition to upsetting, upsetting and active electric power released at the joint, are reproduced with an error of 5–10 times higher than the control system error.

3. To increase the accuracy of control of the FBW process of rails, the list of control parameters in the TS for welding rails, it is appropriate to introduce the control of active electric power at the input of the welding transformer during flashing. At the PWI, a sensor for monitoring such power was designed, which is adapted to the existing control system of welding machines.

- (2016) *New welded rails for railways*. Specifications: TU U 24.1-40075815-002:2016.
- DIN EN 14587-2: *Railway applications — track — flash butt welding of rails. Pt 2: New R220, R260, R260Mn and R350HT grade rails by mobile welding machines at sites other than a fixed plant*.
- Portal of knowledges StatSoft*. URL: <http://statistica.ru/>
- Process capability index*. URL: [https://en.wikipedia.org/wiki/Process\\_capability\\_index](https://en.wikipedia.org/wiki/Process_capability_index)
- Kuchuk-Yatsenko, S.I., Milenin, A.S., Velikoivanenko, E.A. et al. (2018) Mathematical modeling of the process of metal heating in continuous flash-butt welding. *The Paton Welding J.*, **10**, 2–8. DOI: <https://doi.org/10.15407/as2018.10.01>
- Kuchuk-Yatsenko, S.I., Rudenko, P.M., Gavrish, V.S. et al. (2020) Operational control as a method of quality evaluation of welded joints in resistance flash butt welding of modern high-strength steels. *Nauka i Innovatsii*, **16(2)**, 72–78 [in Ukrainian].
- Rao, S., Samant, P., Kadampatta, A., Shenoy, R. (2013) An overview of Taguchi method: Evolution, concept and interdisciplinary applications. *Int. J. of Scientific & Engineering Research*, **4**, 10.

Received 05.04.2021

NEW BOOK



Springer Publishing house (Switzerland) has released in 2020 a new book «**Ferroalloys: theory and practice**» (530 p.) by Gasik M.I., Dashevskii V.Ya., Bizhanov A.M., under supervision of Academician of National Academy of Sciences of Ukraine, Professor Mikhail Ivanovich Gasik.

This book outlines the physical and chemical foundations of high-temperature processes for producing ferroalloys with carbo-, silico- and aluminothermal methods, as well as technology practice for manufacturing of ferroalloys with silicon, manganese, chromium, molybdenum, vanadium, titanium, alkaline earth and rare earth metals, niobium, zirconium, aluminum, boron, nickel, cobalt, phosphorus, selenium and tellurium and also iron-carbon alloys. The chapters introduce the industrial production technologies of these groups of ferroalloys, the characteristics of charge materials, and the technological parameters of the melting processes. Special chapters are devoted to description of ferroalloy furnaces and self-baking electrodes in detail. Additionally, topics related to waste treatment, recycling, and solution of environmental issues are considered.

The book is recommended for specialists and researchers involved in the international ferroalloys production.

[www.springer.com/gp/book/9783030575014](http://www.springer.com/gp/book/9783030575014)

## IMPROVING THE EFFICIENCY OF ROBOTIC FABRICATION OF STEEL TRUSS WELDED STRUCTURES

V.M. Korzhyk<sup>1</sup>, A.A. Grynyuk<sup>1</sup>, V.Yu. Khaskin<sup>1</sup>, Ye.V. Illiashenko<sup>1</sup>, I.M. Klochkov<sup>1</sup>,  
O.V. Ganushchak<sup>1</sup>, Yu Xuefen<sup>2</sup> and Liuyi Huang<sup>2</sup>

<sup>1</sup>E.O. Paton Electric Welding Institute of the NAS of Ukraine

11 Kazymyr Malevych Str., 03150, Kyiv, Ukraine. E-mail: office@paton.kiev.ua

<sup>2</sup>Zhejiang Academy of Special Equipment Science

310016, Jiangan District, Hangzhou, Zhejiang, 211, Kaixuan Road, China

It is shown that to increase the productivity of robotic fabrication of fragments of steel truss RHS (Rectangular Hollow Section) structures it is advisable to make workpieces by precision laser cutting with subsequent assembly of fragments by spot tack welds and consumable-arc seam welding with current-carrying (hot) filler wire. Laser cutting with radiation power of ~1.0 kW and compressed air blowing at the pressure of 1.5 MPa allows obtaining ready for further welding elements of RHS structures with the accuracy of 0–0.1 mm. It is established that in the case of application of consumable-arc welding with hot filler wire, the speed increases by ~1.5 times compared to conventional consumable-arc welding. 13 Ref., 6 Figures.

*Key words*: laser cutting, welding, consumable electrode arc, current-carrying filler wire, fillet joints, carbon steel, structures

Structural advantages of tubular steel elements have become more and more obvious during the last decades owing to investigations and experience in construction [1, 2]. These elements are often used all over the world, particularly in large-span structures. For instance, the first all-welded tubular truss structure of a bridge without supports or connections, was recently commissioned in the Germany. It is an innovation in bridge-building as an integral structure and is an advanced bridge structure as a whole [3]. The truss girders were earlier made from angle-type members, connected into nodes by welded on gussets. In the XXI century new design solutions for truss structures appeared in industry, which include, first of all, use of CHS (Circular Hollow Sections) and RHS (Rectangular Hollow Sections) elements joined by welding directly in the abutment points around the contour [4, 5].

It is known that the elements of hollow structural sections (HSS) have many advantages over the equivalent sections with an open cross-section, including better torsion resistance, as well as tensile and compressive loading, aesthetic character and saving in terms of material costs [5]. At first glance HSS elements can be rather easily joined, having cut the edges and welding them to each other. However, depending on the configuration of the joint connection and num-

ber of connected members, it may lead to producing complex and expensive structures.

In order to reduce the costs and accelerate fabrication of such structures, it is rational to divide them into individual assemblies, which can be welded by industrial robots [6]. In the actual process of truss structure fabrication the elements are usually joined by spot welding on a mounting platform, and then welded entirely in robotic sections [7]. However, this leads to a number of problems, related to preparation and performance of welding.

Robotic welding requires greater adherence to the geometrical dimensions of parts to be welded [8]. This primarily applies to uneven gaps, caused by inaccurate set up, i.e. cutting of the parts for welding. As a rule, cutting is performed by mechanical method using saws. Here, the geometrical dimensions of the parts can change, because of wear of the saw surface. Moreover, cutting is performed, mainly, in semi-automatic machine tools, so that the human factor is added to the accuracy problems. Another problem is the impossibility of obtaining curvilinear shapes of the cut surfaces by saw cutting. This peculiarity leads to appearance of gaps in the butt joint assembled for welding, so that it does not completely meet the requirements of optimum (no gap) assembly. This problem can be solved either by application of certain techniques, or addi-

V.M. Korzhyk — <http://orcid.org/0000-0001-9106-8593>, A.A. Grynyuk — <https://orcid.org/0000-0002-6088-7980>,

V.Yu. Khaskin — <http://orcid.org/0000-0003-3072-6761>, Ye.V. Illiashenko — <https://orcid.org/0000-0001-9876-0320>,

I.M. Klochkov — <https://orcid.org/0000-0001-6490-8905>, O.V. Ganushchak — <http://orcid.org/0000-0003-4392-6682>,

Yu Xuefen — <https://orcid.org/0000-0003-1922-1025>, Liuyi Huang — <https://orcid.org/0000-0003-4155-2824>

tional milling for optimum assembly of the joint for welding. In both the cases, the productivity decreases, while the cost of work performance rises.

Laser technologies are the most promising for preparation of billets with the required geometry of the cut surface [9]. In particular, rather widespread is the process of laser cutting, using industrial robots [10]. At up to 6 mm thicknesses the laser beam ensures a thin (up to 0.5 mm) cut. It enables greatly reducing the metal consumption in cutting, as the width of mechanical CNC cut at up to 6 mm thickness usually is up to 5 mm. [11]. Moreover, the affordability of modern laser equipment is gradually becoming closer to that of CNC machine tools. Compared to plasma cutting, at laser process a smaller number of working tool parts (primarily cutting nozzles) are consumed, and no finishing of the edges is required for further welding [10]. Use of a robot enables making cuts with complex paths in space, which are required to produce the welded joint in terms of its produceability and strength, and also promotes the flexibility of its transition from fillet to butt joints.

In order to produce steel structures from CHS and RHS using robots, more rational and adaptable-to-fabrication is the method of consumable electrode pulsed-arc welding in a mixture of gases (GMAW-P) [12]. Nonetheless, this welding method has certain features, which do not always have a positive impact on the welding process. One of the methods to improve the process of consumable electrode pulsed-arc welding is additional application of filler wire. It enables increasing the amount of metal during welding without raising the welding current. More

over, to increase the effectiveness of welded joint formation when making the fillet welds, it is rational to apply additional filler wire preheated by electric current of different polarity [13]. Such a combination of consumable electrode and additional heated wire enables a certain increase of the speed of welding the fillet welds without increasing the current of the consumable electrode arc, improving the geometry of the weld surface due to reduction or complete elimination of undercuts, reduction of the structure deformation through reducing the heat input at preservation of the amount of metal, involved in weld formation. Moreover, such an approach with application of additional filler wire will allow improvement of the currently available robotic complexes for consumable electrode welding with minimum capital expenditures.

Thus, improvement of the effectiveness of fabrication of truss welded structures from CHS and RHS pipes requires application of a complex approach, which will consist in using the robotic laser cutting of billets from steel shaped pipes and consumable electrode robotic welding with additional heated filler wire.

The objective of the work is increase of the effectiveness of robotic manufacture of fragments of steel truss structures due to application of precision laser cutting of billets with further preparation and consumable-arc welding.

This objective was reached by solving the following task: optimization of the technology of precision laser cutting of carbon steels up to 6 mm thick; preparation of cut billets for consumable-arc robotic welding; consumable-arc robotic welding, also with additional current-carrying (hot) filler wire.

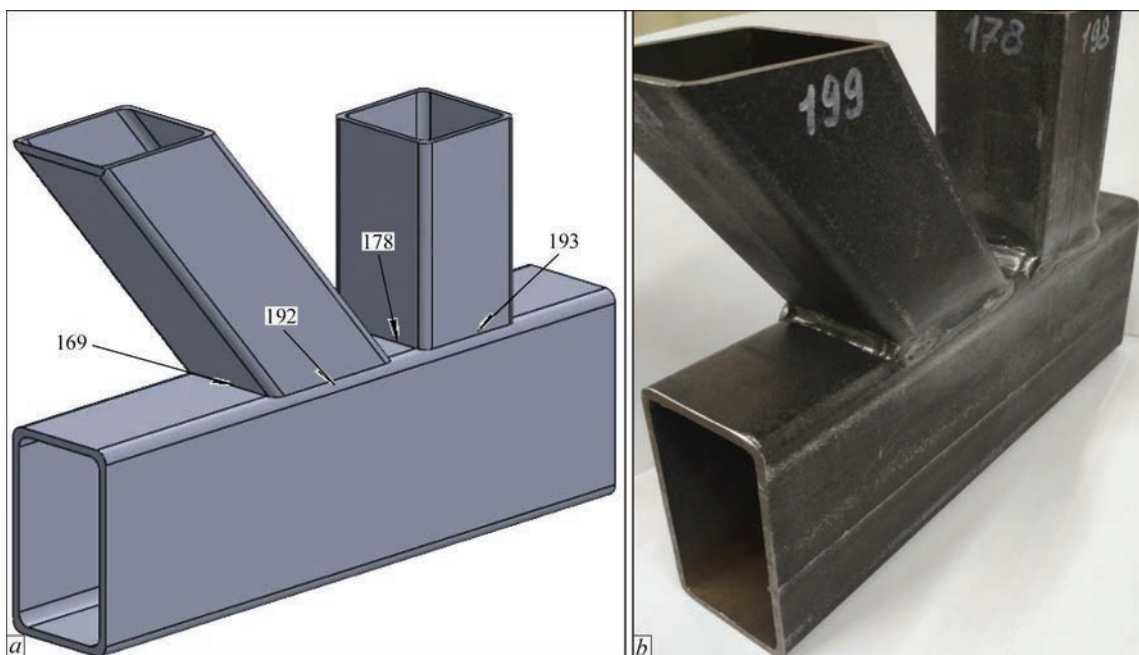


**Figure 1.** Appearance of an assembly of a truss structure from RHS elements: *a* — model with spatial arrangement of welds; *b* — welded fragment

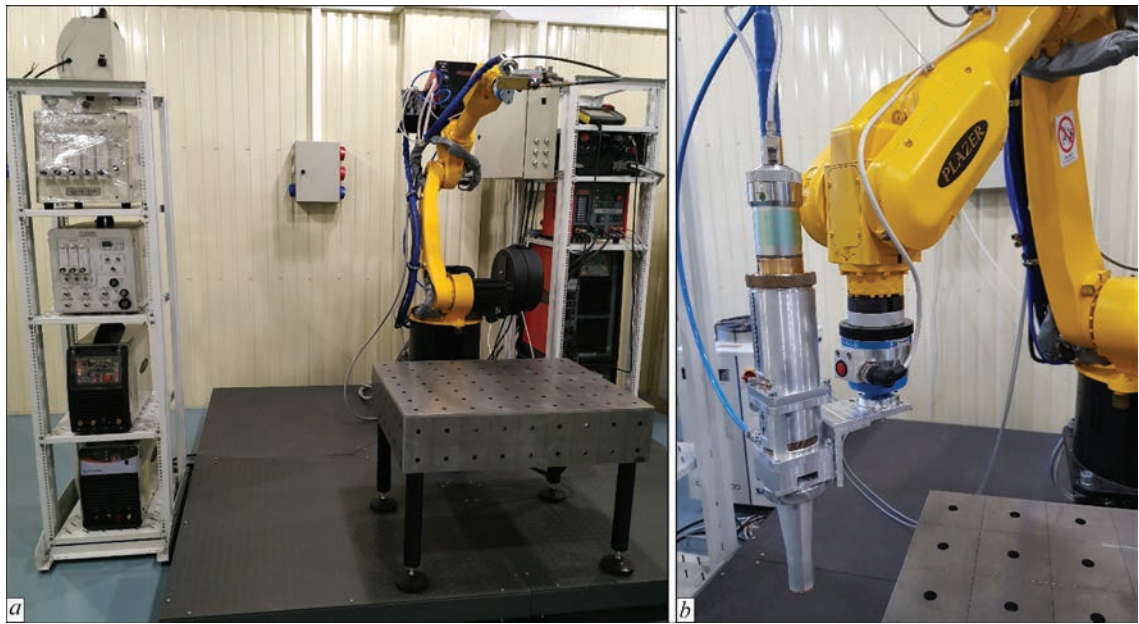


**Figure 2.** Appearance of a laboratory robotic complex (a) and head for laser cutting (b) in the robot arm

The assemblies of truss RHS structures were made from shaped pipe of 60×60 and 120×60 mm size with up to 6 mm wall thickness (Figure 1). Laser cutting was used to make from this pipe 50–300 mm long fragments with square and bevelled edges. Pipe material is Q235 carbon steel (steel St3 analog). This steel is not prone to hot or cold cracking during GMAW, so that the structure does not require heating or monitoring of the cooling rate after welding. Welding experiments were performed using electrode and filler wires of ER-70S grade (Sv-08G2S analog) of 1.0–1.6 mm diameter.

In order to conduct technology studies, a robotic laboratory complex was developed (Figure 2), which includes fiber laser of MFSC-1000 model (MAX Company, PRC) of up to 1.0 kW power, Plazer R1 industrial robot of ingenious design with arm radius of up to 1400 mm and lifting capacity of up to 10 kg; GMAW power source of Fronius TPS 450 model, power source of EWM Tetrax 421 AC/DC model for filler wire heating; gas treatment station, welding heads, welding table, welding-assembly fixtures, etc.

The need to apply precision laser cutting was related to the fact that usually at preassembly of the truss structure components time was consumed in

the preparation section for manual fitting of the parts, which became necessary because of noncompliance with the dimensions of manufacturing the parts. Increase of the accuracy of parts manufacturing up to  $\pm 0.1$  mm eliminated this problem.

Laser cutting head of our own design (Figure 2, b) was used to conduct a series of experiments on cutting carbon steel sheets, as well as shaped steel pipes (Q235 type steel) with wall thickness  $\delta \leq 6$  mm. The best results were obtained in the case of application of compressed air with approximately 1.5 MPa pressure at deepening of the focus for  $\sim 1$  mm under the surface of the material being cut, and not more than 1.0 mm distance between this surface and cutting nozzle edge. At approximately 1.0 kW power of laser radiation the cutting speed decreased from 240 to 60 m/h at increase of sheet thickness from 2.0 to 6.0 mm. The cut width was  $\sim 0.3$  mm, the edges were smooth enough, and a small amount of flash was observed, which was quite easy to separate (Figure 3). The respective shaped pipes were used to cut out the required number of parts for further welding. The accuracy of their preparation was 0–0.1 mm that satisfied the requirements to preassembly of truss structure components.



**Figure 3.** Width (a) and edge (b) of a laser cut of shaped pipe from steel of Q235 type (5 mm wall thickness)

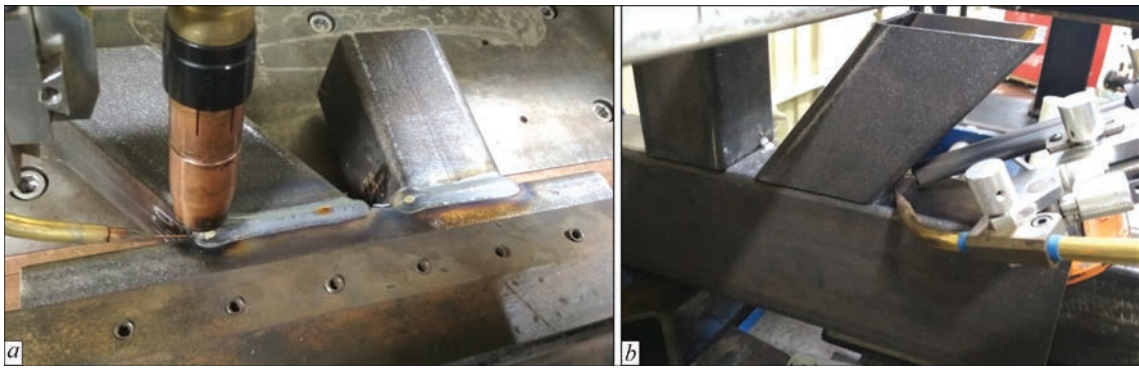


**Figure 4.** Application of a standard torch (*a*) and modified torch with narrowed nozzle part (*b*) for welding the truss structure assembly

The next stage was acceleration of preparation of the cut billets for robotic welding. The main problem which arose at this stage was time consumption for the process of structure assembly, its clamping and disassembly of the clamping devices in the robotic welding section, because of the presence of screw clamps in the structure. In order to eliminate this deficiency, it was proposed to transfer to the robotic welding section the structural elements preassembled by spot welding. With this purpose, PWI developed a project of a section of assembly for welding with all-purpose welding-assembly equipment and respective technology of making the assembly spot welds. The design of simplified fixture for fast fixation of the truss structure part preassembled for welding was developed for the robotic welding section. Such a type of clamping devices was selected, which ensure the minimum time for mounting the billet and its release after spot welding.

The last task, which was addressed within the framework of this study, was consumable-arc robotic welding (GMAW). The first important problem, which was solved here, was caused by the presence of rounding-off radius in the fillet zones of shaped pipe surface, which led to formation of a gap (1.0–1.2 mm) at abutment of the respective elements of the truss structure assembly. The second problem was related to the impossibility of welding with normal electrode extensions (12–16 mm), because of the close arrangement of the structural elements and large diameter of protective nozzle of the standard soldering iron, which did not provide access to 12–16 mm distance from the welding zone (Figure 4, *a*). The third problem concerned the need for welding in different positions in space, as the welded fragment of the truss structure was stationary, while the GMAW torch in the robot arm moved at different angles of inclination by a complex path.

The first of the above problems was eliminated by inclination of the torch axis at 20° angle relative to the conditional plane, which passes through the butt axis normal to the plane of the parts being welded. In order

to enable performance of consumable electrode welding in difficult-of-access places with normal electrode extension (12–16 mm), a modified torch was developed and applied. It has a narrowed nozzle part, which can ensure welding performance at the distance of the order of 13–14 mm between the side walls (Figure 4, *b*). The third problem was eliminated by applying adaptive control of welding current, depending on the direction of movement in space: in the case of uphill welding the current was somewhat reduced, at downhill welding it was somewhat increased. Such a schematic of robotic welding is urgent to manufacture truss structures from steel RHS pipes, but to a greater extent — for structures from CHS pipes, as in the case of welding of one round pipe into another one the torch has to be moved by a saddlelike path.

The robotic experimental complex was used to perform the technological studies of welding the earlier cut by the laser method elements of shaped pipes from steel Q235 with  $\delta = 4$  mm wall thickness with shielding by a gas mixture of 82 % Ar + 18 % CO<sub>2</sub>. GMAW welding was used to make butt and tee (fillet) joints at shielding gas consumption of approximately 20 l/min. Investigations were conducted both for the case of the conventional GMAW, and with additional filler wire (Figure 4). Additional wire was fed backwards in the direction of motion (welding) with shifting relative to the electrode forward in the direction of motion to 2–5 mm distance. The wire was fed both without heating, and with heating. Here, both direct and different polarity current was used for heating. Direct current promoted the welding arc deflection and impaired the welding result. For this reason, symmetrical different-polarity pulses were used for heating of additional filler wire, with current  $I_{HW} = 50$ –100 A at voltage  $U_{HW} = 10$ –15 V, and electric power was in the range from 500 up to 1500 W at frequencies from 75 to 100 Hz.

First, the mode of conventional GMAW at the speed of 27–30 m/h was selected by the criterion of formation of sound welds without undercuts. Studies showed that in this case penetration of the welded

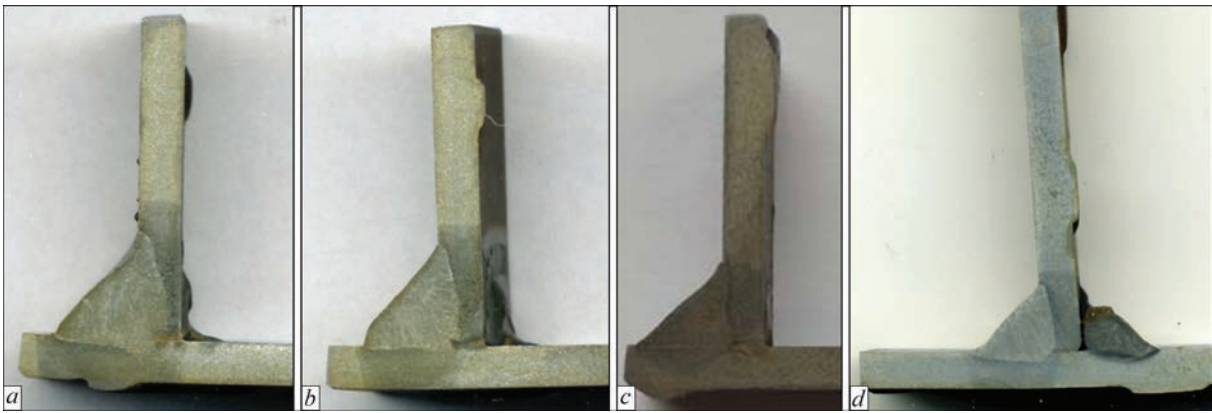


**Figure 5.** Macrostructure of samples with transverse cross-section of fillet welds (left) produced on assembled using tack welds (right) samples from Q235 steel ( $\delta = 4$  mm): *a* — GMAW without filler; *b*, *c* — GMAW with cold filler; *d* — GMAW with hot filler



**Figure 6.** Appearance of welds, produced on samples of an assembly of a truss structure from RHS elements (Q235 steel): *a* — conventional GMAW; *b* — GMAW with hot filler

part wall was equal to about 50 % of the thickness (Figure 5, *a*). In order to raise the welding productivity, the welding speed was increased by 40 % with simultaneous increase of welding current. However, weld formation was considerably impaired, and undercuts appeared. Therefore, the speed was reduced to the initial value, and at the same time filler wire was added. Weld formation became satisfactory, but penetration decreased (to 10–20 % of the wall thickness), and productivity increased (Figure 5, *b*). In the case of an attempt to increase the welding speed by 40–50 %, lack-of-fusion of the weld metal with the base metal was observed (Figure 5, *c*). Introduction of filler wire heating promoted formation of sound welds without undercuts with satisfactory (not less than 30 %) penetration depth of base metal wall (Figure 5, *d*). Here, the welding speed increased up to 1.5 times, compared to conventional GMAW.

Analysis of the produced joints by such indices as weld formation and their strength, showed that conventional GMAW and GMAW with additional conductive (hot) wire are approximately on the same level. However, besides productivity, GMAW with hot

wire features lower spatter and approximately 25 % shorter weld pool (Figure 6).

### Conclusions

1. To increase the productivity of robotic manufacture of fragments of truss structures from steel RHS pipes, it was proposed to produce billets by precision laser cutting with further assembly of fragments by spot tack and consumable-arc seam welding with current-carrying (hot) filler wire.

2. Laser cutting with radiation power of  $\sim 1.0$  kW and blowing compressed air at the pressure of 1.5 MPa allows producing ready for welding RHS structure elements with the accuracy of 0–0.1 mm. Here, 2.0–6.0 mm thick walls were cut at the speed of 240–60 m/h, and the cut width was  $\sim 0.3$  mm.

3. For robotic fabrication of truss structures from steel CHS and RHS pipes a scheme was developed for welding the stationary fragments of such structures by a torch, which is moved by the robot arm in different positions in space. It differs by adaptive control of welding current, depending on the spatial position of the torch with feeding of hot filler wire backwards in the direction of welding.

4. To perform consumable-arc welding with hot filler wire, a specialized torch (narrower nozzle) was developed that enables welding in difficult-of-access places with normal electrode extension (12–16 mm) at 13–14 mm distance between the side walls.

5. It was established that in the case of application of consumable-arc welding with hot filler wire the speed rises by  $\sim 1.5$  times, compared to conventional consumable-arc welding. Here, it is rational to apply symmetrical different-polarity current pulses of 500–1500 W power with 75–100 Hz frequency for wire heating.

1. Radu, D., Radu, B. (2014) Truss beams welded joints strengthening solutions. 41th anniversary faculty of civil engineering subotica. In: *Proc. of Inter. Conf. on Contemporary Achievements in Civil Engineering (24 April 2015, Subotica,*

- Serbia*), 261–269. DOI: <https://doi.org/10.14415/konferencijaGFS> 2015.033.
2. Paton, B.E., Lobanov, L.M., Tereshchenko, V.I. et al. (1994) Robotic production of welded trusses for industrial building overlaps. *Avtomatch. Svarka*, **12**, 26–29 [in Russian].
  3. Casper, H.-J. (2014) The first fully welded integral tube truss bridge of Germany. Ed. by E. Petzek, R. Bancila. In: *Proc. of 8<sup>th</sup> Inter. Conf. on Bridges in Danube Basin*. Springer Vieweg, Wiesbaden, pp. 163–172. DOI: [https://doi.org/10.1007/978-3-658-03714-7\\_11](https://doi.org/10.1007/978-3-658-03714-7_11).
  4. Radu, D., Galatanu, Tf. (2016) Optimization solutions for truss beams elements welded joints. In: *Proc. of 4<sup>th</sup> Int. Conf. on Contemporary Achievements in Civil Engineering» (22 April 2016, Subotica, Serbia)*, 105–111. DOI: <https://doi.org/10.14415/konferencijaGFS> 2016.009.
  5. Zhao, X.L., Tong, L.W. (2011) New development in steel tubular joints. *Advances in Structural Engineering*, **14**(4), 699–715. DOI: <https://doi.org/10.1260/1369-4332.14.4.699>.
  6. Cheav Por Chea, Yu Bai, Xuebei Pan et al. (2020) An integrated review of automation and robotic technologies for structural prefabrication and construction. *Transportation Safety and Environment*, **2**(2), 81–96. DOI: <https://doi.org/10.1093/tse/tdaa007>.
  7. Yang, W., Lin, J., Gao, N., Yan, R. (2018) Experimental study on the static behavior of reinforced warren circular hollow section (CHS) *Tubular Trusses. Appl. Sci*, **8**(11), 2237, 1–22. DOI: <https://doi.org/10.3390/app8112237>.
  8. Grinyuk, A.A., Korzhik, V.N., Shevchenko, V.E. et al. (2015) Main tendencies in development of plasma-arc welding of aluminium alloys. *The Paton Welding J.*, **11**, 31–41. DOI: <https://doi.org/10.15407/tpwj2015.11.04>.
  9. Korzhyk, V., Khaskin, V., Perepychay, A. et al. (2020) Forecasting the results of hybrid laser-plasma cutting of carbon steel. *Eastern-European J. Enterprise Technologies*, **104**(2/1), 6–15. DOI: <https://doi.org/10.15587/1729-4061.2020.198433>.
  10. Kumar, H., Ganesh, P., Kaul, R. et al. (2006) Laser welding of 3 mm thick laser-cut AISI 304 stainless steel sheet. *J. of Mater. Eng. and Perform.*, **15**, 23–31. DOI: <https://doi.org/10.1361/105994906X83385>.
  11. Chuangwen, Xu, Jianming, Dou, Yuzhen, Chai et al. (2018) The relationships between cutting parameters, tool wear, cutting force and vibration depth can improve productivity and control cutting force and vibration. *Advances in Mechanical Engineering*, **10**(1), 1–14. DOI: <https://doi.org/10.1177/1687814017750434>.
  12. Praveen, P., Yarlagadda, P.K.D.V., Kang, M.J. (2005) Advancements in pulse gas metal arc welding. *J. Materials Proc. Technology*, **164–165**, 1113–1119. DOI: <https://doi.org/10.1016/j.jmatprotec.2005.02.100>.
  13. Spaniol, E., Trautmann, M., Ungethüm, T. et al. (2020) Development of a highly productive GMAW hot wire process using a two-dimensional arc deflection. *Weld World*, **64**, 873–883. DOI: <https://doi.org/10.1007/s40194-020-00880-9>.

Received 26.04.2021

WORLD TRADE FAIR FOR WELDING ENGINEERING —  
JOINING, CUTTING, SURFACING

LET'S JOIN  
THE WORLD!

11. – 15. September, 2023

REGISTER NOW!

www.schweissen-schneiden.com

DVS GERMAN WELDING SOCIETY

MESSE ESSEN

# IMPROVING THE EFFICIENCY OF THE SLM-PROCESS BY ADJUSTING THE FOCAL SPOT DIAMETER OF THE LASER BEAM

S.V. Adjamskyi<sup>1</sup>, G.A. Kononenko<sup>1,2</sup> and R.V. Podolskyi<sup>1,2</sup>

<sup>1</sup>LLC «Additive Laser Technology of Ukraine»

144 Rybinska Str., 49000, Dnipro, Ukraine. E-mail: [info@alt-print.com](mailto:info@alt-print.com)

<sup>2</sup>Z.I. Nekrasov Iron and Steel Institute of the NAS of Ukraine

1 Academician Starodubov Sq., 49000, Dnipro, Ukraine. E-mail: [office.isi@nas.gov.ua](mailto:office.isi@nas.gov.ua)

Selective laser melting (SLM) is one of the modern methods of additive manufacturing, which allows creating high-density parts with a unique geometry from metal powder. To improve the efficiency of the SLM process, it is desirable to increase the width of the melt pool, as this will increase the distance between the laser passes and a larger volume will be built in a shorter period of time. However, the formation of the outer surface by large tracks will result in its higher roughness, which can significantly reduce the overall reliability of a product. To improve the surface quality, it is necessary to reduce the size of the melt pools, for example, by reducing the diameter of the laser focal spot. The samples were examined produced at different focal spot diameters using the same laser power. Based on the results of the analysis of technological parameters of the process, it was established that to increase the efficiency of SLM-process, printing of the main body of a product can be performed at an increased laser beam focal spot diameter, and to provide a high surface quality, printing of a contour part (shell) should be more performed using a more localized focal spot. According to the redistribution of power along the cross-section of the beam, a change in the configuration of the melt pool, and accordingly the track occurs. It was established that in order to avoid the formation of deep remelting due to a high concentration of energy in the center of the beam, it is necessary to reduce the laser power. 29 Ref., 6 Figures.

*Keywords*: selective laser melting, technological factors, quality system, AISI 316L, specific linear energy

Additive manufacturing (AM) as a method of parts fabrication is becoming increasingly important in recent years [1]. Selective laser melting (SLM) is the process of AM consisting of three main stages: 1 — deposition of a layer of powder with a thickness from 20 to 50  $\mu\text{m}$  on the construction platform; 2 — melting of the powder layer by a laser source based on previously imported data of 3D-CAD models; 3 — lowering of the construction platform and restart at the point 1. The powder is usually applied with a polymer or rubber scraper. SLM allows manufacturing high-density parts with a unique geometry from metal powder. In addition, due to the possibility of reusing unmelted metal powder, SLM is almost waste-free technology [2, 3]. Moreover, only a small amount of further treatment (polishing, sandblasting, heat treatment) of parts manufactured by the additive method is required, so that expensive value-added processes can be minimized [4]. Studies of the last two decades have mainly focused on the influence of different process parameters on its stability and the resulting microstructure and properties of materials [5–7].

The studies of stainless steel by Gu et al. [8] showed that such parameters as laser power and scanning rate affect the porosity and evolution of the mi-

crostructure in different ways. Yang et al. [9] experimentally showed that quality of a product primarily depends on scanning rate, laser power and layer thickness. In a statistical study, the relative importance of each process parameter was studied and it was found that scanning rate is the parameter that has the most intensive influence [9]. A low scanning rate provides a complete melting of particles and a dense structure, but the process efficiency is significantly reduced. At very low scanning rates, instability of a melt pool causes a nonuniform melting along each track, which leads to a high surface roughness and a high volumetric porosity due to the effect of ball formation [10, 11]. At high scanning rates, a short-term interaction between the material and the laser beam causes the formation of narrow melt pools, which also leads to an increased surface roughness [11]. In addition, very high scanning rates can provoke an increased porosity, as well as the formation of thermal cracks as a result of high cooling rates [12]. According to the results of [13], at a high laser power density, a larger melt pool with a higher temperature is achieved. A fairly large melt pool leads to a good melt distribution and to a completely dense printing.

S.V. Adjamskyi — <https://orcid.org/0000-0002-6095-8646>, G.A. Kononenko — <https://orcid.org/0000-0001-7446-4105>, R.V. Podolskyi — <https://orcid.org/0000-0002-0288-0641>

© S.V. Adjamskyi, G.A. Kononenko and R.V. Podolskyi, 2021

Thus, finding the optimal scanning rate is a compromise between the efficiency and quality of the construction process.

Not only the process parameters have been improved, but also the equipment for the SLM process has undergone significant changes. Modern 3D technologies consider different possibilities of changing technological process of growing parts to increase the efficiency of the equipment preserving a high quality of products. Modern directions of improvement of technological aspects of SLM include an increase in the speed of process by means of a replaceable output chamber, closed control of powder processing, automated powder sieving, multilayer simultaneous printing, two axes of a coating and hoppers with many cavities [14]. Some companies also offer a close cycle powder control system and removable cylinders as new improvements to increase the speed of manufacturing [15–18]. Round platforms prevent powder dispersing and do not require filling or unloading of a powder during the entire fabrication cycle, even during printing at a full capacity [19–21]. This provides a homogeneous process of fabrication, shortens operator time and provides a high level of system security. Some new machines use automatic sieving and powder recycling in order to significantly reduce the time of fabrication. Due to the automation of the sieving process and recirculation of the powder, the time of manual work is reduced, which also increases the efficiency of the process [22, 23].

With an increase in the dimensions of construction a quite large number of technological limitations arises, one of which is a complicated operation of the kinematic system. At a high load on the construction platform, the positioning accuracy of the platform itself should reach several microns, and its horizontality and parallelism relative to the base frame should not exceed a few seconds. The physics of the process and the physical properties of the scanning system do not allow a significant increase in the scanning rate of the laser beam and the specific power with it. As the sizes of the construction platform increase, the fabrication period also increases in direct proportion. To solve this problem, most manufacturers of metal laser printing machines increase the number of scanning systems in combination with an increase in the number of laser radiation sources to 2, 4, 8 and sometimes up to 12 separate systems that scan one working field. On the basis of the analysis of modern 3D printers of world manufacturers, the comparative histogram of the process efficiency was plotted (Figure 1).

The main task in the development of SLM-technology is fabrication of high-quality parts. However, in order to increase the efficiency of the equipment it is necessary to reduce the time spent on fabrication. It

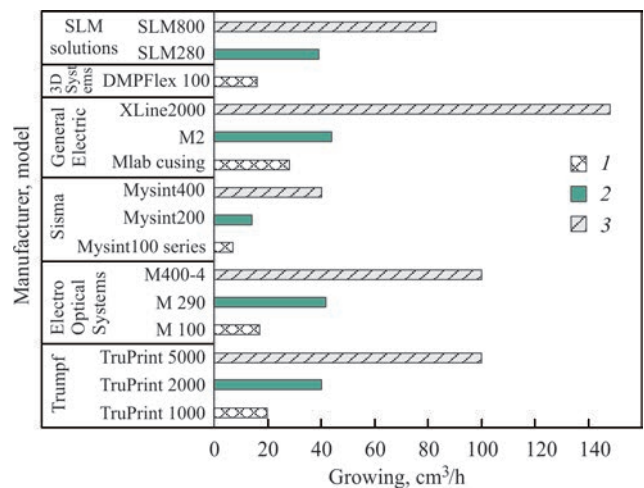


**Figure 1.** Rate of growing parts in the machines of world manufacturers: small machines (1), medium machines (2) and heavy machines (3)

is necessary to find compromise solutions, or to apply fundamentally new approaches to the formation of individual elements of a part.

One of the ways to improve the quality of a part is to reduce the melt pool, as far as the elements of the structure are refined, which leads to improvement in the set of properties, and significantly reduces the surface roughness of a product. However, with a small size of the melt pool, the fabrication time increases, which leads to a decrease in the efficiency of the SLM-process.

A large melt pool allows increasing the efficiency of manufacturing. However, this will increase the surface roughness of a product, and when the power is higher than the optimal, the conditions for evaporation of the substrate or powder may arise, which will lead to the pore formation and an increase in the total porosity of materials [24].

At the same thickness of the working layer, the time required to fill a certain area of a product layer decreases proportionally with an increase in a pool width, for example: at a pool width of 50  $\mu\text{m}$ , taking into account the overlap of tracks by 30 % to fill the area of 0.1  $\times$  0.1 mm, it is necessary to perform 28 scanning passes of the laser beam, and at a track width of 200  $\mu\text{m}$ , under the same conditions it is necessary to perform 7 passes, spending 4 times lower time.

A new solution to the problem is the use of different focal diameters to manufacture individual areas of parts.

The aim of the work is to develop technological approaches to increase the efficiency of the SLM-process while providing a high surface quality of products.

**Material and procedure of studies.** In accordance with modern trends, LLC «Additive laser Technology Ukraine» designed a printing machine ALFA-280 with two scanning systems, each of which can operate at different values of a scanning focal spot. The size of the working chamber of the mentioned

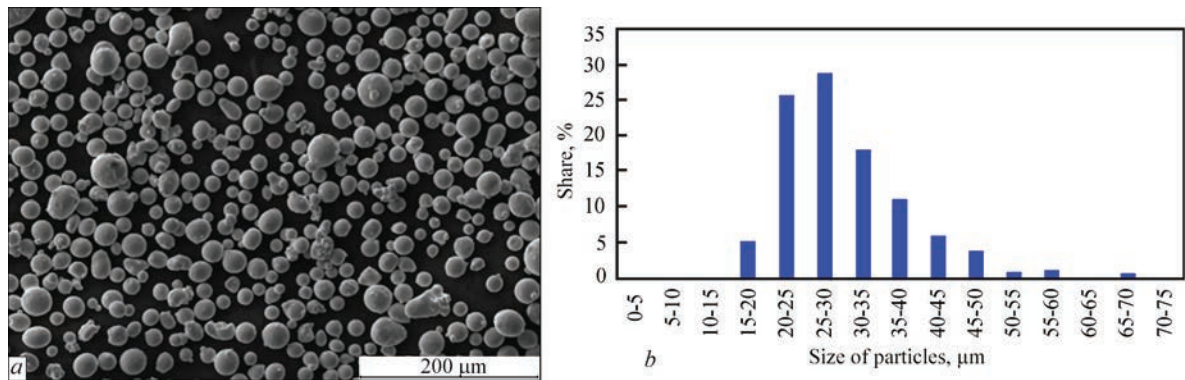


**Figure 2.** Particles of source material 316L ( $\times 200$ ) (a) and results of grain-size analysis (b)

equipment is  $280 \times 280 \times 300$  mm that allows referring it to medium machines.

The studies were performed on samples made of powder material. The samples were printed in the Alfa-280 3D printer produced by «ALT Ukraine» LLC [24]. The material used in this study was stainless steel of the austenitic class 316L with a particle size from 10 to  $45 \mu\text{m}$ . The chemical composition of the powder 316L, wt.% is 17.79 Cr; 12.63 Ni; 2.35 Mo; 0.78 Mn; 0.64 Si; 0.016 C.

The source material was examined using a scanning electron microscope REM-106 (Figure 2, a) to determine the shape and size of the particles. Figure 2, b shows the results of the analysis.

Record of the power distribution along the cross-section of a laser beam with different focal spot diameters was performed in the BeamGage Standard program.

Experimental samples of a cubic shape ( $10 \times 10 \times 10$  mm) were manufactured using different focal spot diameters. During the manufacture of parts the scheme was used shown in Figure 3.

A surface layer (shell) of 1 mm thickness was created using the modes different from those used for the

main body of the sample. The mode of shell scanning is the following: focal spot diameter is  $75 \mu\text{m}$ , scanning rate is 1000 mm/s, power is 200 W, distance between scanning passes is 0.13 mm. To form the area of the main body, different construction modes with different focal spot diameters in the range of 100– $250 \mu\text{m}$  with a step of  $50 \mu\text{m}$  were used. Here, a constant scanning rate of 1000 mm/s, power of 350 W and distance between scanning passes of 0.17 mm were used.

Based on the previous studies of the strategy of construction of the contours of the sample [25], it was found that the order of the beginning of printing the boundaries and the main body does not play a big role in the speed of construction and the quality of manufacturing. Therefore, in this paper, the scheme of construction «main body–boundary of the sample» was chosen.

**Results of studies.** The melt pool of a one track has an arc configuration. This shape is a consequence of the power distribution along the cross-section of the laser beam according to Gauss. The shape and overlap of the melt pools is seen in the microstructure of a product made by SLM [13, 24–26]. Small dendritic and cellular structures with the size of structural elements of a few micrometers are found within each track [24]. For analytical determination of track parameters, the calculation method according to Rosenthal's formula is common [27].

However, this model includes the calculation of local heating only on a single track. In the conditions of the real process an influence of heat from the neighbouring constructed track is present. Based on this, modeling using the finite element method is performed. A number of scientists applied this method for calculation [28, 29]. This model was created for a two-dimensional coordinate system with a transition  $T^{+1}$  (Figure 4) with a fixed values of a focal spot and working layer thickness.

The calculation was performed on the basis of the differential Fourier method, which is based on the replaced functions  $T(x, y)$  of a grid function  $T_{i,k}^j$  where ( $I, K$  is the numbering of nodal two-dimensional grids)

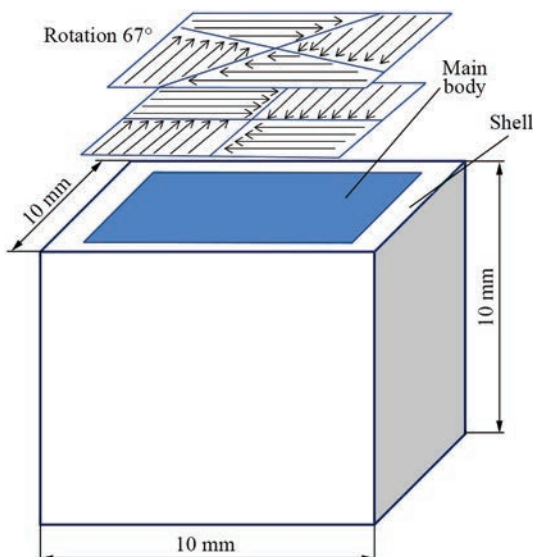


**Figure 3.** Scheme of strategy of construction of studied samples from AISI 316L alloy

under the condition of a uniform grid (step on  $x$  is equal to step on  $y$ ). The temperature distribution in each grid node is determined by the following formula:

$$T_{i,k}^j = \frac{T_{i,k}^{j-1} + T_{i-1,k}^{j-1} + T_{i,k+1}^{j-1} + T_{i,k}^{j-1} - 1}{4}. \quad (1)$$

The temperature field of each moment of time was calculated by means of two templates. The first template displays the starting moment of time. This temperature distribution is described using the boundary conditions of the first kind, i.e. the temperature on the surface of the powder layer is set, which is equal to the ambient temperature. The second template is used to calculate the temperatures at the next moment of time ( $J + 1$ ) based on the formula (1). The results of calculating the temperature distribution for different focal spot diameters of the beam at a constant power of 200 W are shown in Figure 5. It can be seen that at a small diameter of a focal spot, an increase in the power density in the center of the beam leads to heating the powder to a much higher temperature, which can cause a decrease in the metal density of a finished product under the condition of deep penetration. Taken that into account, when reducing the beam diameter, it is necessary to adjust the laser power to provide high quality products.

According to the results of the calculation, it is shown that a decrease in the diameter of a focal

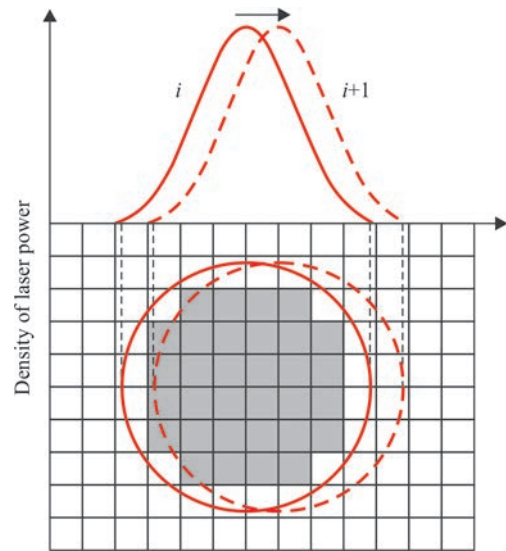
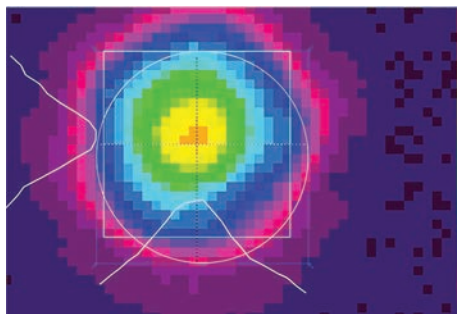


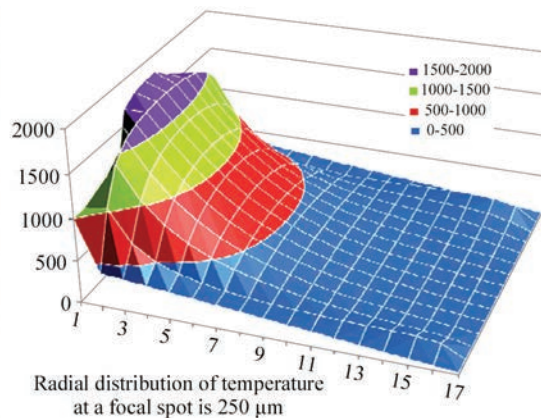
**Figure 4.** Scheme of model of moving heat source (grid diagram) [28]

spot leads to the redistribution of power along the cross-section of the beam, an increase in the energy concentration in the center of a focal spot, and a growth in the gradient. As the diameter of a focal spot (defocus) increases in the central part of the beam, the energy concentration decreases.

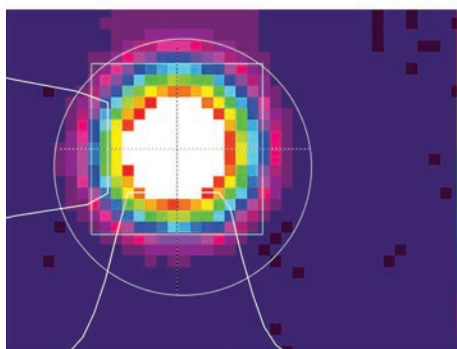
Also from the analysis of calculation results it is seen that during construction of the main body of a part with application of larger diameter of a focal spot, tracks of



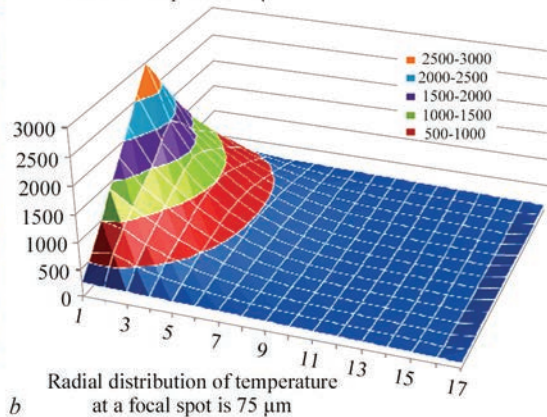
Focal spot diameter of laser beam is 250 μm



Radial distribution of temperature at a focal spot is 250 μm



Focal spot diameter of laser beam is 75 μm



Radial distribution of temperature at a focal spot is 75 μm

**Figure 5.** Power distribution along the cross-section of the laser beam with different focal spot diameters (a), results of calculation of temperature distribution for different focal spot diameters of the laser beam at a constant power of 200 W and a layer thickness of 40 μm (b)

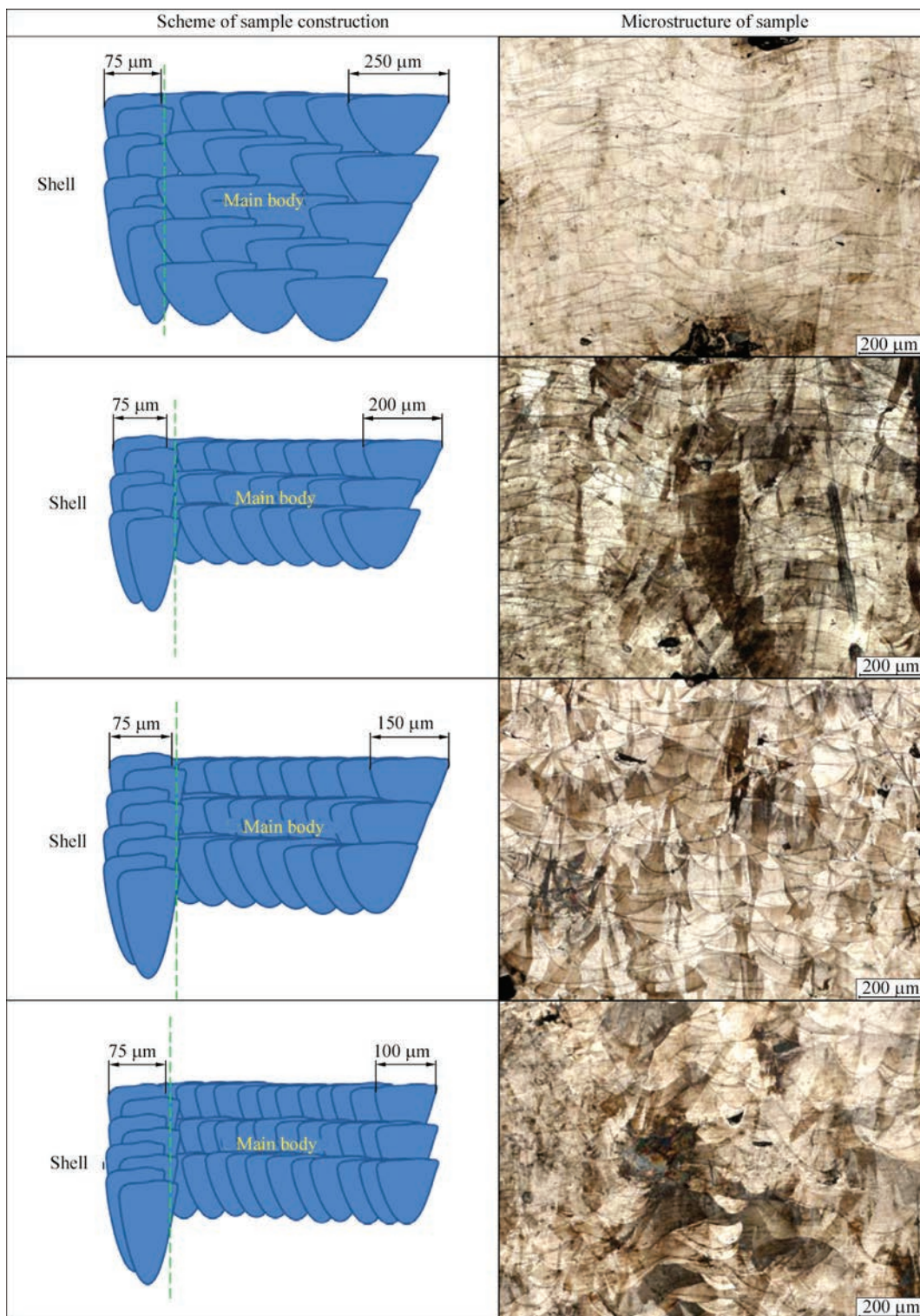


**Figure 6.** Scheme of formation and microstructure of samples manufactured by SLM-technology with different focal spot diameter of the laser beam

larger width will be formed. Therefore, less time can be spent on construction of a product as a whole.

Figure 6 presents the results of metallographic analysis of test samples and a schematic representation of the scheme of construction of the outer layer (shell) and the main body of the sample.

During the metallographic examination of the samples it was found that it is necessary to adjust the

laser power with a change in the focal spot diameter of the laser beam to achieve a high density of metal products manufactured by SLM-technology.

**Conclusions**

1. The analysis of modern equipment for SLM-process realization was performed. It is shown that for medium and heavy machines one of the directions of

increasing efficiency of the process is an increase in a quantity of sources of laser radiation and separate systems scanning one working field.

2. According to the results of the analysis of technological parameters of the process it was established that to increase the efficiency of the SLM process, printing of the main body of a product can be performed with an increased diameter of a focal spot of the laser beam, and to provide a high surface quality, printing of a contour part (shell) should be performed using a more localized focal beam.

3. It is shown that it is necessary to adjust the power of the laser beam when changing the focal spot diameter of the laser beam to achieve a high density of metal products manufactured by SLM-technology.

1. Frazier, W.E. (2014) Metal additive manufacturing: A review. *J. Mater. Eng. and Performance*, **23**(6), 1917–1928.
2. Huang, R. et al. (2016) Energy and emissions saving potential of additive manufacturing: The case of lightweight aircraft components. *J. of Cleaner Production*, **135**, 1559–1570.
3. Ford, S., Despeisse, M. (2016) Additive manufacturing and sustainability: An exploratory study of the advantages and challenges. *J. of Cleaner Production*, **137**, 1573–1587.
4. Conner, B.P., Manogharan, G.P., Martof, A.N. et al. (2014) Making sense of 3-D printing; Creating a map of additive manufacturing products and services, *Additive Manufacturing*, **1–4**, 64–74.
5. Liverani, E. et al. (2017) Effect of selective laser melting (SLM) process parameters on microstructure and mechanical properties of 316L austenitic stainless steel. *J. Mater. Proc. Technology*, **249**, 255–263.
6. Yadroitsev, I. et al. (2013) Energy input effect on morphology and microstructure of selective laser melting single track from metallic powder. *J. Materials Proc. Technology*, **213**(4), 606–613.
7. Yadollahi, A. et al. (2015) Effects of process time interval and heat treatment on the mechanical and microstructural properties of direct laser deposited 316L stainless steel. *Mater. Sci. and Engineering: A*, **644**, 171–183.
8. Kamath, C. (2016) Data mining and statistical inference in selective laser melting. *Int. J. Adv. Manuf. Technol.*, **86**, 1659–1677.
9. Sames, W.J., List, F., Pannala, S. et al. (2016) The metallurgy and processing science of metal additive manufacturing. *Int. Mater. Rev.*, **61**, 315–360.
10. Kempen, K., Thijs, L., Yasa, E. et al. (2011) Process optimization and microstructural analysis for selective laser melting of AlSi10Mg. *Solid Freeform Fabrication Symposium*, **22**, 484–495.
11. Kamath, C., Eldasher, B., Gallegos, G.F. et al. (2014) Density of additively-manufactured, 316L SS parts using laser powder-bed fusion at powers up to 400 W. *Int. J. Adv. Manuf. Technol.*, **74**, 65–78.
12. Amato, K.N., Gaytan, S.M., Murr, L.E. et al. (2012) Microstructures and mechanical behavior of Inconel 718 fabricated by selective laser melting. *Acta Mater.*, **60**, 2229–2239.
13. Adzhamskyi, S.V., Kononenko, A.A., Podolskyi, R.V. (2020) 2D modeling of nonstationary temperature field of simple track of heat-resistant alloy Inconel 718. In: *Proc. of All-Ukrainian Scientific-Methodical Conf. on Problems of Mathematical Modeling*, 1, 42–45 [in Ukrainian]. [https://www.dstu.dp.ua/uni/downloads/material\\_konf\\_traven\\_%202020.pdf](https://www.dstu.dp.ua/uni/downloads/material_konf_traven_%202020.pdf).
14. Khorasani, A., Gibson, I., Kozhuthala, J. Veetil, Ghasemi, A.H. (2020). A review of technological improvements in laser-based powder bed fusion of metal printers. *Int. J. Adv. Manuf Technol.*, **108**, 191–209.
15. SLM Solutions (2019) SLM MACHINES. Last modified March 20, 2019, accessed March 21, 2019. <https://slmsolutions.com/products/machines>
16. Akbari, M., Kovacevic, R. (2019) Closed loop control of melt pool width in robotized laser powder-directed energy deposition process. *Int. J. Adv. Manuf. Technol.*, 1–12.
17. Shrestha, R., Shamsaei, N., Seifi, M., Phan, N. (2019) An investigation into specimen property to part performance relationships for laser beam powder bed fusion additive manufacturing. *Addit. Manuf.*, **29**, 100807.
18. Urhal, P., Weightman, A., Diver, C., Bartolo, P. (2019) Robot assisted additive manufacturing: A review. *Robot Comput. Integr. Manuf.*, **59**, 335–345.
19. SISMA (2019) *LMF «laser metal fusion» technology, last modified March 20, 2019, accessed March 21, 2019*. <https://www.sisma.com/en/additive-manufacturing/>
20. Jafari, R. et al. (2019) Recent progress and challenges with 3D printing of patterned hydrophobic and superhydrophobic surfaces. *Int. J. Adv. Manuf. Technol.*, 1–14.
21. Rausch, A.M., Markl, M., Körner, C. (2019) Predictive simulation of process windows for powder bed fusion additive manufacturing: Influence of the powder size distribution. *Comput. Math. Appl.*, **78**(7), 2351–2359.
22. Renishaw (2019) *Additive manufacturing products, last modified March 20, 2019*. <https://www.renishaw.com/en/additive-manufacturing-products%2D%2D17475>. Accessed March 21, 2019.
23. Yeung, H., Lane, B., Fox, J. (2019) *Part geometry and conduction based laser power control for powder bed fusion additive manufacturing*. *Addit. Manuf.* **30**:100844.
24. Adjamskyi, S.V., Kononenko, G.A., Podolskyi, R.V. (2020) Influence of technological parameters of SLM-process on porosity of metal products. *The Paton Welding J.*, **10**, 13–18. DOI: <https://doi.org/10.37434/as2020.10.03>
25. Adjamskyi, S.V., Kononenko, G.A., Podolskyi, R.V. (2020) Simulation of influence of residual stresses and parameters of SLM technology on formation of boundary areas of heat-resistant alloy Inconel 718 products. In: *Proc. of Sci. and Tech. Conf. on Information Technology in Metallurgy and Machine Engineering (17-19 March 2020, Dnepr)*. Dnepr, 4–6 [in Russian]. DOI: <https://doi.org/10.34185/1991-7848.itmm.2020.01.001>
26. Adjamskyi, S.V., Kononenko, G.A., Podolskyi, R.V. (2020) Investigation of influence of SLM-process modes on quality in contour area of products. In: *Proc. of Int. Conf. on University Science-2020*, **1**, 157–158. [http://eir.pstu.edu/bitstream/handle/123456789/17421/%D0%A3\\_%D0%BA%D0%B0%D1%8F%20%D0%BD%D0%B0%D1%83%D0%BA%D0%B0\\_2020\\_%D0%A2\\_1.pdf](http://eir.pstu.edu/bitstream/handle/123456789/17421/%D0%A3_%D0%BA%D0%B0%D1%8F%20%D0%BD%D0%B0%D1%83%D0%BA%D0%B0_2020_%D0%A2_1.pdf)
27. Rosenthal, D. (1941) Mathematical theory of heat distribution during welding and cutting. *Weld J.*, **20**(5), 220–34.
28. Du, Y., You, X., Qiao, F. et al. (2018) A model for predicting the temperature field during selective laser melting.
29. Promoppatum, P., Shi-Ch Yao, Pistorius, P.C., Rollett, A. (2017) A comprehensive comparison of the analytical and numerical prediction of the thermal history and solidification microstructure of Inconel 718 products made by laser powder-bed fusion. *Engineering*, **3**, 685–694.

Received 14.04.2021

## PULSED-DISCHARGE TREATMENT OF THE Al–Ti–C SYSTEM MODIFIER

**L.M. Lobanov<sup>1</sup>, O.M. Syzonenko<sup>2</sup>, V.V. Holovko<sup>1</sup>, P. Tashev<sup>3</sup>, Ye.V. Lypian<sup>2</sup>, M.S. Prystash<sup>2</sup>,  
A.S. Torpakov<sup>2</sup>, M.O. Pashchin<sup>1</sup>, O.L. Mikhodui<sup>1</sup> and V.O. Shcheretskiy<sup>1</sup>**

<sup>1</sup>E.O. Paton Electric Welding Institute of the NAS of Ukraine

11 Kazymyr Malevych Str., 03150, Kyiv, Ukraine. E-mail: office@paton.kiev.ua

<sup>2</sup>Institute of Pulse Processes and Technologies of the NAS of Ukraine

43-a Bohoyavlenskiy Prosp., 54018, Mykolaiv, Ukraine. E-mail: dioo@iipt.com.ua

<sup>3</sup>Institute of Metal Science, Equipment and Technologies

«Acad. A. Balevsci» with Hydroaerodynamics Centre of the BAS

15474, Sofia, Bulgaria, Shipchenski Prohod Str., 67. E-mail: ptashev@ims.bas.bg

The results of studying the influence of the modifier of the Al–Ti–C system, obtained by high-voltage electric discharge treatment in a hydrocarbon liquid, on the structure and properties of the cast AK7<sup>peh</sup> (A357) alloy are presented. The prospects for the use of a modifier produced by the method of a high-voltage electric discharge treatment of metal powders to improve the structure of cast alloys and weld metal are shown. 25 Ref., 1 Table, 4 Figures.

*Keywords:* welded joint, weld metal, high-voltage electric discharge, modifier of the structure of cast alloys, metallurgy, dispersion, carbidization

The introduction of modifiers into the melt is one of the traditional methods of producing fine-grained metal structures, as far as the more nuclei are in the unit volume of a melt, the more crystals are formed and the smaller they are, and therefore, the better mechanical properties of the metal in foundry and welding. Modern tasks of materials science and engineering practice are the study of the efficiency of nanomodification in welding and surfacing technologies by introducing nanoparticles of refractory chemical compounds into the welding pool [1]. During surfacing with heat-resistant alloys based on iron, nickel and chromium and carbon steels, which are modified by nanoparticles, the stability of the deposited tool is increased. Nanoparticles also eliminate transcristallization zones in the deposited metal or a weld, the sizes of dendrites are sharply reduced, the morphology and topography of the strengthening phases is improved. This increases the heat resistance, structural stability and life of welded joints [2, 3]. The efficiency of modification of cast metal with nanostructured powders is confirmed, for example, in the conditions of production of gas turbines at modification of heat-resistant SM88U alloy [4]. Taking into account the peculiarities of foundry production and fusion welding in

terms of modification of liquid metal, the conceptual approaches to the creation of modifiers for the mentioned technologies are quite close. Thus, the positive results of using liquid metal modifiers in the process of casting are the basis for creation of technologies for modifying the liquid metal of the welding pool under fusion welding conditions. Based on the abovementioned, in the future the modern method of manufacturing modifiers for foundry production can also be used in welding production.

Most modifiers are manufactured by powder metallurgy. Moreover, ultradisersion nanostructured powder mixtures are the most promising for use. Now the main directions of development of methods of obtaining such mixtures are as follows [5–8]:

improvement of existing equipment and technological processes based on widespread mechanical methods of grinding materials; search for fundamentally new ways of grinding, research and development of effective types of equipment and technology on their basis.

The first direction is aimed at increasing the efficiency of destruction and specific efficiency and improving the existing and creating the new machines (crushers and mills) of increased efficiency [7, 8] and is accom-

L.M. Lobanov — <https://orcid.org/0000-0001-9296-2335>, O.M. Syzonenko — <https://orcid.org/0000-0002-8449-2481>,  
P. Tashev — <https://orcid.org/0000-0002-7906-487X>, Ye.V. Lypian — <https://orcid.org/0000-0001-9483-1793>,  
M.S. Prystash — <https://orcid.org/0000-0002-7617-6200>, A.S. Torpakov — <https://orcid.org/0000-0002-9805-3914>,  
M.O. Pashchin — <https://orcid.org/0000-0002-2201-5137>, O.L. Mikhodui — <https://orcid.org/0000-0001-6660-7540>,  
V.O. Shcheretskiy — <https://orcid.org/0000-0002-8561-4444>

© L.M. Lobanov, O.M. Syzonenko, V.V. Holovko, P. Tashev, Ye.V. Lypian, M.S. Prystash, A.S. Torpakov, M.O. Pashchin, O.L. Mikhodui and V.O. Shcheretskiy, 2021

panied by an increased power consumption, metal consumption of structures, using of expensive high quality steels and alloys along with a disproportionately small growth in technical and economic indices.

The second direction is aimed at finding fundamentally new methods of grinding, in particular, electrophysical [9–11]. Thus, one of the efficient electrophysical methods is a pulsed discharge preparation of powders by using high-voltage electric discharge (HED) in the disperse system «liquid–powder». This is a cyclic process, which is characterized by the release of power in the discharge channel during microseconds and is accompanied by the action of compression waves (which under the certain conditions is transformed into a shock one), powerful hydraulic flows, cavitation, electromagnetic and thermal fields [9–11].

At the cyclic action of HED the possibility of fine grinding by pressure waves is created due to the presence of a large number of defects in the powder, which reduces the power of destruction of crystals and the formation of a large number of active centers and facilitates the chemical interaction between the system elements under a dynamic load.

The use of a hydrocarbon liquid as a working medium in HED-treatment of mixtures of powders allows not only eliminating their oxidation, but also creating thermodynamic conditions for pyrolysis of kerosene with the formation of solid carbon, which is able to enter the carbidization reaction with powder particles, forming nanostructured strengthening phases [12].

In [13], an example of using a modifier in casting showed that the introduction of 0.01 wt.% of the Ti–TiC modifier, synthesized by a high-voltage electrodischarge treatment of Ti powder in kerosene and briquetted by spark plasma sintering, allowed reducing the grain size from 1–2 to 0.2–0.6 mm in all modified specimens of heat-resistant SM88U alloy. In this case, the tensile strength at a temperature of 900 °C was 65–69 MPa, and the long-term strength increased by an average of 20 %. This indicates the prospects of using metal powders after HED-treatment to modify the structure of cast alloys.

However, the possibility of using metal powders after HED-treatment to modify the cast metal structure of welds has not yet been sufficiently studied. To establish the prospects of using metal powders after HED-treatment to modify the structure of welds, it is advisable to analyze the effect of a modifier of the Ti–Al–C system after HED-synthesis to grind the structure and improve the properties of cast AK7<sub>pch</sub> (A357) alloy.

The aim of the work consists in the fact that to establish the prospects of application of metal powders after HED-treatment in fusion welding to modify the structure of welds, it is advisable to investigate the

effect of a modifier of Ti–Al–C system after HED to grind the structure and improve the properties of cast AK7<sub>pch</sub> (A357) alloy.

**Procedure of studies.** Modification of aluminium alloys was considered on the example of silumins and involved the obtainment of a fine-grained eutectic silicon in a cast structure. Such a structure of eutectic silicon increases the mechanical properties of the casting, including relative elongation, as well as, in many cases, casting properties of the aluminium melt. As a rule, modification of silumin is carried out by adding small amounts of sodium or strontium [14–17].

In silumins with a silicon content of more than 7 %, eutectic silicon occupies most of the area of the metallographic specimen. With a silicon content from 7 to 13 %, the type of eutectic structure (e.g., granular or modified) significantly affects the mechanical properties of the material, in particular, ductility, which is defined as a relative elongation  $\delta$ . Therefore, when during the tests of the specimen it is necessary to increase the value  $\delta$ , aluminium alloys with a silicon content from 7 to 13 % are modified by adding approximately 0.0040–0.0100 % of sodium [18, 19].

In silumins with a silicon content of about 11 %, especially for low pressure casting, as a long-term modifier, strontium is used. The difference between strontium and sodium as a modifier consists in the fact that it burns out much less from the melt, which is especially important in fusion welding. Strontium is added in an amount of 0.014–0.040 %.

Since sodium burns out from the melt relatively quickly, further modification of silumins with sodium should be carried out at certain intervals, which complicates its use in welding, where the process of introducing a modifier should be continuous. In addition, high cost and complexity of the technology of applying sodium and strontium creates the need in finding cheaper and no less effective weld modifiers on the basis of those studied in the works [20–22].

To study the effect of modifier on crystallization of the cast aluminium AK7<sub>pch</sub> (A357) alloy, a modifier obtained by HED treatment of a mixture of powders of 15 % Al + 85 % Ti with an average diameter  $d_{av} = 40 \mu\text{m}$  in illuminating kerosene was used. The study was performed in an experimental bench, described in detail in [9, 10, 23].

To evaluate the degree of influence of HED in kerosene on the morphology and size of powder particles, as well as to study the structure of cast alloy specimens, the following equipment was used: BIOLAM-I optical microscope with the maximum magnification  $\times 1350$ , JEOL JEM-2100F scanning electron microscope with a magnification range from 50 to 1500000 and Canon digital camera.



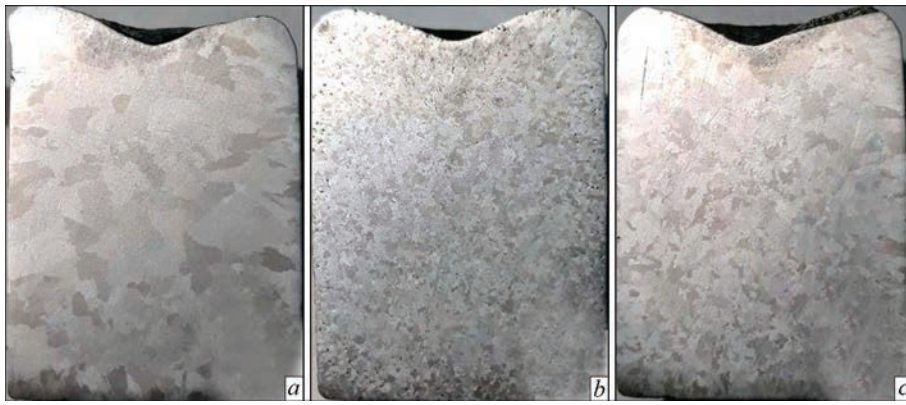


**Figure 3.** Macrostructure of AK7<sub>pch</sub> (A357) alloy: *a* — reference specimen; *b* — specimen modified by 0.7 wt.% of AlTiB; *c* — specimen modified by 0.2 wt.% of the Ti–Al–C mixture produced by HED-treatment

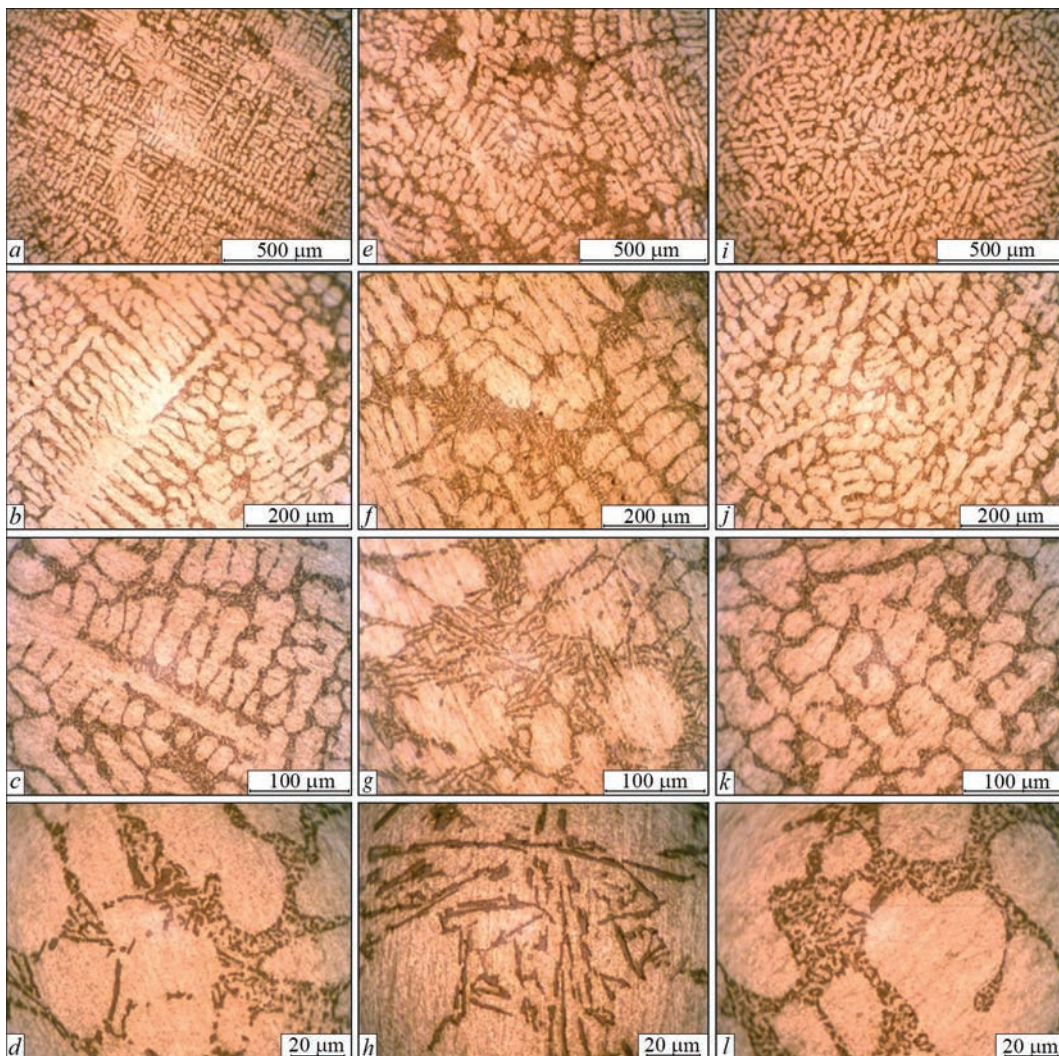
from 1.5 to 2.0 mm, the structure is uniform, grains have a size of 1.5–3.5 mm.

Figure 4 shows the microstructure of reference (*a, b, c, d*), modified 0.7 wt.% of AlTiB (*e, f, g, h*) and modified 0.2 wt.% HED-treated mixture (*i, j, k, l*) of AK7<sub>pch</sub> alloy.

Metallographic analysis of the reference specimen revealed dendrites of  $\alpha$ -solid solution, the size of

which exceeds 1500  $\mu\text{m}$  and a significant amount of eutectic silicon, which has a rounded shape.

Melt modification of 0.2 wt.% of AlTiB leads to insignificant dispersion of dendrites of  $\alpha$ -solid solution, but at the same time the growth of separate  $\alpha$  grains is observed. This modifier had a negative effect on eutectic silicon, which received a needle shape with the size of individual needles of up to 80  $\mu\text{m}$ ,



**Figure 4.** Microstructures of AK7<sub>pch</sub> alloy: *a, b, c, d* — reference specimen; *e, f, g, h* — specimen modified by 0.7 wt.% of AlTiB; *i, j, k, l* — specimen modified by 0.2 wt.% of the Ti–Al–C mixture produced by HED-treatment

Specimen	$\sigma_r$ , MPa	$\sigma_{0.2}$ , MPa	HB
Reference specimen	148	62	48
	143	65	
Specimen modified by 0.7 wt.% of AlTiB	133	62	36
	131	61	
Specimen modified by 0.2 wt.% of mixture of Al–Ti–C-system after HED-treatment	135	66	48
	140	65	

which negatively affects the fatigue strength of the modified metal.

Modification of the specimen of alloy 0.2 wt.% by HED-treated mixture of powders 15 % Al + 85 % Ti led to a significant reduction in the size of the dendrites of  $\alpha$ -solid solution from 1500 to 300  $\mu\text{m}$ , the grains obtained a round shape, also a significant modification of eutectic silicon (Figure 5, *i, j, k, l*) is observed. The obtained grain shape has a positive effect on the fatigue strength of the metal modified by HED-treated mixture. Such results are associated with the presence of carbon nanoparticles and nanostructured particles of refractory TiC, Ti<sub>3</sub>AlC + Ti<sub>2</sub>AlC compounds in the powder mixture, which act as additional crystallization centers.

The hardness of the reference specimen was HB 48, and for those modified by AlTiB and HED-treated mixture, it was HB 36 and HB 48, respectively (Table).

Studies of the change in the ultimate strength  $\sigma_t$  and yield strength  $\sigma_{0.2}$  of modified specimens (see Table) show that in contrast to the modification of 0.7 wt.% of AlTiB, adding 0.2 wt.% of the mixture of Al–Ti–C system after HED-treatment does not lead to a decrease in these characteristics as compared to the reference specimen.

The obtained results in combination with the results presented in [13] indicate that the use of HED-treated powders of the Al–Ti–C system in a hydrocarbon liquid as a modifier leads to a significant reduction in the structural elements of a crystallized alloy. In turn, the refinement of the structure of welds allows increasing heat resistance, structural stability and fatigue strength and long life of welded joints. This allows predicting the possibility of using HED-treated particles of metal powders metal in a hydrocarbon liquid to modify the structure of welds with the purpose of improving the service characteristics of parts and structures produced by different methods of fusion welding.

## Conclusions

1. The possibility of using HED-treated particles of metal powders in a hydrocarbon liquid to modify the structure of welds is shown.

2. It is shown that introduction of the mixture of powders of the initial composition 15 % Al + 85 % Ti ob-

tained by HED-treatment in kerosene as a modifier by the «bell» method allows influencing the structure and properties of the cast aluminium AK7<sub>pch</sub> alloy (A357).

3. Adding of 0.2 wt.% HED-treated mixture of powders 15 % Al + 85 % Ti to AK7<sub>pch</sub> (A357) alloy led to a significant change in the size of the dendrites of the  $\alpha$ -solid solution from 1500 to 300  $\mu\text{m}$ . The hardness of the modified specimens is HB 48, and the yield strength is at the level of 66 MPa.

1. Tashev, P., Aleksiev, N., Manolov, V., Cherepanov, A.N. (2017) Nanomodification in welding and surfacing processes. *Kosmicheskie Apparaty i Tekhnologii*, 19(1), 16–21 [in Russian].
2. Eremin, E.N., Shalai, V.V., Filippov, Yu.O., Sumleninov, V.K. (2012) Use of modification in electroslag welding of heat-resistant alloys. *Vysoki Tekhnologii v Mashynobuduvanni*, 22(1), 115–120 [in Russian].
3. Eremin, E.N., Filippov, Yu.O., Rummyantsev, G.P. (2011) Structural changes in high-temperature nickel alloys at its modification by refractory joint nanoparticles. *Ibid.*, 21(1), 98–104 [in Russian].
4. Syzonenko, O.M., Prokhorenko, S.V., Lypyan, E.V. (2020) Pulsed discharge preparation of a modifier of Ti–TiC system and its influence on the structure and properties of the metal. *Materials Sci.*, 56(2), 232–239. ISSN 1068-820X (Print), 1573-885X (Electronic). DOI: <https://doi.org/10.1007/s11003-020-00421-1>.
5. Syzonenko, O.M., Prystash, M.S., Zaichenko, A.D. et al. (2020) *Application of high-concentrated energy flows in powder metallurgy for producing carbide-steels*. Kiev, Naukova Dumka [in Russian]. ISBN 978-966-00-1756-6.
6. Sizonenko, O.N., Ivliev, A.I., Baglyuk, G.A. (2014) *Advanced processes of manufacture of powder materials*. Nikolaev, NUK [in Russian]. ISBN 978–966–321-292-0.
7. Savyak, M.P., Melnik, O.B., Uvarova, I.V. (2016) Crystallographic features of formation of nanodisperse titanium carbide during grinding of titanium and carbide in planetary milling. *Poroshk. Metallurgiya*, 5–6, 3–12 [in Ukrainian].
8. Hong, S.-M., Park, J.-J., Park, E.-K. et al. (2015) Fabrication of titanium carbide nano-powders by a very high speed planetary ball milling with a help of process control agents. *Powder Technology*, 274, 393–401. DOI: <https://doi.org/10.1016/j.powtec.2015.01.047>.
9. Sizonenko, O., Vovchenko, A. (2014) Pulsed discharge technologies of processing and obtaining of new materials (Kiev). *Int. Virtual J. for Science, Technics and Innovations for the Industry*, 12, 41–44.
10. Sizonenko, O.N., Baglyuk, G.A., Raichenko, A.I. (2012) Variation in the particle size of Fe–Ti–B<sub>4</sub>C powders induced by high-voltage electrical discharge. *Powder Metallurgy and Metal Ceramics*, 51(3–4), 129–136. DOI: <https://doi.org/10.1007/s11106-012-9407-4>.

11. Sizonenko, O.N., Baglyuk, G.A., Raichenko, A.I. (2011) Effect of high-voltage discharge on the particle size of hard alloy powders. *Ibid.*, 49(11–12), 630–636. DOI: <https://doi.org/10.1007/s11106-011-9280-6>.
12. Lipyay, E.V., Sizonenko, O.N., Torpakov, A.S., Zhdanov, A.A. (2015) Thermodynamic analysis of heterogeneous chemical reactions in system «powder mixture Fe–Ti-hydrocarbon liquid» under action of high-voltage electric discharges. *Visnyk NTU KhPI. Series: Tekhnika ta Elektrofizyka Vysokykh Naprug*, 51(1160) 59–65 [in Russian]. ISSN 2079-0740.
13. Syzonenko, O.M., Prokhorenko, S.V., Lypyan, E.V. et al. (2020) Pulsed discharge preparation of a modifier of Ti–TiC system and its influence on the structure and properties of the metal. *Materials Sci.*, 56(2), 232–239. ISSN 1068-820X (Print), 1573-885X (Electronic). DOI: <https://doi.org/10.1007/s11003-020-00421-1>.
14. Stroganov, G.B., Rotenberg, V.A., Gershman, G.B. (1977) *Alloys of aluminium with silicon*. Moscow, Metallurgiya [in Russian].
15. Crubes, U.G. (1983) Veredelung von Aluminium gublegierung mit Al–Sr 3,5-Vorlegierung in Drahtform. *Giesserei*, 70(8), 257–258.
16. Abramov, A.A. (2012) About modification of silumins. *Litejnoe Proizvodstvo*, 7, 19 [in Russian].
17. Korolyov, S.P., Nemenenok, B.M., Mikhajlovsky, V.M. et al. (2005) Problems and practice of modification of hypereutectic silumins for piston alloy. *Litejshchik Rossii*, 10, 19–22 [in Russian].
18. Stetsenko, V.Yu. (2008) On modification of hypoeutectic and eutectic silumins. *Litio i Metallurgiya*, 1, 149–150 [in Russian].
19. Xu, C.L., Jiang, Q.C., Yang, Y.F. et al. (2006) Effect of Nd on primary silicon and eutectic silicon in hypereutectic Al–Si alloy. *J. of Alloys and Compounds*, 422(1–2), 1–4.
20. Xu, C.L., Wang, H.Y., Yang, Y.F. (2006) Effect of La<sub>2</sub>O<sub>3</sub> in the Al–P–Ti–TiCl<sub>2</sub>O<sub>3</sub> modifier on primary silicon in hypereutectic Al–Si alloy. *Ibid.*, 421(1), 128–132.
21. Stetsenko, V.Yu. (2008) On mechanism of modification of silumins. *Metallurgiya Mashinostroeniya*, 1, 20–23 [in Russian].
22. Popova, M.V., Ruzhilo, A.A. (2000) Hereditary effect of batch and melt processing on thermal expansion of hypereutectic silumins. *Litejnoe Proizvodstvo*, 10, 4–6 [in Russian].
23. Sizonenko, O., Prokhorenko, S., Torpakov, A. et al. (2018) The metal-matrix composites reinforced by the fullerenes. *AIP Advances*. 085317. ISSN 2158-3226. DOI: <https://doi.org/10.1063/1.5031195>.
24. Sizonenko, O.N., Grigoryev, E.G., Zaichenko, A.D. (2017) Plasma methods of obtainment of multifunctional composite materials, dispersion-hardened by nanoparticles. *High Temperature Materials and Processes*, 36(9), 891–896. ISSN 0334-6455. DOI: <https://doi.org/10.1515/htmp-2016-0049>.
25. Bethune, D.S., Meijer, G., Tang, W.C., Rosen, H.J. (1990) The vibrational Raman spectra of purified solid films of C<sub>60</sub> and C<sub>70</sub>. *Chem. Phys. Lett.*, 174, 219–222. DOI: [https://doi.org/10.1016/0009-2614\(90\)85335-A](https://doi.org/10.1016/0009-2614(90)85335-A).

Received 08.04.2021

## XX INTERNATIONAL INDUSTRIAL FORUM - 2021

INTERNATIONAL TRADE FAIRS

# November 16-19

METAL WORKING

WELDING

HYDRAULICS PNEUMATICS

BEARINGS

UKROSER

UKRFOUNDRY

UKRSPORN AUTOMATIZATION

PATTERNS, STANDARDS AND INSTRUMENTS

HOISTING AND TRANSPORTING STOREHOUSE EQUIPMENT

INDUSTRIAL SAFETY

**ORGANIZER:**  
International Exhibition Centre

General Information Partner:

Exclusive Media Partner:

Technical Partner:

International Exhibition Centre  
15 Brovarskyi Ave., Kyiv, Ukraine  
“Livoberezhna” underground station  
☎ +38 044 201 11 65, 201 11 56, 201 11 58  
e-mail: alexk@iec-expo.com.ua  
[www.iec-expo.com.ua](http://www.iec-expo.com.ua)  
[www.tech-expo.com.ua](http://www.tech-expo.com.ua)

# ARGON-ARC WELDING OF HIGH-STRENGTH SPARSELY-DOPED PSEUDO- $\beta$ -TITANIUM ALLOY Ti-2.8Al-5.1Mo-4.9Fe

**S.V. Akhonin, V.Yu. Bilous, R.V. Selin, I.K. Petrychenko and L.M. Radchenko**

E.O. Paton Electric Welding Institute of the NAS of Ukraine

11 Kazymyr Malevych Str., 03150, Kyiv, Ukraine. E-mail: [office@paton.kiev.ua](mailto:office@paton.kiev.ua)

Structural sparsely-doped titanium alloys are developed with the purpose of lowering the finished product cost. Possibility of application of tungsten electrode argon-arc welding (AAW) for sparsely-doped pseudo- $\beta$ -titanium alloy Ti-2.8Al-5.1Mo-4.9Fe was evaluated. Influence of different kinds of argon-arc welding on weld formation and mechanical properties of Ti-2.8Al-5.1Mo-4.9Fe alloy joints were assessed. The effect of through penetration AAW, semi-submerged AAW, AAW with feeding unalloyed titanium welding filler wire VT1-00sv was studied. It was found that the structure of metal of the weld and HAZ in welded joints of sparsely-doped titanium alloy Ti-2.8Al-5.1Mo-4.9Fe made by AAW consists mainly of  $\beta$ -phase with precipitates of metastable  $\alpha$ -phase. Lowering of AAW heat input for Ti-2.8Al-5.1Mo-4.9Fe alloy has a positive impact on the joint strength. So, among the welded joints made without changing the weld metal composition, the joints produced by semi-submerged arc welding have the highest strength of 972 MPa and the highest impact toughness on the level of 5.7 J/cm<sup>2</sup>. 15 Ref., 3 Tables, 3 Figures.

*Keywords:* titanium, titanium alloys, argon-arc welding, heat input, flux, wire, mechanical properties

Tungsten-electrode argon-arc welding (AAW) became the most widely accepted for welding titanium alloys owing to the fact that this welding process is the least expensive and the most versatile [1, 2]. It allows making joints in different positions in space, under the conditions of limited space, and does not require complex readjustment of the equipment at the change of welded product thickness or joint type. Welding can be performed both with application of filler metal, and without it. Used as filler metal are welding wires or rods from titanium alloys [3]. There is a number of variants of this method: welding with through penetration, and semi-submerged arc welding, which expand its technological capabilities [4]. In order to lower the cost of the production process and the cost of titanium alloy products, the concept of «sparse doping» of titanium alloys became widely accepted. It is based on selection of such alloying elements for the alloys which would have relatively low cost. Iron is the most widely spread alloying element for such alloys [5, 6]. Iron, owing to its stabilizing impact on  $\beta$ -phase, is also used for alloying several low-cost alloys, based on  $\beta$ -phase [7–9]. Welding such alloys based on  $\beta$ -phase is a little studied process. A large quantity of iron can cause considerable deterioration of welded joint properties due to brittle phase formation [10]. The currently available fluxes can have a refining effect in welding of sparsely-doped alloys

[11]. Therefore, the possibility of applying fluxes for welding these alloys should be considered separately. In addition, in view of the absence of welding wires from sparsely-doped titanium alloys, it is rational to consider the impact of low-alloyed titanium wire on the properties of joints of such an alloy [12, 13].

The objective of the work was studying the impact of argon-arc welding modes on weld formation and mechanical properties of the produced joints of sparsely-doped pseudo- $\beta$ -titanium alloy Ti-2.8Al-5.1Mo-4.9Fe.

Unalloyed titanium welding wire VT1-00sv of 2 mm diameter was used as the filler metal. It allows changing the degree of weld metal alloying within narrow limits. The relative quantity of filler metal in the weld metal was determined by calculation of the area of joint metal penetration on transverse weld sections.

Samples of titanium pseudo- $\beta$ -alloy Ti-2.8Al-5.1Mo-4.9Fe of 200×100×6 mm were welded. Welding was performed from one side. Modes of through penetration tungsten electrode argon-arc welding from one side of sparsely-doped titanium pseudo- $\beta$ -alloy Ti-2.8Al-5.1Mo-4.9Fe are given in Table 1.

Welding modes were selected under the condition of providing through penetration of joints of 6 mm Ti-2.8Al-5.1Mo-4.9Fe alloy. Tungsten electrode argon-arc welding can be performed in wide ranges of welding speed and welding current values. The most

**Table 1.** Modes of through penetration AAW from one side of sparsely-doped titanium pseudo-  $\beta$ -alloy Ti-2.8Al-5.1Mo-4.9Fe

Mode number	Welding current, $I_w$ , A	Arc voltage $U_a$ , V	Welding speed $v_w$ , m/h	Wire feed rate $v_{f.w}$	Preset arc length $L_a$ , mm	Preheating temperature, $T_{preh}$ , °C
1	330	12	10	–	2	–
2	350	12	10	30	2	–
3	350	12	10	60	2	–
4	310	12	10	–	2	400
5 (over a layer of flux)	240	12	16	–	2	–

widely used range of speeds of automatic AAW for titanium alloys is 10–20 m/h range. Full penetration of 6 mm samples occurs at through penetration AAW without filler at welding current of 330 A and welding speed of 10 m/h. Addition of filler wire leads to increase of welding current. Welding with preheating allows somewhat lowering the welding current to 310 A. Semi-submerged AAW due to argon arc constriction enables an essential lowering of welding current to 240 A, increasing the welding speed and providing full penetration of Ti-2.8Al-5.1Mo-4.9Fe alloy metal 6 mm thick. Thus, semi-submerged AAW allows welding titanium pseudo- $\beta$ -alloy Ti-2.8Al-5.1Mo-4.9Fe in modes with minimum heat input and cross-sectional area of the metal of weld and HAZ (Table 2).

Transverse macrosections of the produced welds are given in Figure 1. An example of through penetration tungsten electrode welding (Figure 2) confirms formation of a through hole under the tungsten electrode at through penetration welding. When welding current is switched off, a hole forms under the tungsten electrode, if the crater welding up mode is not used.

Calculation of filler metal quantity in the weld metal was performed by the results of studying the prepared transverse macrosections. It was found that at 60 m/h feed rate of 2 mm VT1-00sv filler wire and 8 m/h welding speed the quantity of VT1-00 fill-

er metal in the weld metal is 21–25 %. Accordingly, at 30 m/h feed rate of the filler wire, the quantity of VT1-00 filler metal in the weld metal is 10–13 %.

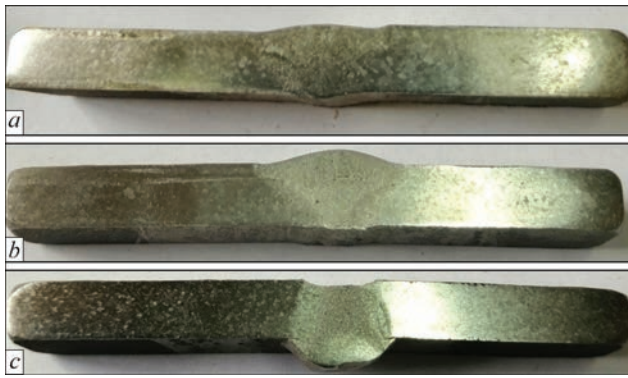
The base metal of welded joint of sparsely-doped titanium pseudo  $\beta$ -alloy Ti-2.8Al-5.1Mo-4.9Fe consists of recrystallized grains (Figure 3, a), equiaxed polyhedral  $\beta$ -grains, both in the near-surface layers, and inside the metal. The size of  $\beta$ -grains is equal to 200–600  $\mu$ m. Located inside  $\beta$ -grains are dispersed particles of  $\alpha$ -phase. Dispersed particles of different shape and dimensions precipitate in base metal microstructure, both in the surface areas, and those remote from the surface. Precipitate dimensions vary within a broad range (from less than 1  $\mu$ m up to 15  $\mu$ m), and are nonuniformly distributed in the grain body.

Figure 3, b–f shows the weld metal microstructure. The weld structure is dendritic (modes No.1 and No.2, see Table 1). Particles of another precipitating phase are smaller than those in the base metal, and their dimensions are from less than 1 to 3–4  $\mu$ m (Figure 3, b, c). In the weld of a joint made by AAW with filler wire feeding at the rate of 60 m/h that ensures 21–25 %, unlike the above-considered cases, the weld microstructure also changed, as a result of considerable change of the weld metal chemical composition and its dilution. In the weld metal of this joint, the instability of  $\beta$ -solid solution leads to a significant

**Table 2.** Parameters of welds in AAW joints of sparsely-doped titanium alloy Ti-2.8Al-5.1Mo-4.9Fe made by AAW\*

Mode number	Sample type, $I_w$ , $v_w$ , $v_{f.w}$	Weld width, mm	HAZ width, mm	Weld area, mm <sup>2</sup>	Heat input, J/cm	Quantity of $\beta$ -phase, %
BM	Base metal	–	–	–	–	76
1	Welded joint without filler, $I_w = 330$ A, $v_w = 10$ m/h	13	21	53	14256	77
2	Welded joint with filler, $I_w = 350$ A, $v_w = 10$ m/h, $v_{f.w} = 30$ m/h	15.1	24.1	59.8	15120	75
3	Welded joint with filler, $I_w = 350$ A, $v_w = 10$ m/h, $v_{f.w} = 60$ m/h	16.5	25.5	73.1	1511.9	56
4	Welded joint with preheating to 400 °C, $I_w = 310$ A, $v_w = 10$ m/h	17	25	65.0	13392	75
5	Welded joint produced by semi-submerged-arc welding $I_w = 240$ A, $v_w = 16$ m/h	7.2	17.2	33.9	6480	63

\*Joint thickness is 6 mm.



**Figure 1.** Transverse macrosection of the joint of sparsely-doped titanium pseudo- $\beta$ -alloy Ti-2.8Al-5.1Mo-4.9Fe made by AAW: *a* — through penetration without filler wire application; *b* — with filler metal addition to the weld in the quantity of 10 %; *c* — made by semi-submerged AAW without filler wire

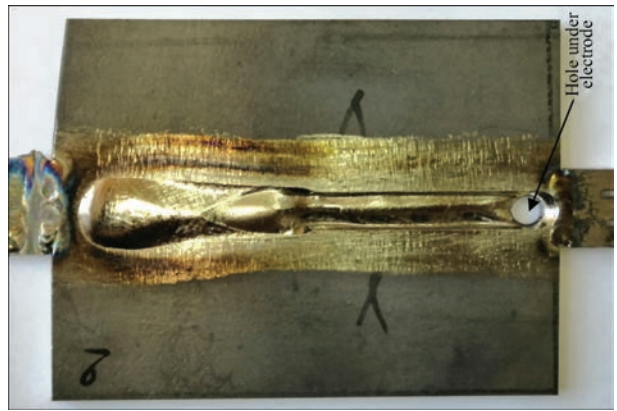


**Figure 2.** Example of welded joint of a sparsely-doped pseudo- $\beta$ -alloy Ti-2.8Al-5.1Mo-4.9Fe, made by through penetration AAW without filler wire, mode No.1

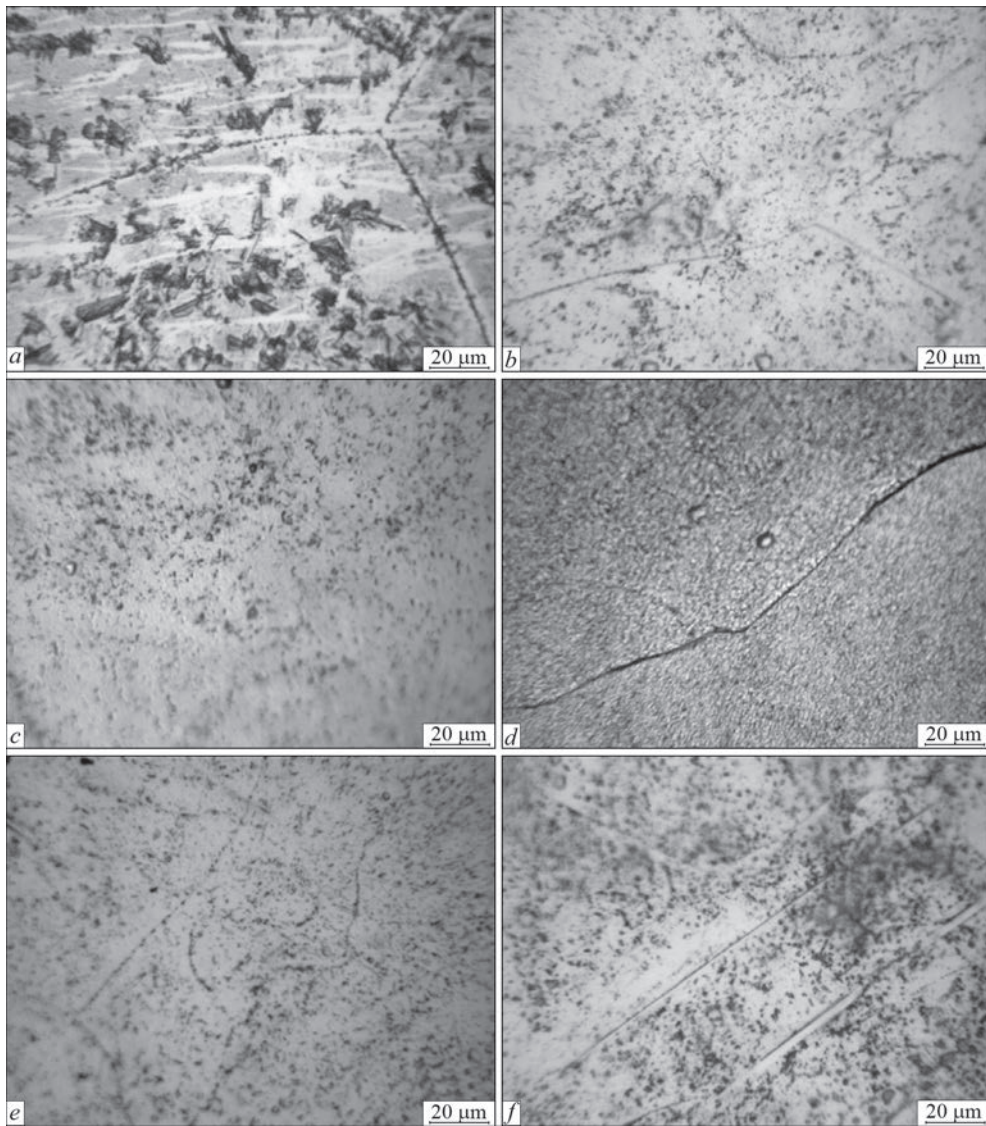


**Figure 3.** Microstructure of base metal and weld metal of joints of sparsely-doped titanium alloy Ti-2.8Al-5.1Mo-4.9Fe, made by AAW in as-welded condition: *a* — base metal; *b* — through penetration without filler wire, mode No.1; *c* — through-penetration with filler wire, mode No.2; *d* — through penetration with filler wire, mode No.3; *e* — through penetration without filler wire with preheating, mode No.4; *f* — semi-submerged arc welding without filler wire, mode No.5

**Table 3.** Mechanical properties of base metal and joints of sparsely-doped titanium alloy Ti–2.8Al–5.1Mo–4.9Fe, made by AAW in as-welded condition

Mode number	Sample type	Tensile strength $\sigma_t$ , MPa	Yield limit $\sigma_y$ , MPa	Relative elongation $\delta$ , %	Reduction in area $\psi$ , %	Impact toughness, KCV, J/cm <sup>2</sup>
BM	Base metal	1071	971	2.0	–	5.3
1	Joint	921	–	–	–	4.9
2	Same	1002(968)	936	10	27	5.5
3	–	960	–	–	–	3.5
4	–	799	–	–	–	4.3
5	–	972	925	8.0	23	5.7

decomposition at weld metal cooling after welding with precipitation of a considerable quantity of  $\alpha$ -phase (Figure 3, *d*). The welds of the joints made by through-penetration AAW method without feeding the filler wire (mode No.4, see Table 1) with joint preheating to 400 °C temperature and over a layer of flux (mode No.5, see Table 1) are based on  $\beta$ -phase, similar to welding in modes No.1 and No.2 (Figure 3, *e, f*).

Thus, in the structure of the metal of welds the most finely-dispersed precipitates of metastable  $\alpha$ -phase of up to 1–2  $\mu\text{m}$  size, are found in joints made by semi-submerged arc welding. Joints made by AAW with preheating, alongside large dimensions of welds and HAZ in as-welded state demonstrate nonuniform precipitation of fine particles of metastable  $\alpha$ -phase: finer in the weld upper part than in the lower one. It may point to a too high temperature of the applied preheating which in this case was 400 °C [14]. On the whole, application of preheating for AAW of joints of sparsely-doped titanium alloy Ti–2.8Al–5.1Mo–4.9Fe is undesirable.

The smallest quantity of  $\beta$ -phase was registered in welds, made by AAW with feeding VT1-00 filler wire at the rate of 60 m/h that ensures 21–25 % content of filler wire in the weld, and is equal to 56 % (Table 2) which is attributable to lowering of the degree of weld metal alloying. In welds, made by semi-submerged AAW the quantity of  $\beta$ -phase also decreased to 63 %. Note that at semi-submerged AAW the joints made with the lowest heat input values (see Table 2), have the smallest width of the weld and HAZ, and the weld area. In other welds made without any change of weld alloying, the quantity of  $\beta$ -phase in as-welded condition is equal to 75–77 %.

Establishing the mechanical properties of welded joints of sparsely-doped titanium alloy Ti–2.8Al–5.1Mo–4.9Fe made by AAW, led to the conclusion that the lowest values of strength in as-welded condition are determined for joints made with preheating to 400 °C, and they are equal to 799 MPa that is 75 % of base metal strength (Table 3). The strength of joints made with application of VT1-00sv filler wire in the modes that ensure the content of VT1-00 metal in the weld on the level of 10–13 %, is the highest. In this case, the strength values reach 1002 MPa, or 93 % of base metal strength. Impact toughness of

weld metal samples with a sharp-angled notch (KCV) made with application of VT1-00sv filler wire at feed rate of 30 m/h at VT1-00 metal content in the weld on the level of 10–13 % reaches maximum values (5.5 J/cm<sup>2</sup>). Impact toughness values of samples with a sharp-angled notch from AAW joints are almost on the same level of 4.9–5.7 J/cm<sup>2</sup>. The highest values are found in samples, made with flux application.

As the strength of VT1-00sv filler wire material (295–470 MPa) is much lower than that of base metal of Ti–2.8Al–5.1Mo–4.9Fe titanium alloy (1071 MPa), and it cannot be used as the strengthening alloying material, the cause for increased strength of the joints is the change of the structure and phase composition in welding with addition of VT1-00sv filler wire and loss of weld metal alloying. Quantity of  $\beta$ -phase decreases, so welded joints with loss of alloying will have higher strength values compared to joints without any change in weld alloying.

If we separately consider the properties of welded joints of Ti–2.8Al–5.1Mo–4.9Fe alloy, made without changing the weld metal composition, then the highest strength of the joints on the level of 972 MPa and the highest impact toughness of weld metal on the level of 5.7 J/cm<sup>2</sup> are found in joints made in the modes with lower heat input. So, semi-submerged arc welding has minimum heat input of the process on the level of 6480 J/cm, which is almost two times higher than that of through penetration AAW (14256 J/cm) and AAW with preheating (13392 J/cm). Note that the cross-sectional area of weld metal is the largest at AAW with preheating (see Table 2). Increase in the strength of joints made in the modes with lower heat input is attributable to a smaller quantity of  $\beta$ -phase in the weld metal. Reduction of the quantity of  $\beta$ -phase in the weld metal occurs under the conditions of lowering of the cooling rates in the temperature range of  $\beta \rightarrow \alpha + \beta$  polymorphous transformations at joint cooling.

Obtained data lead to the conclusion that the highest strength is found in joints where the weld metal composition is different from that of the base metal. If we compare joints, in which the chemical composition of the metal did not change, then the highest strength (972 MPa or 90 % of base metal strength) is demonstrated by joints made with flux application.

It leads to the conclusion about the rationality of application of tungsten electrode semi-submerged AAW for producing joints of sparsely-doped titanium alloy Ti–2.8Al–5.1Mo–4.9Fe. Semi-submerged AAW ensures the lowest values of the heat input and minimal dimensions of the weld and HAZ.

Contrarily, the joints made with preheating up to 400 °C have the lowest strength values, which is indicative of the unsuitability of this welding process for producing joints of sparsely-doped titanium alloy Ti–2.8Al–5.1Mo–4.9Fe.

Note that as a result of the impact of AAW on joints of VT19 pseudo- $\beta$ -alloy, also  $\beta$ -phase is predominantly reported in the welds [15]. Here, the level of strength of the joints at AAW with application of VT1-00sv filler wire in the quantity of 22 % is on the level of  $\sigma_t = 965$  MPa. In joints of VT19 alloy made by TIG-welding without filler wire application, the values of tensile strength are on the level of  $\sigma_t = 860$  MPa, that is much lower than the strength of Ti–2.8Al–5.1Mo–4.9Fe alloy.

Thus, the properties of welded joints of sparsely-doped titanium alloy Ti–2.8Al–5.1Mo–4.9Fe made by tungsten electrode AAW were studied, and it was established that joints made with application of VT1-00sv filler wire in the quantity of 10–13 %, demonstrate the highest strength on the level of 1002 MPa, or 93 % of that of the base metal. Here, the quantity of  $\beta$ -phase in the weld metal is 75 %. In order to ensure a homogeneous structure, and decomposition of metastable phases, and to produce full strength joints, they have to be subjected to further heat treatment.

## Conclusions

1. The modes of argon-arc welding with lower heat input for sparsely-doped pseudo- $\beta$ -alloy Ti–2.8Al–5.1Mo–4.9Fe have a positive impact on joint strength. So, among the welded joints, made without any change of weld metal composition, the joints produced by semi-submerged welding with minimum heat input and cross-sectional area of the weld metal, demonstrate the highest strength of 972 MPa and the highest impact toughness at the level of 5.7 J/cm<sup>2</sup>.

2. The structure of the metal of weld and HAZ of the joints of sparsely-doped titanium alloy Ti–2.8Al–5.1Mo–4.9Fe made by AAW, consists mainly of  $\beta$ -phase, with precipitates of metastable  $\alpha$ -phase; the size of  $\alpha$ -phase particles precipitates is smaller, than in the base metal, and it is equal from less than 1  $\mu$ m to 3–4  $\mu$ m. The finest precipitates of metastable  $\alpha$ -phase are found in joints made by semi-submerged AAW, precipitate size being up to 1–2  $\mu$ m.

3. The strength of joints of Ti–2.8Al–5.1Mo–4.9Fe titanium alloy made by AAW with application of

VT1-00sv filler wire in the quantity of 10–13 % in as-welded condition is equal to 1002 MPa or 93 % of that of the base metal. Here, the quantity of  $\beta$ -phase in the weld metal is equal to 75 %. To ensure a homogeneous structure of the weld, HAZ and base metal and decomposition of metastable phases, and to produce full strength joints, all the joints have to be subjected to further heat treatment.

- Dhinakaran, V., Shriragav, S.V., Fahmidha, A.F.Y., Ravichandran, M. (2020) A review on the categorization of the welding process of pure titanium and its characterization. *Materials Today, Proceedings*, **27**, 742–747.
- Pasang, T., Tao, Y., Azizi, M. et al. (2017) Welding of titanium alloys. In: *MATEC Web of Conf.*, **123**, 00001. EDP Sciences.
- Ströber, K., Abele, C. (2018) Titanium welding technology for series production. *Lightweight Design Worldwide*, **11**(4), 12–15.
- Reddy, M.K.P., Naik, R.P., Samatham, M., Kumar, C.H. (2020) Review on different welding techniques of Titanium and its alloys. *Int. J. of Sci. Research in Science. Engineering and Technology* (www.ijrsret.com)© 2020IJSRSET | Volume 7 | Issue 1 | Print ISSN: 2395-1990 | Online ISSN: 2394-4099.
- Nochovnaya, N.A., Antashev, V.G. (2007) Titanium alloys of «LOW-COST»series and possibilities of their application. In: *Proc. of Int. Conf. on Ti-2007 in CIS* (Kiev, IMF), 191–192.
- Dobrescu, M., Dimitriu, S., Vasilescu, M. (2011) Studies on Ti–Al–Fe low-cost titanium alloys manufacturing, processing and applications. *Metalurgia Int.*, **16**(4), 73.
- Lin, D.J., Ju, C.P., Lin, J.H.C. (1999) Structure and properties of cast Ti–Fe alloys. *Transact. of the American Foundry men's Society*, **107**, 859–864.
- Holden, F.C., Ogden, H.R., Jaffee, R.I. (1956) Heat treatment and mechanical properties of Ti–Fe alloys. *Transact. of the American Institute of Mining and Metallurgical Engineers*, **206**(5), 521–528.
- Lee, D.B., Park, K.B., Jeong, H.W., Kim, S.E. (2002) Mechanical and oxidation properties of Ti–xFe–ySi alloys. *Materials Sci. and Eng. A*, **328**(1–2), 161–168.
- Lütjering, G., Williams, J.C. (2003) *Titanium (engineering materials and processes)*. Berlin, Springer-Verlag. 3.
- Gurevich, S.M., Blashchuk, V.E. (1968) Consumable electrode shielded-gas welding. *Avtomatich. Svarka*, **11**, 87–89 [in Russian].
- Hong, S.H., Hwang, Y.J., Park, S.W. et al. (2019) Low-cost beta titanium cast alloys with good tensile properties developed with addition of commercial material. *J. of Alloys and Compounds*, **793**, 271–276.
- Zheng, B., Dong, F., Zhang, Y. et al. (2018) Microstructure, mechanical properties and deformation behavior of new V-free low-cost Ti–6Al–xFe–yCr alloys. *Materials Research Express*, **6**(2), 026551.
- Akhonin, S.V., Belous, V.Y., Selin, R.V., Kostin, V.A. (2021) Influence of TIG welding thermal cycle on temperature distribution and phase transformation in low-cost titanium alloy. In: *Proc. of IOP Conf. Series: Earth and Environmental Sci.*, **688**(1), 012012. IOP Publ.
- Akhonin, S.V., Bilous, V.Yu., Selin, R.V., Petrychenko, I.K. (2020) Impact of TIG welding on the structure and mechanical properties of joints of pseudo- $\beta$ -titanium alloy. *The Paton Welding J.*, **2**, 9–15. <https://doi.org/10.37434/tpwj2020.02.02>

Received 16.04.2021

# EFFECT OF THERMAL CYCLES IN ELECTRON BEAM WELDING OF ALUMINIUM 1570 ALLOY ON MECHANICAL PROPERTIES OF WELDED JOINTS

V.M. Nesterenkov, V.V. Skryabinskyi and M.O. Rusynyk

E.O. Paton Electric Welding Institute of the NAS of Ukraine

11 Kazymyr Malevych Str., 03150, Kyiv, Ukraine. E-mail: [office@paton.kiev.ua](mailto:office@paton.kiev.ua)

The effect of welding speed on strength of joints and size of the heat-affected-zone in electron beam welding of 1570 alloy was investigated. Thermal cycles in the tail part of the welding pool and spots in the metal surface in the near-weld zone were determined. According to the thermal cycles of the welding pool, the rate of hardening of the weld metal was calculated and its effect on mechanical properties of the joints before and after artificial aging was investigated. Decrease in the welding speed and, consequently, increase in the lifetime of the liquid phase leads to the growth of hardness of the weld metal after aging, which is probably associated with a more complete dissolution of primary scandium intermetallics and its transition to a supersaturated solid solution during cooling. Measuring the hardness of metal in the cross-section of the joints, according to the thermal cycles of the corresponding points, it was determined that the temperature of the beginning of the loss of strength of the metal in electron beam welding of 1570 alloy is in the range of 450–560 °C. It was found that artificial aging provides full strength welded joints with stamped semi-finished products, and explosion treatment is ineffective. It is possible to increase the strength of joints to the level of strength of hardened plates by 20 % applying plastic deformation and a subsequent artificial aging. 7 Ref., 3 Tables, 8 Figures.

*Key words:* electron beam welding, aluminium alloy, welded joints, thermal cycles, mechanical properties, artificial aging

1570 alloy of the Al–Mg–Sc system is considered to be thermally unstrengthening, as far as during its production a strengthening heat treatment in the form of hardening and artificial aging is not used. However, during casting of semi-finished products of alloys, scandium is fixed in a supersaturated solid solution (i.e., hardening) and the alloy is strengthened during subsequent heating (i.e., aging) [1]. The high mechanical properties of the alloy are predetermined by the formation of strengthening particles of Al<sub>3</sub>Sc phase, which is precipitated during heating and deformation from a supersaturated solid solution. One of the causes for the positive effect of scandium on the strength characteristics of alloys of the Al–Mg system is the stability of a nonrecrystallized structure formed as a result of pressure treatment, which is predetermined by the formation of secondary particles of Al<sub>3</sub>Sc phase, precipitated during heating and deformation from a supersaturated solid solution. The second cause for strengthening is a direct strengthening action of the Al<sub>3</sub>Sc phase particles [2].

Scandium refers to refractory elements and its introduction into low-melting aluminium alloys presents the known difficulties. To facilitate the assimilation of aluminium melt, the refractory element— scandium is introduced in the form of a master alloy Al – 2 % Sc.

Moreover, the concentration of a solid solution of scandium in aluminium in the master alloy does not exceed 0.7–0.8 %. And most of scandium is in the form of primary Al<sub>3</sub>Sc intermetallics, which have a high thermal stability and are extremely slowly soluble in the aluminium melt. To accelerate this process, the melt is overheated [3]. Therefore, the dissolution of Al<sub>3</sub>Sc intermetallics is significantly affected by the temperature and time of a melt existence. In the production of semi-finished products of 1570 alloy, some part of scandium does not pass into a solid solution, but precipitated from the melt in the form of primary intermetallics, which contain Sc and Zr [1]. Thus, in the existing technologies of production, some part of the main strengthening and most expensive component of the alloy 1570 — scandium does not participate in its strengthening.

On the experimental Al–Mg–Sc alloys, at a scandium content of 0.4–1.0 %, it was found that at a hardening rate of 10<sup>2</sup> °C/s, scandium partially turns into a supersaturated solid solution, and partially crystallizes in the form of intermetallics. At a hardening rate of 10<sup>5</sup> °C/s much more scandium passes into a supersaturated solid solution, which facilitates 10<sup>2</sup> times increase in the density of precipitates of the strengthening Al<sub>3</sub>Sc phase, formed during aging [4, 5]. With the use of such a highly concentrated heat source for welding as electron beam, it is possible to change the welding speed in a wide range, changing

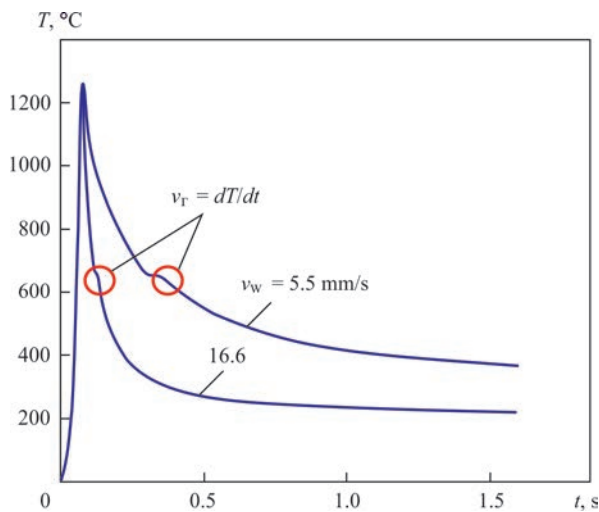


**Figure 1.** Measured experimental curves of cooling of welding pool metal in EBW of AMg6 alloy at different rates

the temperature of the welding pool, the lifetime of the liquid phase, and also the cooling rate of the weld metal immediately after solidification (i.e. hardening rate). Thus, we will probably be able to change the amount of fixed scandium in the solid solution, which will affect the strength of welded joints after further artificial aging.

The aim of the work is to experimentally determine the thermal cycles in the tail part of the welding pool and points on the metal surface in the heat-affected-zone (HAZ) during electron beam welding (EBW) of 1570 alloy. According to the thermal cycles of the welding pool, the hardening rate of the weld metal was calculated and its effect on the mechanical properties of joints was investigated before and after artificial aging. By measuring the hardness of the metal in the cross-section of the joints, the temperature of the beginning of softening of the alloy was found by the thermal cycles of the respective points. The effect of thermomechanical treatment on the strengthening of welded joints was also determined.

**Experimental procedure.** The thermal cycles of the welding pool and HAZ were determined in EBW of plates of aluminium AMg6 alloy (closest to 1570 alloy as to the chemical composition) of 15 mm thickness. Welding modes were selected in such a way as to provide a guaranteed penetration with the formation of a uniform weld reinforcement. When determining the thermal cycles of the welding pool in its tail part the brazed joint of chromel-alumel thermocouple was immersed and its readings were recorded with a re-

recorder [6]. The temperature of the welding pool was recorded directly, and the instantaneous cooling rate was determined as the tangent of the angle of inclination of the temperature tangent to the function diagram at a point of interest to us. HAZ thermal cycles were determined from the readings of thermocouples that were caulked-in at a distance of 1, 3, 5, and 7 mm from the fusion line. In order to reduce the inertia of the measurements, the diameter of the wire for the manufacture of thermocouples was chosen as the minimum possible (0.1 mm). The readings of thermocouples were recorded with a N338 type recorder. The speed of the tape was 100 mm/s.

**Experimental part.** The curves of cooling the weld pool and the weld metal for different speeds of EBW are shown in Figure 1. From Figure 1 it is seen that after reaching its maximum, the temperature decreases according to exponential law. From the obtained curves, the rates of cooling the weld metal immediately after crystallization (quenching rate) were calculated. As the welding speed increases from 2.8 to 16.8 mm/s, the cooling rate grows from  $5 \cdot 10^2$  to  $1 \cdot 10^4$  °C/s. Investigations of the effect of hardening rate of the weld metal on the strength of welded joints were performed on stamped plates of 1570 alloy with a thickness of 30 mm. The chemical composition of the base metal and weld metal are given in Table 1.

The experiments were performed in an electron beam welding machine UL 209M with a power source ELA 60/60 with a voltage of 60 kV. During EBW, the beam current and the focusing current were selected from the condition of a guaranteed penetration and formation of a reverse weld bead. A circular scanning of a beam with a diameter of 1.5 mm and a frequency of 600 Hz was used. Welds had a width of about 3 mm with almost parallel boundaries of the penetration zone in the central and lower part.

Hardness measurements were used to evaluate the degree of loss of strength and changes in the properties of the weld metal and the HAZ Rockwell device with a load on a steel ball of 600 N according to the scale of B with a ball diameter of 1.0 mm was used. Thermal cycles of points on the surface of welding plates are shown in Figure 2, and the results of hardness measurements are presented in Figure 3. The figures show that for welding speeds of 2.8 and 16.8 mm/s, the width of HAZ does not exceed 3 mm. A short-term heating of 1570 alloy to 450 °C is not ac-

**Table 1.** Chemical composition (wt.%) of base metal and weld metal of stamped semi-finished product of 1570 alloy

Place of determination	Al	Mg	Mn	Sc	Zr	Si	Fe	Cu	Zn
Base metal	Base	6.45	0.32	0.16	0.025	0.041	0.07	0.014	0.02
Weld	»	6.35	0.31	0.16	0.025	0.040	0.06	0.015	0.02

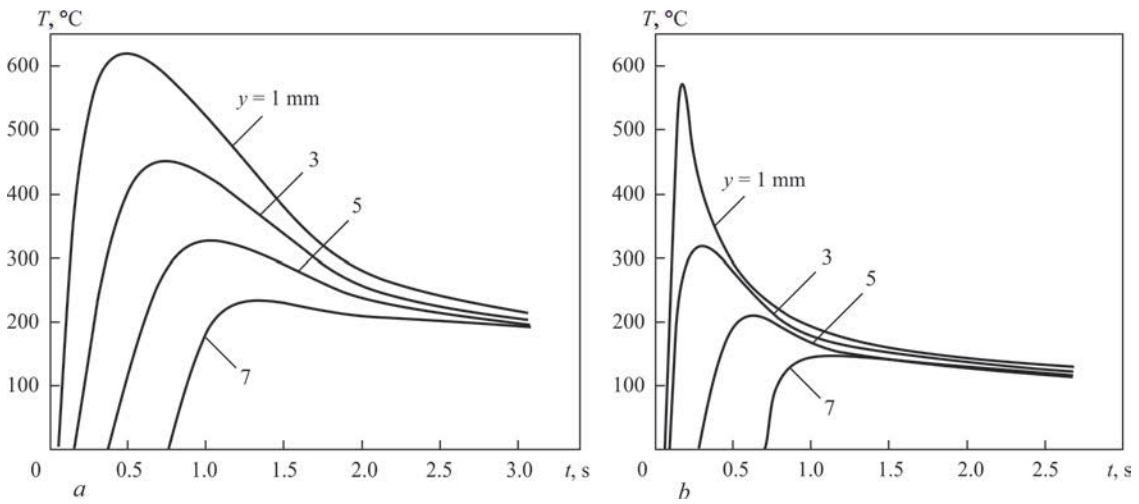


**Figure 2.** Thermal cycles of points on the surface of the plates of AMg6 alloy in EBW at a speed of: *a* — 2.8 mm/s; *b* — 16.8 (y is the distance from the fusion line)

accompanied by a decrease in hardness. Short-term rises in temperature to 560 °C and higher lead to a decrease in hardness by 2–3 HRB units.

A part of the welded specimens was heat-treated for 1 h at a temperature of 350 °C. Hardness measurements in the cross-section of the joints and mechanical tensile tests of the specimens were performed (Table 2). Prior to heat treatment, the hardness of the weld metal was HRB 81–82 units. After artificial ageing, the hardness of the weld metal increased to a level exceeding the hardness of the base metal by HRB 1–2 units at a welding speed of 16.8 mm/s and by HRB 5–6 units at a welding speed of 2.8 mm/s. Therefore, with a decrease in welding speed, the hardness of the weld metal increased. Therefore, more reinforcing secondary Al<sub>3</sub>Sc particles precipitated at low welding speeds after heat treatment. After welding, all the

scandium contained in the weld metal should be either in a supersaturated solid solution, the decomposition of which causes strengthening of the alloy during ageing, or in the form of primary intermetallics, which do not participate in strengthening of the alloy. The lower the welding speed, the lower the cooling rate, but the longer the time when the weld metal stays in a liquid state in the affected zone of the electron beam. Probably, an increase in the lifetime of the liquid phase led to the dissolution of more primary intermetallics and, accordingly, to the fixation of more scandium in a solid solution under cooling. Thus, the transition of scandium to a solid solution of the weld metal is affected by the welding speed more than the rate of further cooling and hardening of the metal. Thus, after electron beam remelting and a subsequent ageing, the hardness of the weld metal is higher than the hard-

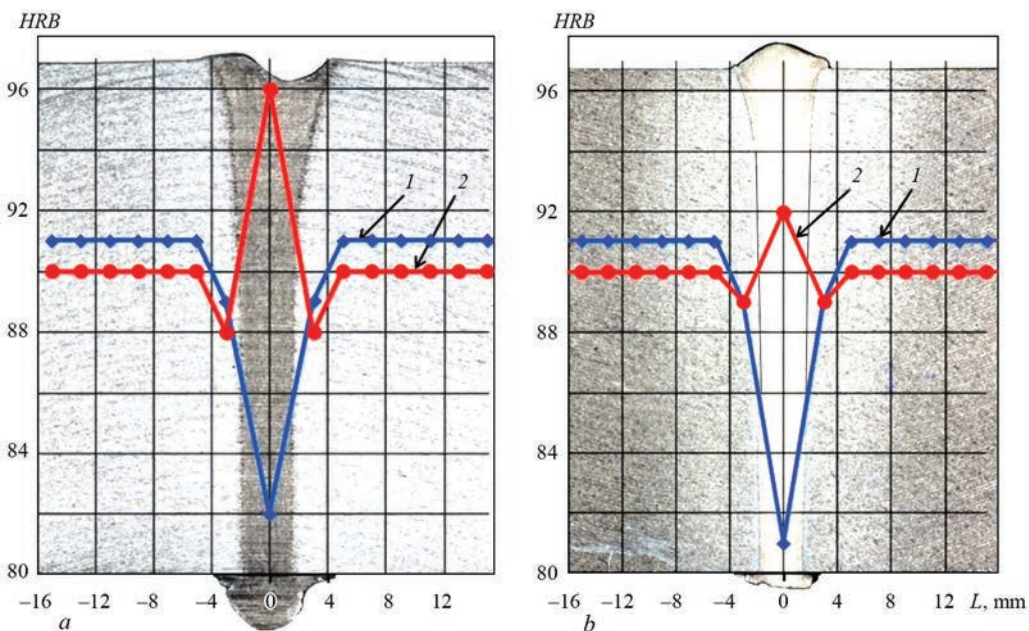


**Figure 3.** Hardness distribution in the cross-section of joints welded at a speed of 2.8 (*a*) and 16.8 mm/s (*b*). Curves 1 — welded joints without heat treatment; 2 — after artificial ageing

**Table 2.** Ultimate tensile strength  $\sigma_t$  (MPa) of welded joints of stamped semi-finished product of 1570 alloy with a thickness of 30 mm without heat treatment and after artificial aging for different welding speeds

Welding speed, mm/s	Rate of hardening of weld metal, °C/s	$\sigma_t$ of welded joint, MPa	$\sigma_t$ of welded joint after artificial aging, MPa
2.8	$>5 \cdot 10^2$	$\frac{326-332}{328}$	$\frac{383-386}{384 (*)}$
16.8	$>1 \cdot 10^4$	$\frac{329-332}{331}$	$\frac{385-387}{386 (*)}$

*Note.* In the numerator the minimum and maximum values are shown, in the denominator the average value of the three measurements is shown. (\*) is the fracture of 100 % of the specimens occurred on the base metal outside the HAZ.

ness of the original stamped semi-finished products of 1570 alloy. Probably, this occurs due to a more complete assimilation of scandium in the alloy.

From Table 2 it is seen that the strength of welded joints both before and after heat treatment depends little on the rate of hardening of the weld metal. The fracture of rupture specimens (Figure 4) occurs in the area with the lowest strength. Prior to artificial aging, such an area is a weld. After aging, all the specimens fractured on the base metal outside the HAZ, i.e. aging at 350 °C strengthens the weld metal to a level higher than the strength of the base metal. In cases where heat treatment of joints is provided after welding, the speed of EBW of 1570 alloy can be adjusted within wide ranges without a fear of decreasing their strength.

In some cases, it is possible to improve the strength properties of the weld and the heat-affected zone of aluminium alloys by explosion treatment of welded joints [7]. Studies of the effectiveness of such treatment as-applied to the joints of 1570 alloy were performed on stamped plates with a thickness of 60 mm, welded with an electron beam. Using explosives, the facial and then the reverse side of the joints were

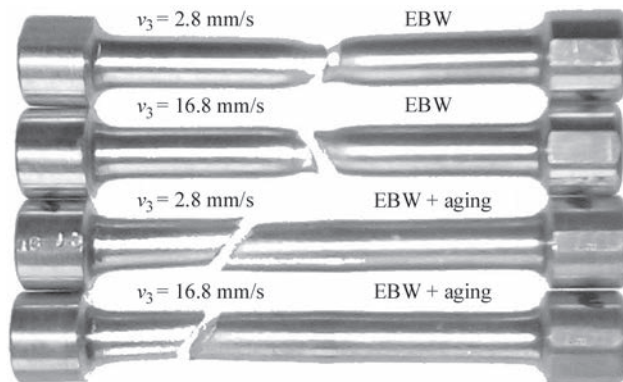


**Figure 4.** Nature of fracture of specimens after the test on rupture of joints of 1570 alloy without heat treatment and after artificial aging (welded joints are located in the center of specimens)

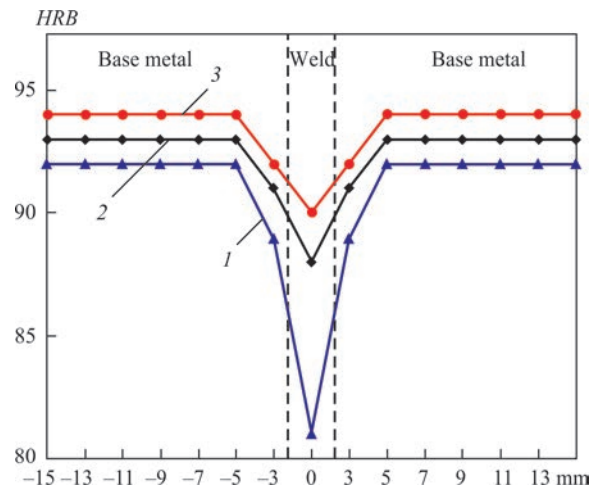


**Figure 5.** Distribution of hardness in the cross-section of welded joints of 1570 alloy at a distance of 10 mm from the surface of the plates (1 — after welding; 2 — welding + explosion treatment on mode 1; 3 — welding + explosion treatment on mode 2)

sequentially treated. The weld and adjacent areas of about 50 mm width were treated. Two treatment modes were used, which differed in the power of the explosive. When using a weak charge (mode 1), no noticeable deformation occurred on the surface of the treated plates. A more powerful explosive (mode 2) deformed the treated plates up to 0.5 mm at the locations of the explosive. In Figure 5 the results of hardness measurements in the cross-section of welded joints are shown.

Explosion treatment increases the hardness of the weld metal at a distance of 10 mm from the surface of plates with HRB 82–83 to HRB 88–90. In the part of the weld, which is central as to the thickness of the joint, the hardness increased to HRB 86–88. The hardness of the base metal and HAZ after treatment increased slightly (by HRB 1–3 units). Some of the specimens after explosion treatment were artificially aged at 320 °C for 1 h. Heat treatment increased the hardness of the weld metal to the level of the base met-

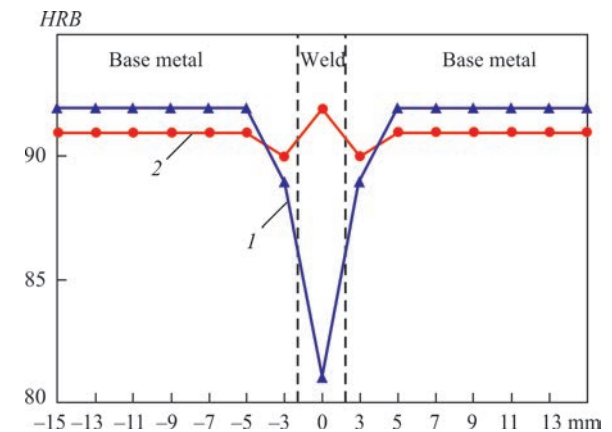


**Figure 6.** Hardness distribution in the cross-section of welded joints of 1570 alloy (1 — after welding; 2 — welding + explosion treatment on mode 2 + artificial aging)

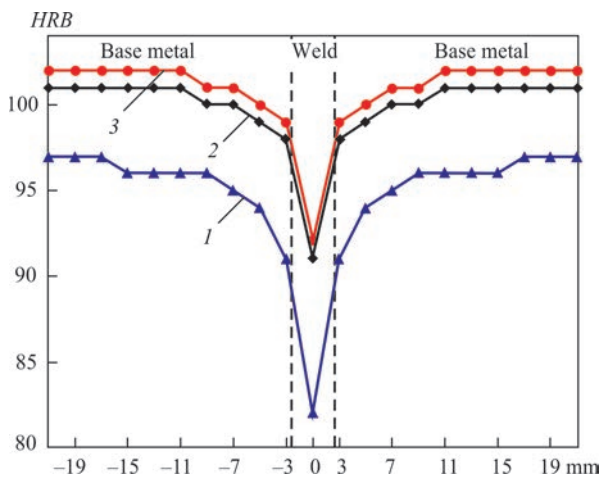


**Figure 7.** Hardness distribution in the cross-section of welded joints of hardened plates of 1570 alloy with a thickness of 26 mm (1 — after welding; 2 — welding + hardening 20 %; 3 — welding + hardening 40 %)

al (Figure 6). Some decrease in hardness (by *HRB* 1–2 units) is observed only in HAZ, whose width does not exceed 3 mm.

The subsequent studies revealed that explosion treatment in the mode 1 did not affect the mechanical properties of the welded joints. As the explosive power increases (treatment on the mode 2), the ultimate tensile strength of the joints increases slightly (by 10–20 MPa). A subsequent heat treatment increases the ultimate tensile strength to the same level that is achieved also without an explosion treatment. Thus, the explosion treatment of welded joints of 1570 alloy is not only technologically complex, but inefficient and, therefore, is not rational.

Studies of the effect of plastic deformation on the mechanical properties of the joints of 1570 alloy were performed on hardened plates with a thickness of 26 mm. Cold plastic deformation was carried out by rolling. Before rolling, the reinforcement and the root of the weld were removed by mechanical treatment to the level of the base metal surface. The direction of rolling coincided with the direction of welding. The results of measuring hardness in the cross-section of welded joints are shown in Figure 7. Plastic deformation increases the hardness of the weld metal by *HRB*

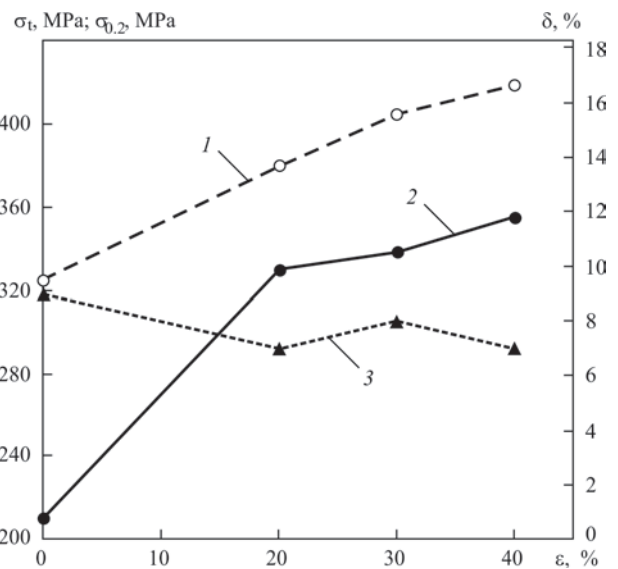


**Figure 8.** Mechanical properties of welded joints of hardened plates of 1570 alloy with a thickness of 26 mm depending on the degree of hardening (1 — ultimate tensile strength  $\sigma_t$ , MPa; 2 — conditional yield strength  $\sigma_{0.2}$ , MPa; 3 — relative elongation  $\delta$ , %)

81–82 to 91–93, and the base metal by *HRB* 94–95 to 101–103. The main increase in hardness occurs at the degree of plastic deformation from 0 to 30 %. A subsequent plastic deformation has no significant effect on the increase in hardness.

Mechanical properties of the joints after rolling are shown in Figure 8. With an increase in the degree of deformation to 40 %, the ultimate tensile strength grows from 320 to 420 MPa, and the conditional yield strength grows from 210 to 350 MPa. It is important that plasticity of the joints does not change. At a deformation of 30 %, the strength of welded joints reaches the level of strength of hardened semi-finished products.

A part of the specimens after plastic deformation were aged at a temperature of 350 °C for 1 h. The test results of these specimens are given in Table 3. From Table 3 it is seen that the ultimate tensile strength of heat-treated specimens grows with an increase in the degree of plastic deformation. In all cases, artificial aging additionally increases the strength of the joints by 10–80 MPa.

**Table 3.** Ultimate tensile strength of base metal and welded joints  $\sigma_t$  (MPa) of hardened plates of 1570 alloy after hardening and artificial aging

Object of tests	Degree of plastic deformation, %			
	0	20	30	40
Base metal	$\frac{402-415}{410}$	–	–	–
Welded joint	$\frac{320-332}{325}$	$\frac{362-384}{376}$	$\frac{402-411}{408}$	$\frac{412-424}{419}$
Welded joint after artificial aging	$\frac{392-402}{396}$	$\frac{401-405}{404}$	$\frac{415-419}{417}$	$\frac{424-426}{425}$

## Conclusions

It was found that artificial aging of welded joints produced by the EBW method, increases the hardness of the weld metal to the level, higher than the hardness level of the base metal of stamped semi-finished products. The greatest increase in hardness (5–6 units *HRB*) occurs at a low welding speed (2.8 mm/s) and, accordingly, at a low rate of hardening ( $5 \cdot 10^2$  °C/s). Therefore, the rate of hardening does not play a crucial role in strengthening the weld metal during aging. On the other hand, a decrease in the welding speed increases the time when the metal stays in a liquid state in the zone of influence of the electron beam. Here, probably, not only dissolution of fine secondary  $Al_3Sc$  particles, but also a more complete dissolution of large primary scandium intermetallics occurs. During cooling, scandium turns into a supersaturated solid solution, followed by precipitation of more reinforcing secondary  $Al_3Sc$  particles during artificial aging.

After artificial aging, all specimens are fractured on the base metal outside the HAZ, i.e. in the cases when after welding heat treatment of joints is provided, the speed of EBW of 1570 alloy can be adjusted in a wide range without fear of reducing their strength.

The temperature of start of weakening the metal in the HAZ during EBW is in the range of 450–560 °C. The width of the HAZ in a wide range of welding speed change does not exceed 3 mm.

The effect of heat and explosion treatment, as well as plastic deformation on mechanical properties of 1570 alloy joints was studied. It was found that artificial aging makes welded joints equally strength with stamped semi-finished products, and explosion treatment has a low efficiency. It is possible to increase the strength of joints to the level of strength of hardened plates by 20 % applying plastic deformation and a subsequent artificial aging.

1. Filatov, Yu.A. (2014) Alloys of Al–Mg–Sc system as a special group of wrought aluminium alloys. *Tekhnologiya Lyogkikh Splavov*, **2**, 34–41 [in Russian].
2. Drits, M.E., Pavlenko, S.G., Toropova, L.S. et al. (1981) About mechanism of scandium effect on improvement of strength and thermal stability of Al–Mg system alloys. *DAN SSSR*, **257(2)**, 353–356 [in Russian].
3. Zakharov, V.V., Fisenko, I.A. (2013) On saving scandium when alloying aluminium alloys with it. *Tekhnologiya Lyogkikh Splavov*, **4**, 52–60 [in Russian].
4. Berezina, A.L., Segida, E.A., Monastyrskaya, T.A., Kotko, A.V. (2008) Influence of solidification rate on anomalous supersaturation of Al–Mg–Sc alloys. *Metallofizika i Novejshie Tekhnologii*, **30(6)**, 849–857 [in Russian].
5. Fedorchuk, V.E., Kushnaryova, O.S., Alekseenko, T.A., Falchenko, Yu.V. (2014) Peculiarities of alloying of weld metal of high-strength aluminium alloy welded joints with scandium. *The Paton Welding J.*, **5**, 28–32.
6. Skryabinskyi, V.V., Nesterenkov, V.M., Rusynyk, M.O., Strashko, V.R. (2020) Effect of mode of electron beam welding, heat treatment and plastic deformation on strength of joints of aluminium 1570 alloy. *Ibid.*, **5**, 9–14.
7. Tretyak, N.G., Saenko, M.I., Petushkov, V.G. (1980) Explosion strengthening of welded joints of 1201 alloy. *Avtomatich. Svarka*, **9**, 67–68 [in Russian].

Received 14.04.2021

**MAY 2, 1969**



Ocean liner «Queen Elizabeth 2» went on its first voyage Southampton — New York. For 35 years it was the flagship of the British Shipping Company «Cunard». The all-welded structure of the ship hull was divided into 13 waterproof transverse bulkheads. The outdoor deck, which is wood sheathed, was fastened on welded-on studs. As regards aluminium decks, because of application of thin material, the «springing» effect appeared when walking on the ship. This was largely overcome by cross-welding stiffeners on larger areas of the deck.

**MAY 3, 1973**

One day before the completion of the 108-storey building of Sears-Tower — a skyscraper in Chicago, USA, it becomes the tallest building in the world at that time (442.1 m). It is the hallmark of Chicago. Construction of such a building structure is a challenge for the construction and welding companies. About 76000 t of steels were used in construction. Lincoln Electric Company participated in the project as a construction partner. Its design contained 268 km of the main welds. Both electric arc and electroslag welding was used in construction of the building.



**MAY 9, 1981**

The sculpture-monument «Motherland», the largest statue in Ukraine (17<sup>th</sup> in the world), was opened on Victory Day. The figure of a woman holding up the shield and sword is faced with stainless steel sheets. The Statue height from the pedestal to the tip of the blade is 62 m, absolute height is 102 m, its weight is about 500 t. For the first time in the USSR, the sculpture of such a scale was manufactured at the Kiev Parizhskaya Kommuna Plant with technical support of PWI. More than 30 km of welds were made during its construction.



# ANALYSIS OF THE PROPERTIES OF ELECTRON BEAM WELDED JOINTS OF ALUMINIUM LITHIUM ALLOY LATEST GENERATION

**Mir. Sahul<sup>1</sup>, Mar. Sahul<sup>2</sup>, L. Čaplovič<sup>2</sup>, M. Marônek<sup>1</sup>, I. Klochkov<sup>3</sup> and S. Motrunich<sup>3</sup>**

<sup>1</sup>Slovak University of Technology in Bratislava, Faculty of Materials Science and Technology in Trnava,  
Department of Welding and Joining of Materials

J. Bottu 25, 917 24 Trnava, Slovakia. E-mail: miroslav.sahul@stuba.sk

<sup>2</sup>Slovak University of Technology in Bratislava, Faculty of Materials Science and Technology in Trnava,  
Institute of Materials Science

J. Bottu 25, 917 24, Trnava, Slovakia

<sup>3</sup>E.O. Paton Electric Welding Institute of the NAS of Ukraine

11 Kazymyr Malevych Str., 03150, Kyiv, Ukraine. E-mail: office@paton.kiev.ua

Electron beam welded joints made on AW2099 aluminium lithium alloy with the thickness of 4 mm were analysed. The third generation of aluminium lithium alloys was developed to improve the drawbacks of the second one. Various electron beam welding parameters (beam current, welding speed) were tested. Accelerating voltage was constant, i.e., 55 kV. Defect free welded joints were produced under optimized welding parameters. Weld metal microstructure and welded joints mechanical properties were investigated. Microstructure of weld metal matrix consists of  $\alpha$ -aluminium solid solution. Inter-dendrite areas were enriched in alloying elements due to segregation. Narrow equiaxed zone was observed at the location close to the fusion boundary being characteristic for welded joints made on aluminium lithium alloys. The character of the grains changed in the direction towards weld metal centre to columnar dendritic and equiaxed dendritic. Microhardness values reduction in the weld metal was observed which is associated to the dissolution of strengthening precipitates. 19 Ref., 1 Table, 9 Figures.

*Keywords:* AW2099 aluminium lithium alloy, electron beam welding, equiaxed zone, scanning electron microscopy, drop of microhardness

Aluminium lithium alloys have received extensive attention in aerospace industry due to low density, high strength/weight ratio, high Young's modulus, improved fatigue crack growth resistance and resistance to corrosion. It is known that adding of 1 % of lithium resulted in the decrease in density by 3 % and improvement in Young's modulus by 6 % [1–7].

The third generation of aluminium lithium alloys was developed to remove the disadvantages of previous generation. Important representatives of newly developed alloys are 2099 and 2199 being applied in the fuselage's skin stringer components [8]. Al–Li alloys of the new generation are characteristic by higher Cu/Li ratio than previous generation [9]. The application of 2099 alloy caused the reduction of weight of wing components by 14 % and cryogenic tanks by 21 % [10].

Currently, worldwide research focuses on the welding of aluminium lithium alloys. Friction stir welding belongs to the possible joining methods [11–18]. The main issues when fusion welding of these alloys is

carried out are porosity, hot cracking, evaporation of alloying elements and decrease in mechanical properties. Drop in mechanical properties is associated with the dissolution of strengthening precipitates due to thermal cycle of welding. From this point of view, the application of low heat input electron beam welding could be more convenient. High welding speeds lead to formation of minimum deformations and residual stresses. Furthermore, narrower weld metal and HAZ represents softening region of much smaller dimensions in comparison to conventional arc welding processes [19, 20].

Only a few papers focus on the electron beam weldability of AW2099 aluminium lithium alloy have been published. The purpose of the paper is to analyse the properties of electron beam welded joints made on latest generation AW2099 aluminium lithium alloy.

**Materials and methods.** AW2099 aluminium lithium alloy, 4 mm thick, was suggested as experimental material. Initial thickness of as delivered alloy

Mir. Sahul — <https://orcid.org/0000-0001-5091-6381>, Mar. Sahul — <https://orcid.org/0000-0001-9472-500X>,  
L. Čaplovič — <https://orcid.org/0000-0002-2280-008X>, M. Marônek — <https://orcid.org/0000-0002-4716-8092>,  
I. Klochkov — <https://orcid.org/0000-0001-6490-8905>, S. Motrunich — <https://orcid.org/0000-0002-8841-8609>

© Mir. Sahul, Mar. Sahul, L. Čaplovič, M. Marônek, I. Klochkov and S. Motrunich, 2021

Chemical composition of AW2099 aluminium lithium alloy

Cu	Li	Zn	Mg	Mn	Zr	Ti	Fe	Si	Be	others	Al
2.7	1.8	0.70	0.30	0.30	0.09	0.10	0.07	0.05	0.0001	0.03	Bal.

was 25.4 mm. The thickness of AW2099 alloy was reduced to 4 mm. Solution annealing at 530 °C/1 hr. was carried out before hot rolling. The chemical composition of the AW 2099 alloy provided by Smiths High Performance is given in Table.

PZ EZ 30 STU electron beam welding machine from First Welding Company, Inc. in Bratislava with the maximum accelerating voltage of 60 kV was used for manufacturing of welded joints (Figure 1). The maximum beam current 500 mA and output power are 30 kW. Welded joints were produced in the Centre of Excellence of 5-axis Machining (CE5AM) of the Faculty of Materials Science and Technology in Trnava, Slovakia. The vertical electron beam welding was carried out within experiments. The volume of vacuum chamber is 14.3 m<sup>3</sup>. The vacuum level during welding was 10<sup>-2</sup> Pa. Accelerating voltage of 55 kV and focusing current of 885 mA were used.

After metallographic preparation, the samples were etched with Keller’s reagent (chemical composition 1 ml HF + 1.5 ml HCl + 2.5 ml HNO<sub>3</sub> + 95 ml distilled H<sub>2</sub>O). High resolution field emission gun scanning electron microscope JEOL JSM 7600 F with EDS analyser X-max 50 mm<sup>2</sup> of Oxford Instruments was used to identify elemental distribution across investigated location. Microhardness measurements across base metal–HAZ–weld metal interface was carried out on Buehler IndentaMet 1100™ Series microhardness tester. The parameters of measurements were as follows: loading force 0.98 N, dwell time 10 s. Distance between indents in base metal and HAZ was 100 and 500 μm within the weld metal.

**Results.** Effect of welding parameters on the weld bead appearance and weld defects is given in Figure 2. When beam current of 50 mA was used, the

application of welding speeds up to 20 mm/s resulted in the drop through. The heat input was too high in such cases. Increasing the welding speed to 30 mm/s resulted in the elimination of mentioned burn through. On the other hand, slight undercut was observed. Increase of beam current to 60 and 70 mA (at welding speed of 30 mm/s) resulted in solidification cracking. Smooth surface without weld defects was observed when lower heat inputs were applied. Beam currents 60 and 65 mA and welding speeds from 50 to 80 mm/s resulted in the production of defect-free welded joints with smooth surface.

Microstructure of weld metal–heat affected zone interface (welded joint produced with beam current of 50 mA and welding speed of 30 mm/s) is given in Figure 3. The equiaxed zone (EQZ) was observed close to the fusion boundary. Equiaxed grains were probably formed due to heterogeneous nucleation at the lithium and zirconium rich precipitates.

In the direction towards weld center, the change in the dendrite morphology was observed. Columnar dendrite zone and equiaxed dendrite zone were found. The width of EQZ of about 20 μm consisting of equiaxed grains of average size 7 μm was documented between the fusion boundary and weld metal. Wang et al. observed that the grain volume was without precipitates and similarly found eutectics at the EQZ boundaries [11].

Chen et al. found EQZ in the un-fused region in the welded joints produced by newly developed fusion-diffusion electron beam welding of 2195-T3 aluminium lithium alloy. The diameter of equi-axed crystals was 50 μm. Weld metal and EQZ were characteristic by the presence of Al<sub>2</sub>Cu and T1 precipitates [21].



Figure 1. PZ EZ 30 STU electron beam welding machine

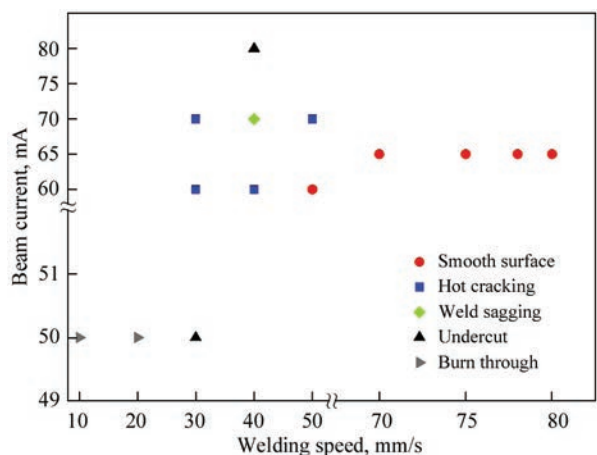
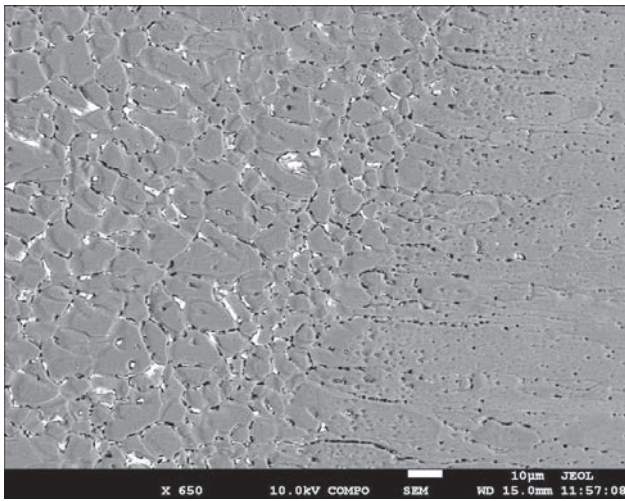


Figure 2. Effect of welding parameters on bead appearance and type of weld defects



**Figure 3.** Microstructure of weld metal–HAZ interface ( $I_b = 50$  mA,  $v = 30$  mm/s)

The microstructure of HAZ–weld metal interface of welded joint produced with lower heat input 45 J/mm (beam current of 65 mA and welding speed of 80 mm/s) is documented in Figure 4. Lower heat input caused that the width of EQZ decreased to about 10  $\mu\text{m}$  and was non-uniform across weld depth. EQZ is formed in some locations along fusion boundary only by one grain.

The weld root area of welded joint produced with the beam current of 60 mA and welding speed of 50 mm/s is given in Figure 5. The structure has a typical casting character, with a dendritic morphology. The matrix is formed by a  $\alpha$ -solid solution of alloying elements Cu and Li in aluminium and at the inter-dendrite locations depending on the maximum temperature and holding, the precipitation of secondary phases  $\delta'$ -Al<sub>3</sub>Li,  $\beta'$ -Al<sub>3</sub>Zr,  $\theta$ -Al<sub>2</sub>Cu could be expected.

Inter-dendrite precipitate documented by electron microscopy is given in Figure 6. EDS «linescan» across aluminium matrix–precipitate–aluminium matrix interface is given in Figure 7. The increase in copper, iron, and manganese content was observed in the

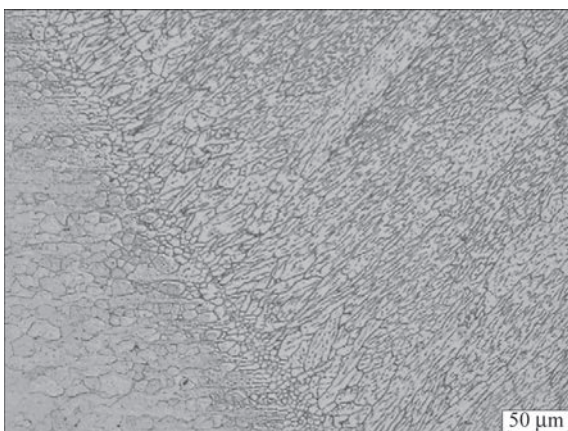


**Figure 4.** Microstructure of HAZ–weld metal interface ( $I_b = 65$  mA,  $v = 80$  mm/s)



**Figure 5.** The microstructure of the equiaxed dendrite zone in the weld metal centre ( $I_b = 60$  mA,  $v = 50$  mm/s)

site where precipitate is present. On the other hand, aluminium content remarkably decreased.

The course of microhardness across welded joints interfaces are given in Figure 8. The average microhardness of base material was 109 *HV*0.1. Welded joint produced with beam current of 50 mA and welding speed of 30 mm/s, i.e., heat input 92 J/mm was characterized by drop of microhardness in the weld metal. The average microhardness measured in the weld metal is about 75 *HV*0.1, representing about 69 % of the microhardness of the base material.

Microhardness trend for welded joint produced with higher heat input, following welding parameters: beam current 80 mA and welding speed of 40 mm/s is given in Figure 9. The calculated heat input is 110 J/mm. Similarly, the drop of microhardness was recorded in the weld metal. The averaged microhardness reached the value of 81 *HV*0.1 being about 74 % of the averaged values measured in the AW2099 aluminium lithium alloy.

Chen et al. investigated the reasons for lower mechanical properties of electron beam welded joints on 2195-T3 aluminium lithium alloy with the thickness of 5 mm. Similarly, authors also observed the decrease in the hardness in the welded joint averaging

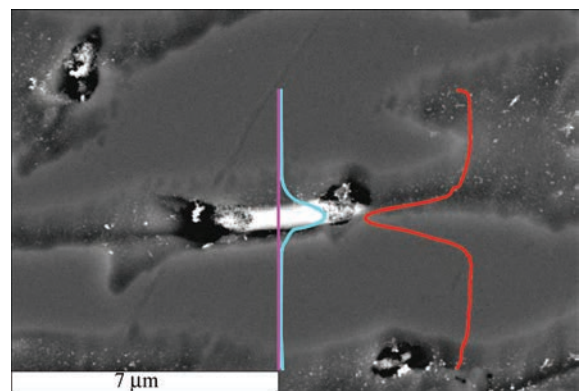


**Figure 6.** Inter-dendrite precipitate in the weld metal

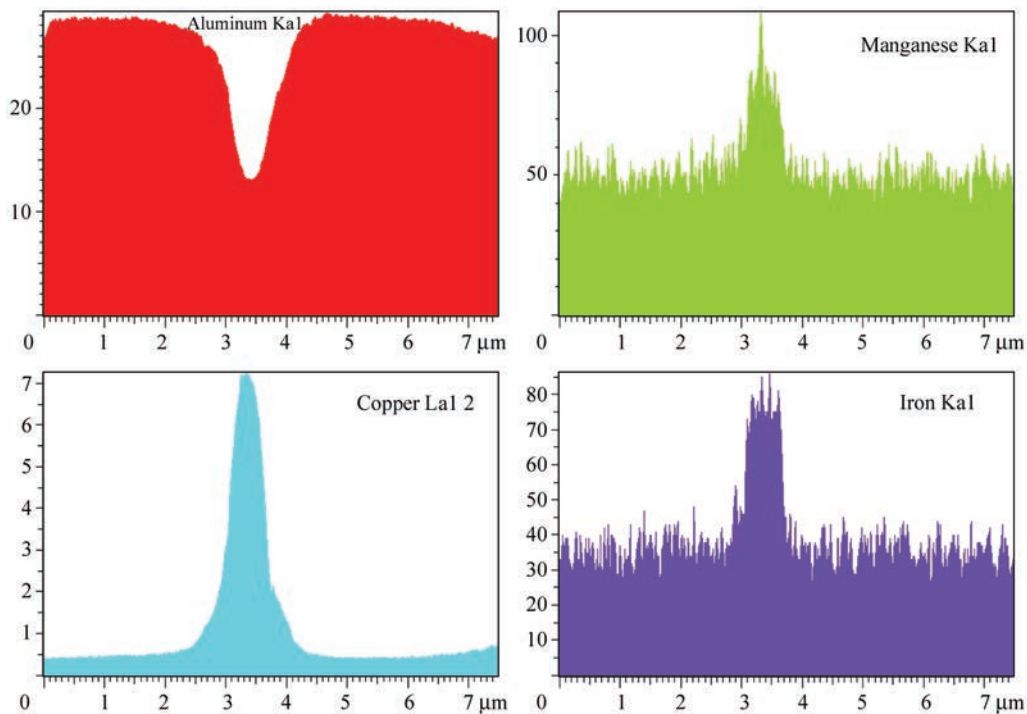


**Figure 7.** Course of aluminium, copper, manganese and iron across dendrite boundary (the value on the ordinate axis must be increased 1000 times)

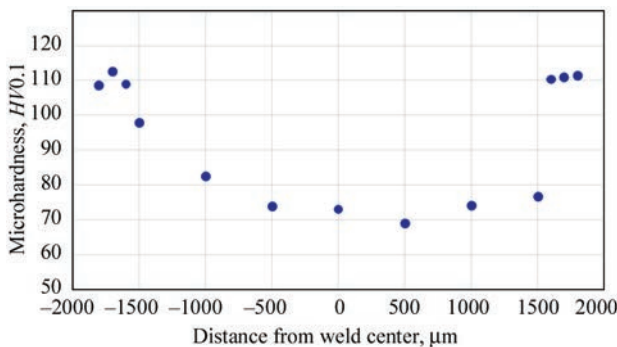


**Figure 8.** The course of microhardness across welded joint produced by beam current 50 mA and welding speed 30 mm/s

72 HV, representing about 60 % of the base materials hardness [22].

Based on the course of the measured values of microhardness, it can be stated that the microhardness of the weld metal decreased in comparison to the base material. Due to the thermal influence of the material by the welding thermal cycle, main precipitates T1 ( $Al_2CuLi$ ), most significantly contributing to the increase of mechanical properties during the heat treatment of mentioned aluminium alloy dissolved in the weld metal region. Reheating and melting of the base material resulted in the dissolution of phase T1.

**Conclusions**

The following could be concluded according to the results attained by the analysis of the electron beam welded joints made on AW2099 aluminium lithium alloy:

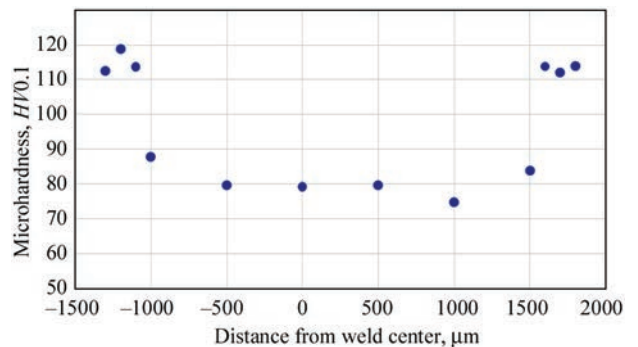


**Figure 9.** The course of microhardness across welded joint produced by beam current 80 mA and welding speed 40 mm/s

- electron beam welding of latest generation aluminium lithium led to the production of sound joints by optimization of welding parameters;
- higher heat input resulted in burn through and formation of solidification cracking;
- non-dendritic equiaxed zone was observed in the location close to the fusion boundary;
- the width of EQZ decreased when lower heat input was used;
- increase in the copper content was observed at the inter-dendrite areas due to segregation;
- decrease in average microhardness of weld metal was found and it was probably caused by dissolution of precipitates.

*Acknowledgement.* This work was supported by the Slovak Research and Development Agency under the contract No. APVV-15-0337.

The paper was prepared under the support of the KEGA cultural and educational grant agency of the Ministry of Education, Science, Research, and Sport of the Slovak Republic, project No. 001STU-4/2019.

This publication was supported by the Operational Programme Research and Innovation for the project: Scientific and Research Centre of Excellence SlovAKION for Material and Interdisciplinary Research, code of the project ITMS2014+:313011W085 co-financed by the European Regional Development Fund.

The work was carried out also within the framework of the departmental order programme of the National Academy of Sciences of Ukraine by E.O. Paton Electric Welding Institute (basic research no.6541230) titled «Supporting Development of the Priority Research Areas».

- Xiao, R., Zhang, X. (2014) Problems and issues in laser beam welding of aluminum-lithium alloys. *J. Materials. Proc. Technology*, **16**, 166–175.
- Gao, Ch., Gao, R., Ma, Y. (2015) Microstructure and mechanical properties of friction spot welding aluminium-lithium 2A97 alloy. *Mater. Des.*, **83**, 719–727.
- Han, B., Tao, W., Chen, Y., Li, H. (2017) Double-sided laser beam welded T-joints for aluminium-lithium alloy aircraft fuselage panels: Effects of filler elements on microstructure and mechanical properties. *Opt. Laser Technol.*, **93**, 99–108.
- Lee, H.-S., Yoon, J.-H., Yoo, J.-T., No, K. (2016) Friction stir welding process of aluminum-lithium alloy 2195. *Procedia Eng.*, **149**, 62–66.
- Ma, Y.E., Xia, Z.C., Jiang, R.R., Li, W.Y. (2013) Effect of welding parameters on mechanical and fatigue properties of friction stir welded 2198 T8 aluminum-lithium alloy joints. *Eng. Fract. Mech.*, **114**, 1–11.
- Zhang, F., Shen, J., Yan, X.-D. et al. (2014) Homogenization heat treatment of 2099 Al–Li alloy. *Rare Met.*, **33**, 28–36.
- Tao, Y., Ni, D.R., Xiao, B.L. et al. (2017) Origin of unusual fracture in stirred zone for friction stir welded 2198-T8 Al–Li alloy joints. *Mater. Sci. Eng.*, A **693**, 1–13.
- Rajan, R., Kah, P., Mvola, B., Martikainen, J. (2016) Trends in aluminium alloy development and their joining methods. *Rev. Adv. Mater. Sci.*, **44**, 383–397.
- Dursun, T., Soutis, C. (2014) Recent developments in advanced aircraft aluminium alloys. *Mater. Des.*, **56**, 862–871.
- Romios, M., Tiraschi, R., Ogren, J.R., Babel, H.W. (2005) Design of multistep aging treatments of 2099 (C458) Al–Li alloy. *J. Mater. Eng. Perform.*, **14**, 641–646.
- Wang, G., Zhao, Y., Hao, Y. (2018) Friction stir welding of high-strength aerospace aluminium alloy and application in rocket tank manufacturing. *J. of Mater. Sci. and Technology*, **34**, 73–91.
- Poklyatsky, A.G., Knysh, V.V., Klochkov, I.N., Motrunich, S.I. (2016) Features and advantages of the process of friction stir welding of butt joints of sheet aluminium-lithium alloys. *The Paton Welding J.*, **6**, 93–98.
- Milagre, M.X., Mogili, N.V., Donatus, U. et al. (2018) On the microstructure characterization of the AA2098-T351 alloy welded by FSW. *Mater. Charact.*, **140**, 233–246, DSC vyzera byt fajm.
- Li, W.Y., Chu, Q., Yang, X.W. et al. (2018) Microstructure and morphology evolution of probeless friction stir spot welded joints of aluminum alloy. *J. of Materials Proc. Technology*, **252**, 69–80.
- Knysh, V.V., Klochkov, I.M., Motrunich, S.I., Poklyatsky, A.G. (2021) Influence of irregular cyclic load on fatigue resistance of thinsheet welded joints of heat-strengthened aluminium alloys. *The Paton Welding J.*, **1**, 9–13.
- de Castro, C.C., Plaine, A.H., Dias G.P. et al. (2018) Investigation of geometrical features on mechanical properties of AA2198 refill friction stir spot welds. *J. Manuf. Processes*, **36**, 330–339.
- Hatamleh, O., Rivero, I.V., Swain S.E. (2009) An investigation of the residual stress characterization and relaxation in peened friction stir welded aluminium-lithium alloy joints. *Mater. Des.*, **30**, 3367–3373.
- Motrunich, S., Klochkov, I., Poklyatsky, A. (2020) High cycle fatigue behaviour of thin sheet joints of aluminium-lithium alloys under constant and variable amplitude loading. *Weld World*, **64**, 1971–1979.
- Weglowski, M.St., Blacha, S., Phillips, A. (2016) Electron beam welding — Techniques and trends — Review. *Vacuum*, **130**, 72–92.
- Cui, L., Li, X., He, D. et al. (2012) Effect of Nd:YAG laser welding on microstructure and hardness of an Al–Li based alloy. *Mater. Charact.*, **71**, 95–102.
- Chen, G., Yin, Q., Zhang, G., Zhang, B. (2020) Fusion-diffusion electron beam welding of aluminium-lithium alloy with Cu nano-coating. *Mater. Des.*, **188**, 108439.
- Chen, G., Yin, Q., Zhang, G., Zhang, B. (2020) Underlying causes of poor mechanical properties of aluminum-lithium alloy electron beam welded joints. *J. Manuf. Process.*, **50**, 216–223.

Received 22.03.2021

**MAY 15, 2006** Cloud Gate sculpture was opened. It is located in the business quarter of Chicago, USA. Its author is the Indian-born British artist Anish Kapoor (born in 1954). The sculpture consists of 168 stainless steel plates, welded together and polished so well that its exterior has no visible welds. The dimensions of the sculpture are 10 (height), 20 (length) and 13 (width) m, its weight is about 100 t. Welders used hybrid laser-arc welding. Cloud Gate is one of the most famous and recognizable monuments of our time. It is believed that the sculpture form was inspired by a mercury drop.



**MAY 22, 2012** Opening of Tokyo Skytree — TV tower in Sumida district (Tokyo, Japan). It is the world's tallest TV tower of 634 m height and the second in height construction in the world after «Burge-Halifa». The entire structure of the tower consists of «lattice» elements, each of which is a combination of triangles, as part of other components. These elements are connected through branch joints and pipes. All the structures are joined by welding directly to the main support, without application of any other fastening systems or methods. This type of connection has a very simple appearance and high seismic resistance.



## CALCULATION OF RESIDUAL STRESS-STRAIN STATE OF DEPOSITED STEEL SHEET PLATES

I.K. Senchenkov<sup>1</sup>, I.O. Ryabtsev<sup>2</sup>, O.P. Chervinko<sup>1</sup> and A.A. Babinets<sup>2</sup>

<sup>1</sup>S.P. Timoshenko Institute of Mechanics of the NAS of Ukraine  
3 Nesterov Str., 02000, Kyiv, Ukraine

<sup>2</sup>E.O. Paton Electric Welding Institute of the NAS of Ukraine  
11 Kazymyr Malevych Str., 03150, Kyiv, Ukraine. E-mail: office@paton.kiev.ua

Finite-element calculation procedure was developed and stress-strain and microstructural state was studied at single- and two-layer surfacing of 3 mm sheets from St3 steel by Sv-Kh19N18G6M3V2, PP-Np-25Kh5FMS and Sv-08A wires. Calculations of SSS, microstructural state and shape change of the sheets at surfacing under the smooth support conditions were performed. The model of plane-deformation state (PDS) predicts greater deflections, compared to the model of plane-stress state (PSS), except for materials with martensite transformations (PP-Np-25Kh5FMS). At surfacing by materials with martensite transformations, greater deflections are in place due to volumetric effects of transformation. Except for deposited metal with martensite transformations (25Kh5FMS), the model of simultaneous deposition of a layer predicts greater deflection, compared to that of bead-by-bead deposition and it can be used for assessment of upper deflection limit. Satisfactory correlation was obtained for calculated and experimental data on surfaced sheet deflections. Rational schemes of supporting and fastening the element edges were determined, which provide minimum residual deflections. Ref. 7, 1 Table, 7 Figures.

*Keywords:* arc surfacing, stress-strain state, surfaced sheet deformations, Bodner–Partom model, deflection calculation procedure

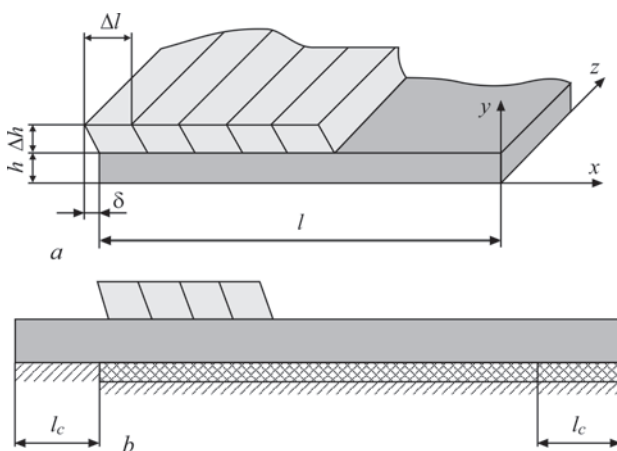
The work is devoted to development of a procedure of calculation of the current and residual stress-strain and microstructural state, as well as deflections of 3 mm steel sheets at deposition of steel layers with different structure and properties. Processes with single- and two-layer surfacing are considered. St3 sheets of 3 mm thickness surfaced by Sv-Kh19N18G6M3V2, PP-Np-25Kh5FMS and Sv-08A wires were selected as the objects of study.

Figure 1 shows the scheme of deposition and shape of beads, as well as conditions of fastening the side edges of the sheets during surfacing, which were accepted when developing the calculation procedure. A scheme of rigid fastening of the sheet left edge and movable fastening of its right edge is considered. The following is assumed:  $l = 100$  mm;  $h = 3$  mm;  $\Delta h = 2.4$  mm,  $\Delta l = 5$  mm,  $l_c = 25$  mm. The bead deposition rate was 31 m/h. Sheet length along  $Oz$  axis was  $L = 200$  mm.

The scheme of simultaneous (instantaneous) deposition of the bead in  $Oz$  direction is used in order to reduce the three-dimensional problem to a two-dimensional one. The task is now limited to the problem of plane deformation state (PDS) or plane stress state (PSS) in  $Oxy$  plane, depending on the conditions of fastening and supporting of the sheet.

At two-layer surfacing, the schemes of deposition of second layer beads without shifting (Figure 2, *a*) and with their 50 % shifting are considered (Figure 2, *b*). The scheme with sequential simultaneous deposition of applied metal layers with an interval, which is dictated by deposition conditions (Figure 2, *b*) is considered as the simplified one.

Experimental studies of deformation of 3 mm St3 steel sheets during surfacing were conducted by the following scheme. Surfacing with Sv-Kh19N18G-



**Figure 1.** Scheme of deposition and shape of the beads (*a*) and conditions of fastening the side edges of the sheets during surfacing (*b*)

6M3V2 wire ensured producing deposited metal with an austenitic structure; with PP-Np-25Kh5FMS wire — martensitic-bainitic deposited metal with a small quantity of residual austenite; with Sv-08A wire — producing ferritic-pearlitic deposited metal, close in its chemical composition to base metal. Selection of exactly such surfacing materials is attributable to the difference in their physico-mechanical properties and structural state, compared to base metal, and, accordingly, to their anticipated different impact on the level of residual stresses and strains in the surfaced sheets.

So, at surfacing by Sv-Kh19N18G6M3V2 wire the level of deformations of St3 sheets will depend on the impact of local heating and considerable difference in the coefficient of thermal expansion (CTE) of the base and deposited metal. For PP-Np-25Kh5FMS wire it will depend on the impact of local heating and martensite transformation, which is accompanied by an increase of the deposited metal volume, as the difference in CTE is minimal in this case. At surfacing by Sv-08A wire the strain level will depend only on the impact of local heating, as there is practically no difference between the base and deposited metal in CTE and structural state.

Surfacing by all the wires was performed as individual beads with  $\approx 50\%$  overlapping of the adjacent beads in the same mode: 150 A current; 22 V voltage; 31 m/h deposition rate. Such a surfacing mode provided a deposited layer  $\approx 2.4$  mm thick. Sheet surfacing was performed in one and two layers for each type of wire.

Sheets to be surfaced were fastened on the welding table with copper surface and were clamped to it using two steel straps in keeping with the design scheme: one of the straps pressed the sheet edge to the table, completely preventing its movement (rigid fastening), and the other did not allow the sheet edge deforming

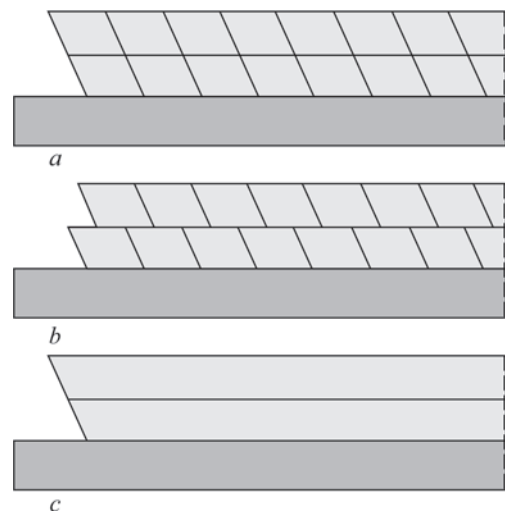


**Figure 2.** Scheme of two-layer surfacing of the sheets: *a* — without displacement of the second layer beads; *b* — with displacement of the second layer beads

in the vertical direction, but enabled its shifting in the horizontal plane (movable fastening) (Figure 3).

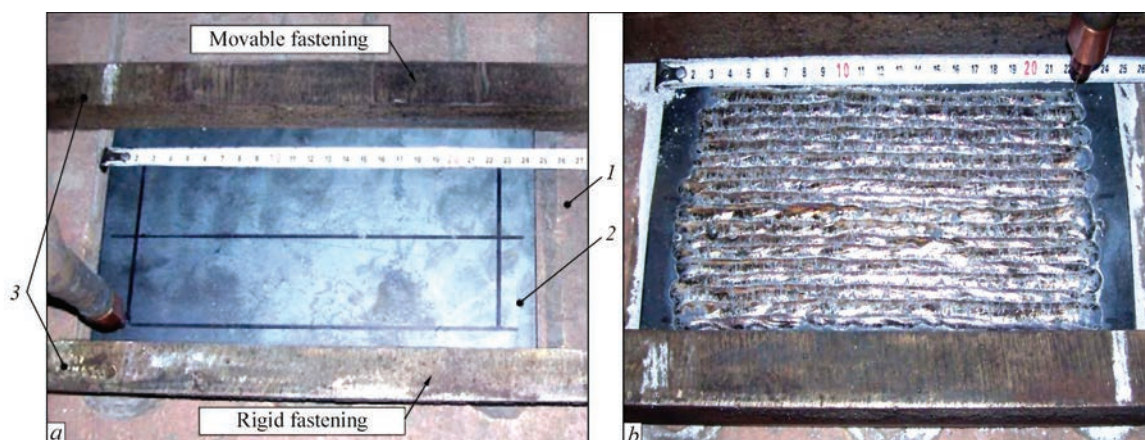
Surfacing of sheets with similar fastening, but with a gap between the sheets and the table was also performed. Surfacing of each sheet was begun from the side of rigid fastening and continued to the other edge without pauses for cooling. After surfacing of the entire sheet, the clamping strap was not removed up to its complete cooling.

Figure 4 shows the sheets after one-layer surfacing by three different wires.

At calculations bead deposition was modeled within a model of growing bodies [1]. This model uses nonclassical boundary conditions on the treated surface [2, 3].

Thermoviscoplastic behaviour of the base metal and deposited beads is described by Bodner–Partom model [4]. Model parameters, as well as thermophysical characteristics are specified using experimental data.

Microstructural transformations are modeled, using thermokinetic diagrams (TKD) of overcooled



**Figure 3.** Method of fastening the sheets on the welding table (*a*): 1 — welding table with copper plate; 2 — sheet being surfaced; 3 — clamping straps; (*b*) — appearance of sheets after surfacing

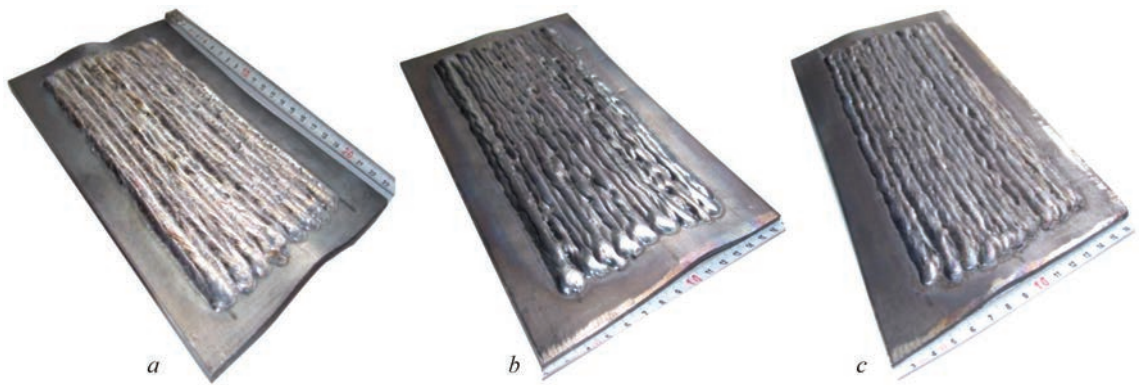


**Figure 4.** Appearance of deformed sheets after one-layer surfacing by the following wires: *a* — Sv-Kh19N18G6M3V2; *b* — Sv-08A; *c* — PP-Np-25Kh5FMS

austenite decomposition [5, 6]. For steels under consideration these diagrams were digitized for use in calculations.

Mathematical definition of the problem includes the following relationships:

- equations of equilibrium and heat conductivity

$$\text{div} \sigma = 0, \quad \bar{c}_v \dot{\theta} = \text{div}(\bar{k} \text{grad } \theta) + Q, \quad (1)$$

with thermal boundary and initial conditions

$$\begin{aligned} -k \bar{n} \text{grad } \theta &= -q + \gamma(\theta - \theta_c) + \sigma \varepsilon(\theta^4 - \theta_0^4); \\ \theta &= \theta_0 \text{ at } t = 0; \end{aligned} \quad (2)$$

- determining equations

$$\varepsilon_{ij} = \varepsilon_{ij}^e + \varepsilon_{ij}^p + \varepsilon_{ij}^{\theta ph} + \varepsilon_{ij}^*, \quad \varepsilon_{kk}^p = 0; \quad (3)$$

$$\begin{aligned} s_{ij} &= 2G(e_{ij} - \varepsilon_{ij}^p - e_{ij}^{\theta ph} + e_{ij}^*), \\ \sigma_{kk} &= 3K_V(\varepsilon_{kk} - \varepsilon_{kk}^{\theta ph} - \varepsilon_{kk}^*); \end{aligned} \quad (4)$$

- flow equations

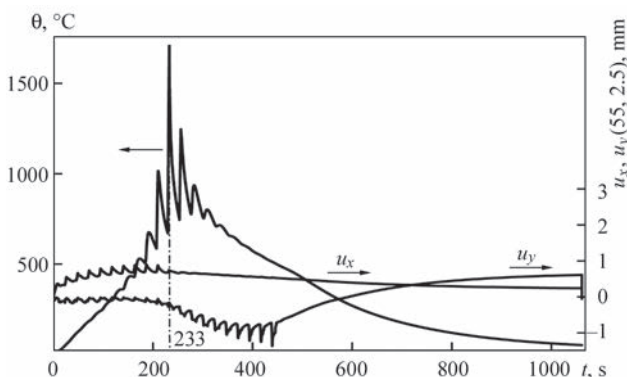


**Figure 5.** Temperature and movement of base point under the 11<sup>th</sup> bead in time. Surfacing with Sv-08A solid wire

$$\begin{aligned} \dot{\varepsilon}_{ij}^p &= D_0 \exp \left\{ -\frac{1}{2} \left[ \frac{(\bar{K}_0 + K)^2}{3J_2} \right]^n \right\} s_{ij} / s_i, \\ \varepsilon_{ij}^p(0) &= 0; \end{aligned} \quad (5)$$

for base metal  $\varepsilon_{ij}^*(0) = 0$ ;

- evolution equation for isotropic strengthening parameter

$$\dot{K} = m_1 (\bar{K}_1 - K) \dot{w}^p, \quad K(0) = 0, \quad (6)$$

where  $G$ ,  $G_f$  and  $K_v$ ,  $K_{vf}$  are the shear and bulk compression moduli; dash on top means calculation by the rule of mixture  $\overline{(\bullet)} = (\bullet)_\xi C_\xi$ ,  $C_\xi$  are the volume phase concentrations,  $\xi = A, F, P, B, M$  of austenite, ferrite, pearlite, bainite and martensite, respectively;  $K_{\xi 0}$ ,  $K_{\xi 1}$ ,  $m_1$ ,  $n$ ,  $D_0$  are the model parameters;  $\dot{w}^p$  is the plastic power;  $s_i$  is the second invariant of the stress tensor;  $\dot{w}^p = \sigma_{ij} \dot{\varepsilon}_{ij}^p$ ;  $s_i^2 = 1/2 s_{ij} s_{ij}$ ;  $Q$  is the heat source;  $\varepsilon_{ij}^*$ ,  $\theta^*$  are the strains and temperature of element  $\Delta v(t^*)$  at the moment of its build-up that ensure conditions  $\sigma_{ij}(\varepsilon_{ij}^*, \theta^*) = 0$  in  $\Delta v(t^*)$  at build-up moment  $t = t^*$ ,  $k$  and  $\bar{c}_v$  are the coefficients of heat conductivity and volumetric heat capacity;  $\varepsilon_{ij}^{\theta ph}$  is the thermal phase strain.

Mechanical boundary conditions are specified by those of surfacing and fastening of the element.

The problem of thermomechanical state of the surfaced parts is solved numerically by finite element method [7]. An eight-node rectangular finite element is used. Nonstationary equations are integrated by implicit time-stepping schemes with variable integration step. Iteration processes at each step are accelerated using Stephenson–Aitken procedure.

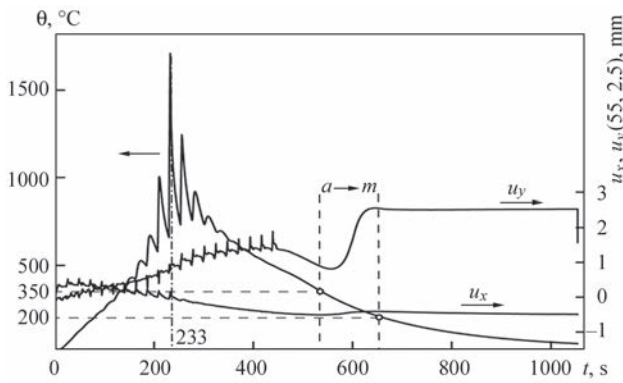


**Figure 6.** Temperature and movement of base point under the 11<sup>th</sup> bead in time. Surfacing by PP-Np-25Kh5FMS flux-cored wire

Influence of martensite transformation on the kinetics of temperature and movements under the conditions of surfacing with a gap between the sheet and support is illustrated in the point in the base material under the 11<sup>th</sup> bead, which is deposited at moment of time  $t_{11} = 2.33$  s. Such curves are given in Figure 5 for surfacing with Sv-08A wire and in Figure 6 for the case of surfacing by PP-Np-25Kh5FMS wire.

In the second case, an essential increase of deflection in the area of martensite transformation is in place. Points on the temperature curve in Figure 6 indicate the moments of entering the region of austenite-martensite transformation and leaving it. Dashed curves limit this area on axes  $\theta$  and  $t$ . Instantaneous change of deflection at  $t \approx 1100$  °C corresponds to releasing the right edge of the sheet from smooth fastening.

Experimentally, the characteristic deflections of the surfaced sheets were determined as follows. After cooling down and releasing of the fastened edges, the sample was placed on a smooth plate and normal displacement of the sheet upper surface relative to the plate was measured by an indicator. The maximum local value of the above-determined deflection in the cross-section of the surfaced part of the sheet was taken as the characteristic deflection (Figure 7). With such a definition the characteristic deflection is always positive.

Experimental and calculated data on deflection of sheets (mm), surfaced by different wires in one layer\*

Supporting conditions	PDS/PSS	Surfacing materials								
		Sv-Kh19N18G6M3V2			PP-Np-25Kh5FMS			Sv-08A		
		1	2	3	1	2	3	1	2	3
Smooth	PDS	1.45	1.61	0.7	1.52	1.69	1.7	1.21	1.22	0.7
	PSS	1.34	1.38		1.93	1.72		1.13	1.12	
With a gap	PDS	2.77	2.18	2.0	2.81	4.96	2.5	2.84	2.27	1.2
	PSS	2.66	1.68		2.55	4.22		2.35	1.69	

*Notes.* \*Columns with numbers 1 and 2 correspond to calculated data at simultaneous and bead-by-bead deposition, respectively. PDS and PSS lines correspond to calculation models. No.3 columns correspond to experimental data. Deflections are determined after cooling and releasing the edges.

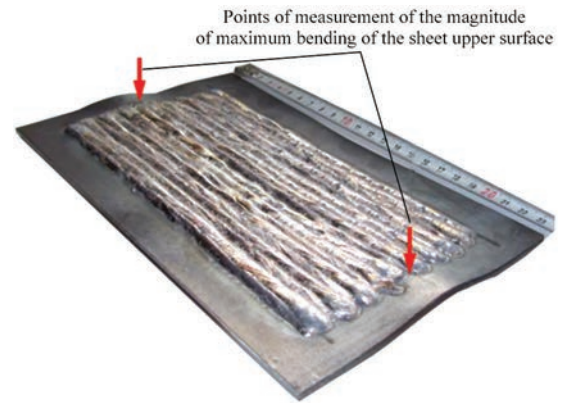


**Figure 7.** Scheme of measurement of the magnitude of sheet deformation after surfacing

For three Sv-Kh19N18G6M3V2, PP-Np-25Kh5FMS and Sv-08A wires the experimental and calculated data for the characteristic deflections at one-layer surfacing under the conditions of smooth support are given in the Table.

As one can see from the tabulated data, PDS model predicts greater deflections, compared to PSS model, except for materials with martensite transformations (25Kh5FMS). At deposition of materials with martensite transformations greater deflections are in place, because of bulk transformation effects. It should be also noted that much greater deformations are observed at surfacing with a gap between the sheet and the welding table, than in the case of tight pressing of the sheet to the table.

Similar calculations were conducted for the case of two-layer surfacing. In particular, at calculation of two-layer surfacing by Sv-08A solid wire the following results on deflections were obtained under the conditions of smooth support: schemes without bead overlapping (Figure 2, a) — 1.02 mm for PDS model, and 0.91 mm for PSS model. The scheme of sequential simultaneous deposition of the layers yields the following deflection values: 1.00 mm for PDS, and 0.91 mm for PSS. Experimental values of deflection were 0.8 mm. Results of calculation of the deflections for the case of bead deposition with overlapping and without overlapping coincide with less than 10 % discrepancy.

Discrepancy of the given calculated and experimental results is determined, on the one hand, by inaccuracy of the mathematical model in terms of ignoring the contact interaction of the sheet with the supporting surface, and on the other hand — by technical difficulties in ensuring experimental studies under all the conditions of fastening the sheet edges.

### Conclusions

1. The numerical finite-element procedure for calculation of the current and residual stress-strain and microstructural state of surfaced sheets was improved, in order to take into account the conditions of their fastening during surfacing.

2. Calculations of SSS, microstructural state and change of the shape of the sheets at surfacing under the conditions of smooth support were performed. It is found that these conditions provide a smaller residual deflection, compared to those of the free boundary on the element lower surface. Influence of the conditions of element fastening on the maximum values of residual deflections, as well as of the effect of microstructural transformations in the deposited metal was assessed.

3. PDS model predicts greater deflections, compared to PSS model, except for materials with martensite transformations (25Kh5FMS). At deposition of materials with martensite transformations greater

deflections are found due to the bulk effects of transformation.

4. Except for the deposited metal with martensite transformations (25Kh5FMS), the model of simultaneous deposition of a layer predicts greater deflection, compared to the model of bead-by-bead deposition, and it can be used for assessment of the upper deflection boundary.

5. Calculation results satisfactorily correlate with the experimental data.

1. Senchenkov, I.K. (2005) Thermomechanical model of growing of cylindrical bodies from nonlinear materials. *Prikl. Mekhanika*, 41(9), 118–126 [in Russian].
2. Ryabtsev, I.A., Senchenkov, I.K., Turyk, E.V. (2015) *Surfacing. Materials, technologies, mathematical modeling*. Gliwice, Silesia Polytechn. In-te, 44–100 [in Polish].
3. Ryabtsev, I.A., Senchenkov, I.K. (2013) *Theory and practice of surfacing works*. Kyiv, Ekotekhnologiya [in Russian].
4. Bodner, S.R. (2000) *Unified plasticity — an engineering approach*. Final Rep. Technion. Israel Inst. of Tech., Haifa.
5. Popov, A.A., Popov, A.E. (1961) *Isothermal and thermokinetic diagrams of overcooled austenite decomposition*: Refer. Book of heat-treater. Moscow-Sverdlovsk. GNTI Mashlit [in Russian].
6. Shorshorov, M.Kh., Belov, V.V. (1972) *Phase transformations and change of steel properties in welding*: Atlas. Moscow, Nauka [in Russian].
7. Motovilovets, I.A., Kozlov, V.I. (1987) *Mechanics of related fields in materials and structure elements*. In: 5 Vol., Vol. 1: *Thermoelasticity*. Kiev, Naukova Dumka [in Russian].

Received 19.04.2021

## SUBSCRIPTION-2021



«The Paton Welding Journal» is Published Monthly Since 2000 in English, ISSN 0957-798X, doi.org/10.37434/tpwj.

«The Paton Welding Journal» is Cover-to-Cover Translation to English of «Automatic Welding» Journal Published Since 1948 in Russian and Ukrainian.

«The Paton Welding Journal» can be also subscribed worldwide from catalogues subscription agency EBSCO.

If You are interested in making subscription directly via Editorial Board, fill, please, the coupon and send application by Fax or E-mail.

12 issues per year, back issues available.

\$384, subscriptions for the printed (hard copy) version, air postage and packaging included.

\$312, subscriptions for the electronic version (sending issues of Journal in pdf format or providing access to IP addresses).

Institutions with current subscriptions on printed version can purchase online access to the electronic versions of any back issues that they have not subscribed to. Issues of the Journal (more than two years old) are available at a substantially reduced price.

The archives for 2009–2019 are free of charge on [www://patonpublishinghouse.com/eng/journals/tpwj](http://www://patonpublishinghouse.com/eng/journals/tpwj)

### Address

11 Kazymyr Malevych Str. (former Bozhenko Str.), 03150, Kyiv, Ukraine

Tel.: (38044) 200 60 16, 200 82 77; Fax: (38044) 200 82 77

E-mail: [journal@paton.kiev.ua](mailto:journal@paton.kiev.ua); [www://patonpublishinghouse.com/eng/journals/tpwj](http://www://patonpublishinghouse.com/eng/journals/tpwj)

# PULSE-PLASMA MODIFICATION OF SURFACE OF STEEL HOT DRAWING DIES OF TITANIUM ALLOY PRODUCTS

**Yu. M. Tyurin<sup>1</sup>, O.V. Kolisnichenko<sup>1</sup>, V.M. Korzhyk<sup>1</sup>, I.D. Gos<sup>1</sup>, O.V. Ganushchak<sup>1</sup>,  
Jin Ying<sup>2</sup> and Zhong Fengping<sup>2</sup>**

<sup>1</sup>E.O. Paton Electric Welding Institute of the NAS of Ukraine

11 Kazymyr Malevych Str., 03150, Kyiv, Ukraine. E-mail: [vnkorzhyk@gmail.com](mailto:vnkorzhyk@gmail.com)

<sup>2</sup>Zhejiang Academy of Special Equipment Science

310016, Jianggan District, Hangzhou, Zhejiang, 211, Kaixuan Road. E-mail: [jinying@zjtj.org](mailto:jinying@zjtj.org)

The technology of pulse-plasma modification of the working surface of the die of 4Kh5MF1S tool steel (analogues are X40CrMoV5-1 in the EU and 4Cr5MoSiV1 in China) was considered. The mentioned tool is used for stamping billets of titanium VT6 alloy (wt.%: Al — 3.0–6.8; V — 3.5–5.0; Ti — base), which is performed at temperatures of up to 700 °C. The die surface is heated, which leads to its oxidation and diffusion redistribution of alloying elements. Pulse-plasma stamping leads to the formation of elastic-plastic deformations of the surface layer in a tool steel, which in combination with pulsed thermal and electromagnetic effects provides a refinement of the alloy structure and intensifies the diffusion mechanisms of alloying elements. The studies showed that the modified layer (over 80 μm thickness) in 4Kh5MF1S steel, formed in the process of pulse-plasma treatment, contains up to 2.5 % carbon, up to 12 % oxygen and up to 3 % tungsten. In the mentioned layer the presence of nanocrystalline structures with a size of less than 100 nm was revealed. The hardness of the modified layer is more than 700  $HV_{0.025}$ . The surface roughness after pulse-plasma treatment did not change. Experience of industrial use of this technology showed that modification of a surface of the die from 4Kh5MF1S steel provided its high serviceability at a deep drawing of products from the heated (to 700 °C) sheet of VT-6 titanium of 3 mm thickness. 11 Ref., 1 Table, 6 Figures.

*Keywords:* plasma treatment, alloying, tool steels, die, titanium deformation, structuring, wear resistance, serviceability

It is known that nanocrystalline materials have high characteristics of strength and heat resistance [1], but their production in large quantities is currently problematic. The technology of pulse-plasma modification allows modifying the surface layer of a metallic product without its heating. The modification process is accompanied by alloying and nanostructuring of the surface layer. The mechanism of this process is described in the monograph [2].

The working surface of a stamping tool is exposed to the highest loads. Therefore, its modification will significantly increase the capabilities of stamping technology during the deformation of titanium-based alloys. It is proposed to nanostructure and alloy the die surface layer by carbon, oxygen and tungsten. The presence of alloying elements in the surface layer of stamped steel blocks the possibility of oxidation and diffusion processes when the die is heated. Extremely high content of carbon and oxygen in the metal alloy eliminates the chemical and thermal processes of its interaction with

titanium, even at high temperatures. Pulse-plasma technology of alloying and nanostructuring of the surface layer is considered in more detail in [3].

The aim of the work is to create a resource-saving effective technology for modifying the surface layer of a stamping tool, which provides its high serviceability in the deformation of chemically active materials and alloys, for example, based on titanium.

Analysis of the work of the tool made of stamped steel after chemical-heat treatment shows [4, 5] that its maximum serviceability is observed after a complex alloying of the surface layer. Thermodiffusion saturation is carried out, as a rule, at a high temperature (900–1100 °C). A long-term heating complicates heat treatment, requires additional power consumption and, furthermore, causes the growth of crystals. Currently, technologies are being developed that allow changing the structural-phase composition of the surface layer to a depth of tens of microns. The technologies of surface laser strengthening, alloying

Yu. M. Tyurin — <http://orcid.org/0000-0002-7901-7395>, O.V. Kolisnichenko — <http://orcid.org/0000-0003-4507-9050>,  
V.M. Korzhyk — <http://orcid.org/0000-0001-9106-8593>, I.D. Gos — <http://orcid.org/0000-0002-9469-8002>,  
O.V. Ganushchak — <http://orcid.org/0000-0003-4392-6682>, Jin Ying — <http://orcid.org/0000-0002-9551-5036>,  
Zhong Fengping — <http://orcid.org/0000-0002-2046-7199>

© Yu. M. Tyurin, O.V. Kolisnichenko, V.M. Korzhyk, I.D. Gos, O.V. Ganushchak, Jin Ying, Zhong Fengping, 2021

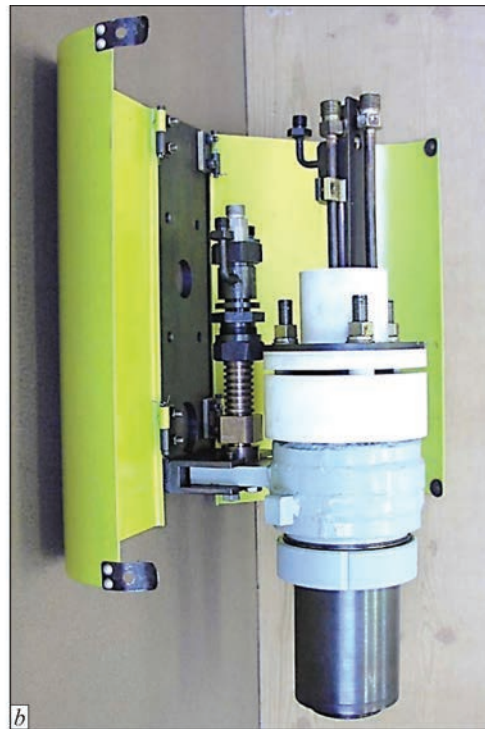
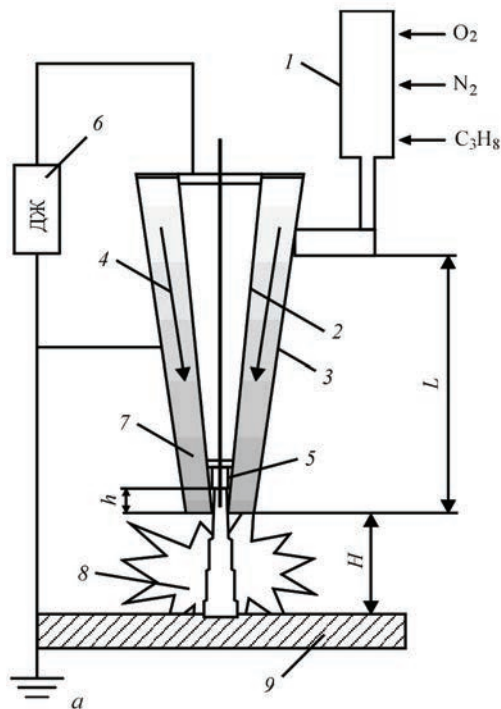


**Figure 1.** Pulse plasma generator for surface modification: scheme of operating generator (a) and appearance of generator on the manipulator arm (b)

and nitriding [5, 6], vacuum plasma devices with adjustable atmospheric composition and pressure for surface treatment of tool materials are used [7]. An axial electromagnetic plasma accelerator for surface modification [8] was created, which represents a ballistic plasmatron based on the principle of adiabatic compression of the plasma-forming medium, [9].

The article presents the results of stamped steel modification applying a coaxial pulse-plasma generator [9]. Pulse-plasma treatment provides a rapid heating ( $10^{-3}$ – $10^{-4}$  s) of the surface layer of steel with a subsequent intensive cooling. High heating and cooling rates up to  $10^7$  K/s lead to deformation of the surface layer and, as a consequence, the formation of nanocrystalline structure and high dislocation density. It is possible to introduce different alloying elements into plasma, which in combination with the pulsed electromagnetic influence and elastic-plastic deformation intensifies the mechanisms of their diffusion into the surface layer [10, 11].

To modify the working surface of the dies, a pulse-plasma generator (Figure 1) was used, consisting of a detonation chamber 1, in which the formation and combustion of a combustible gas mixture ( $C_3H_8$ ,  $O_2$ ,  $N_2$ ) and coaxial electrodes 2, 3 is carried out. A flow of combustion products 4 is formed between the electrodes, having a frequency that can vary within 1–5 Hz. Along the axis of the plasmatron a consumable electrode 5 is located, which evaporates and enriches the plasma with alloying elements.

As a result of detonation combustion of the combustible mixture in the plasma generator, ionized combustion products 7 are formed, which close the  $R-L-C$  circuit of the power source. In the interelectrode gap of the plasma generator, an electric current flows behind the front of the detonation wave along the cross volume of the gas, the degree of ionization of which subsequently increases. Plasma jet 8 from the generator nozzle flows on the modified surface 9 (cathode). Around the central electrode 2 and the plasma jet 9, an azimuthal magnetic field is formed, which interacts with the current  $I$  flowing in the interelectrode gap and creates an electromagnetic force that accelerates and focuses the plasma. In addition, during the flow of electric current, Joule heat is released, which due to the expansion of the heated volume of gas also enhances the gas-dynamic component of the plasma, carrying out rapid heating of the surface layer (Figure 2).

The calculated power characteristics of the plasma jets at the output of the plasma generator have a linear dependence on the electric field strength and the length of the interelectrode gap. Thus, at the length of the interelectrode gap  $L = 300$  mm and the electric field strength of 400 kV/m, the plasma jet can have a temperature of 25000 K and a velocity of 8 km/s [2].

The plasma jet closes the electrical circuit between the consumable electrode and the surface of a product. A thin layer of material at the end of the consumable electrode is overheated and destroyed by an explosion (transition to a stable state from metastable one), which

provides synchronization of the introduction of heated and accelerated elements forming the electrode into the plasma jet. In the zone of inhibition of the plasma jet on the treated surface a layer of shock-compressed plasma and electrode erosion products is formed. The duration of interaction of this layer with the surface of a product is 0.4–0.6 ms, the heat flux varies in the range of  $0.3 \cdot 10^5$ – $1.4 \cdot 10^6$  W/cm<sup>2</sup>. The heat flux is regulated by the  $R$ – $L$ – $C$  parameters of the power source circuit, the distance  $H$  and the depth of the electrode  $h$ . The deepening of the electrode mainly affects the diameter of the spot of the plasma contact with the surface of a product (8–25 mm). This in turn allows adjusting the heat flux density at the same pulse energy. In the course of experiments, it was found that under pulse-plasma exposure for 3–5 ms, the products of plasma-chemical synthesis from the interelectrode gap flow and condense on the surface between the pulses. Subsequent plasma pulse melts a thin surface layer, mixing and saturating it with alloying elements. This provides the possibility of additional alloying of the surface layer by preliminary surfacing of alloying elements on the surface of a product.

On the basis of the theoretical analysis of the non-stationary equation of thermal conductivity, the evaluation of heat flows was carried out and change of temperature in time for one pulse of duration  $t = 0.6$  ms and power  $q = 7.2 \cdot 10^8$  W/m<sup>2</sup> at different distance from the surface at steel surface treatment was calculated. Calculations showed that heating and cooling rates reach  $10^7$  K/s, and the temperature gradients across the thickness of the modified layer are  $2.5 \cdot 10^7$  K/m. In the period between the pulses (at a frequency of 2 Hz), the surface layers heated to the melting point have time to cool. A repeated pulse-plasma effect on the surface leads to a periodic deformation of the surface layers, phase hardening and refinement of the structure.

The experiments were performed on a stamped steel of grade 4Kh5MF1S (the analogues are Kh40CrMoV5-1 in the EU and 4Cr5MoSiV1 in China), which is used for manufacture of tools operating in the conditions of long-term heat changes to the temperatures of 630 °C (press stamp, needles for pipe piercing, hammer and press inserts, tool for upsetting of billets, etc.). To increase the heat resistance of the working layer of the tool, it is proposed to increase the content of tungsten, oxygen and carbon in the surface layer, as well as to change its structure to nanocrystalline. The following technological parameters of pulse-plasma treatment were established: inductance of the discharge circuit  $L$  — 30  $\mu$ H, capacitance of the capacitor bank  $C$  — 960  $\mu$ F and voltage on the coatings of the capacitor bank  $U$  — 3.2 kV, eroded

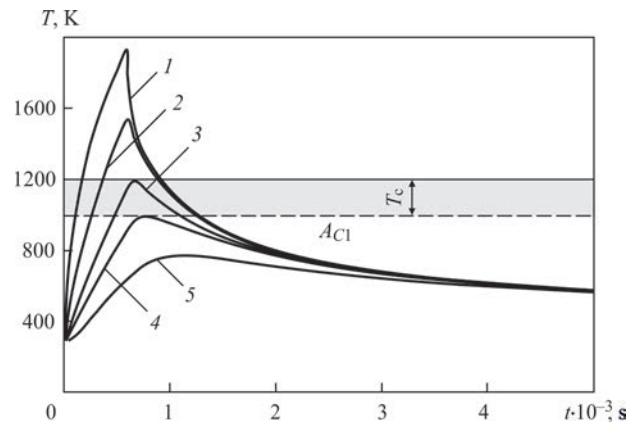


**Figure 2.** Change in temperature in the specimen layer at the depth: 1 — 0; 2 — 20; 3 — 40; 4 — 60; 5 — 100  $\mu$ m

electrode —  $W$ . Additional introduction of carbon is carried out by applying graphite coatings to the surface. Consumption of gases: propane — 0.38; oxygen — 1.04; air — 1.13 m<sup>3</sup>/h. The potential was supplied from the power source to the product/specimen, which enhanced the plasma effect by switching the power of the electric discharge between the generator electrode (anode) and the modified surface (cathode). The number (5 times) of plasma overlaps on the modified surfaces was established. As is noted above, a change in the value of deepening of the consumable electrode leads to a change in the diameter of the treatment spot, and, accordingly, the heat flux density into a product. For pulse-plasma treatment of specimens and a die a depth at a value  $h = 25$  mm was set. The diameter of the visible treatment area was 18 mm. The specimen and dies were treated at a distance  $H = 50$  mm. This mode provided a fairly high power density, which melted and evaporated the material from the specimen surface.

Using the methods of optical metallography, visible traces of surface melting were detected on the specimen. Microscopic analysis of the modified surface layer produced with the supply of potential, performed using an electron-ion scanning microscope Quanta 200 3D, showed that on the surface of the specimen a modified layer of up to 100  $\mu$ m thickness was formed (Figure 3), which has no distinct boundary with the base metal. The hardness of the surface layer increased by 3 times to  $774 HV_{0.025}$ , and the hardness of the specimen material at a depth of 80  $\mu$ m is up to  $674 HV_{0.025}$ , which is twice higher than the hardness of the base.

A high power density provided refinement of the structure of the surface layer due to high temperature gradients. However, element-by-element analysis did not show the presence of elements, forming plasma in the layer, which is probably predetermined by a high temperature, evaporation and destruction of a thin

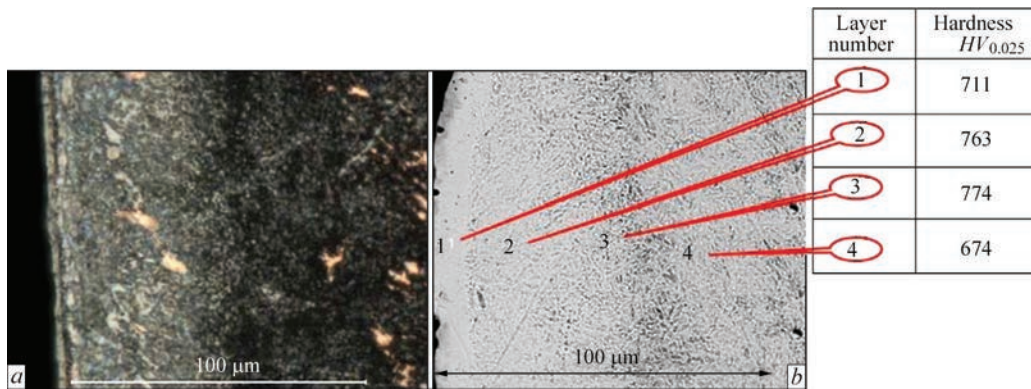


**Figure 3.** Surface analysis with the use of: *a* — optical inverted microscope OLIMPYXS GX 51; *b* — electron-ion scanning microscope Quanta 200 3D

surface layer. The surface of the specimen had roughness and traces of melting, oxidation, carbon deposition and spraying of the material.

X-ray diffraction analysis confirmed a significant oxidation. On the surface carbon is present, deposited from the graphite coating and condensed from the combustion products. Alloying elements in such conditions are oxidized and removed from the surface together with the destroyed layer of the base metal of the specimen.

Examination of the specimen in a transmission electron microscope equipped with a system of energy-dispersive microanalysis allowed determining that alloying of the surface layer was carried out to a depth of 80 μm (Figure 4). The upper molten layer at a depth of up to 5 μm contains up to 11.81 wt.% of oxygen, 2.19 wt.% of tungsten and 1.28 wt.% of carbon. At a depth of 20–80 μm, the modified layer has 2.3 times (points 2, 3, 4 in Figure 3) increased content of tungsten (3.83, 4.36 and 3.50 wt.%, respectively) and carbon (1.2–4.36 wt.%). The bases of the modified layer do not contain oxygen. In a thin «white» layer (point 1 in Figure 4), inhomogeneities are seen, which are probably predetermined by a nonuniform oxidation (oxygen content is up to 11.81 %).

A crystalline structure of the modified layer contains discrete elements smaller than 100 nm (Figure 5). In the surface layer at a depth of up to 6 μm,

the presence of a crystalline structure is not observed. The modified layer consists of a nanocrystalline alloy having apparently amorphous layers.

In the surface layer of stamped steel, the concentration of the main elements (tungsten, oxygen, carbon), affecting the heat resistance of this layer increased. Tungsten was introduced into the plasma jet in the form of erosion products of the metal electrode (rod), carbon was introduced from the surface in the form of an interlayer, and oxygen is a component of the plasma. The formation of a dense oxidized layer on the surface of the stamped steel closes it from the further oxidation and prevents the contact of metals of the stamped alloy and the die. The distribution of alloying elements across the thickness of the modified layer was determined using an atomic emission spectrometer of a glow discharge. Precision quantitative layer-by-layer analysis of a stamped steel after pulse-plasma treatment with the introduction of tungsten, carbon and oxygen into the plasma showed that alloying elements are located at a depth of up to 80 μm (see Figure 4). In the surface layer, a new material with a high content of alloying elements was formed.

It is expected that additional alloying of a stamped steel surface by carbon and oxygen will reduce the effect of oxygen during operation of the dies. Pulse-plasma treatment of a product and a complex alloying will

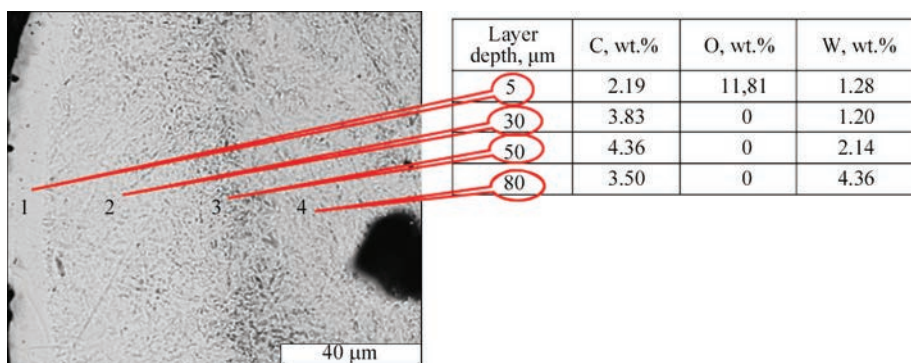


**Figure 4.** Results of analysis of alloying with carbon, oxygen and tungsten. Treatment by direct plasma (with a supply of potential)

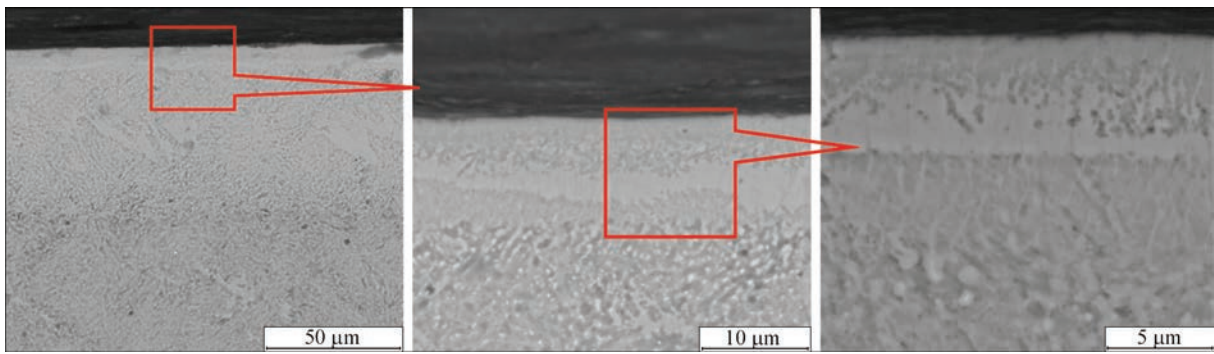


**Figure 5.** Microscopic analysis of the modified surface layer obtained by supply of a potential. Electron-ion scanning microscope Quanta 200 3D. Etching by Rzeszotarski’s reagent



**Figure 6.** Surface of the die for deep drawing of products from VT-6 titanium sheet: *a* — unmodified; *b* — modified with a pulse plasma by complex alloying with carbon, tungsten and oxygen

increase the service life of the stamping tool surface and eliminate failures because of brittle fractures.

Taking into account the previous work, the working surfaces of a large-sized matrix of the die for hot drawing of a titanium sheet from VT-6 alloy of 3 mm thickness were modified (Figure 6). The working area of the die (matrix) was made of a stamped steel 4Kh4VMFS (DI-22), heat-treated applying a standard technology. The surface of the die was ground after heat treatment  $R_a = 1.6$ .

Before stamping, a matrix of the die is heated to a temperature of 650–690 °C. At a temperature of 500 °C and higher, on the matrix surface a scale is formed, which significantly deteriorates sliding of the workpiece during shape drawing. The destruction of the die surface, adhesion of titanium on the surface, oxidation and roughness violation are observed (see Figure 6, *a*).

To increase the serviceability of a stamping tool, the surface was modified with a pulse-plasma. Treatment was carried out using a pulse-plasma generator «Impuls» (Figure 1).

Elastic-plastic deformations of the surface layer in combination with pulsed thermal and electromagnetic influence provide a refinement of the alloy structure and intensify the diffusion mechanisms of alloying

Results of industrial tests of a modified pulse plasma stamping tool

Description of the tool	Without mod. t/unit	After mod. t/unit	Efficiency, %
Detachable matrix	24.4	79.35	325
Supporting matrix	4.5	29.23	650
Slotted punch	1.8	7.08	393
Deformation punch	10.85	22.5	207
Forming matrix	18.0	54.0	300

elements. Previous studies of reference specimens showed that the modified layer contains such alloying elements as carbon, tungsten and oxygen, has a three-fold increase in hardness and reduced characteristic sizes of crystal structures (< 100 nm). The modified surface has a low roughness.

The dies were used in the technological process of deep drawing of a titanium sheet with a thickness of 3 mm. The sheet was heated to a temperature of 700 °C. After the use of dies on an intended purpose, no traces of oxidation and roughness violation were observed on their surface (see Figure 6, *b*).

Technology and technological equipment for pulse-plasma strengthening of the tool are used in the hardware production of JSC «Cherepovets Steel Rolling Plant». An experience of industrial operation demonstrated that serviceability of the tool made of

stamped steel subjected to pulse-plasma treatment, increased by 2–6 times (see Table [10]).

**Conclusions**

The proposed technology and equipment for pulse-plasma modification provide alloying and nano-structuring of the surface layer of tool steels to a depth of more than 80 μm.

Industrial tests confirmed the effectiveness of modification. After pulse-plasma treatment of working surfaces of a large-sized matrix of the die for hot drawing of a titanium sheet from VT-6 alloy with a thickness of 3 mm, during heating to a temperature of 700 °C the tool of a stamped steel 4Kh5MF1S did not have failures because of adhesion wear, brittle fracture or breakdown. The serviceability of the tool was 2–6 times increased. The only cause for the failure of the tool is incandescence of working surfaces.

1. Gusev, A.I. (2009) *Nanomaterials, nanostructures, nanotechnologies*. 2<sup>nd</sup> Ed. Moscow, FIZMATLIT [in Russian].
2. Tyurin, Yu.N., Zhadkevich, M.L. (2008) *Plasma hardening technologies*. Kiev, Naukova Dumka [in Russian].
3. Tyurin, Yu.N., Kolisnichenko, O.V. (2009) Plasma-detonation technology for modification of the surface layer of metal parts. *The Open Surface Sci. J.*, **1**, 13–19.

4. Lyakhovich, L.S., Voroshnin, L.G., Panich, G.G., Shcherbakov, E.D. (1974) *Multicomponent diffusion coatings*. Minsk, Nauka i Tekhnika [in Russian].
5. Ershov, G.S., Poznyak, L.A. (1993) *Structure formation and formation of properties of steels and alloys*. Kiev, Naukova Dumka [in Russian].
6. Abboud, J., Benyounis, K., Olabi, A. (2007) Laser surface treatments of iron-based substrates for automotive application. *J. Mater. Proc. Technology*, **182**, 427–431.
7. Cherenda, N.N., Uglov, V.V., Anishchik, V.M. et al. (2005) Structure-phase transformations in high-speed steel treated by compression plasma flow. *Vacuum*, **78**, 483–487.
8. Rott, M., Raif, M., Igenbergs, E. (2006) Surface modification processes by hypervelocity plasma pulses. *Int. J. of Impact Engineering*, **33**, 691–702.
9. Shmelev, V., Podoynitsyn, S., Vasilik, N. (2006) Application of the ballistic plasmatron of superadiabatic compression for surface treatment. *Surface & Coatings Technology*, **200**, 4939–4946.
10. Tyurin, Yu.N., Kolisnichenko, O.V., Tsygankov, N.G. (2001) Pulse plasma hardening of tools. *The Paton Welding J.*, **1**, 38–44.
11. Korzyk, V., Changgen, Feng, Tyurin, Y. et al. (2020) Pulse-plasma technologies of modification and increasing durability of metal working tool. In: *The 394<sup>th</sup> Young Scientists Forum of China Association for Science and Technology*, 325–339.

Received 29.04.2021



E.O. Paton Electric Welding Institute of the NAS of Ukraine  
 National Technical University of Ukraine  
 «Ihor Sikorsky Kyiv Polytechnic Institute»  
 International Association «Welding»

The Tenth International Conference  
**BEAM TECHNOLOGIES in WELDING  
 and MATERIALS PROCESSING**

6 – 11 September 2021

Ukraine, Odesa

**Conference Chairmen**

Prof. I. Krivtsun

**Conference topics**

- Laser and electron-beam welding, cutting, surfacing, heat treatment, coating deposition
- Electron-beam melting and refining
- Hybrid processes
- 3D-technologies
- Modelling and materials science of laser and electron-beam technologies

**EQUIPMENT ♦ TECHNOLOGIES ♦ MODELLING**



**LTVMP 2021 Organizing Committee**  
 03150, 11, Kazymyr Malevych str., Kyiv, Ukraine  
 E.O. Paton Electric Welding Institute of the NAS of Ukraine  
 Tel./fax: (38044) 200-82-77  
 E-mail: journal@paton.kiev.ua  
 www.pwi-scientists.com/eng/ltwmp2021



## EFFECT OF MODIFICATION OF WELD METAL OF HIGH-STRENGTH LOW-ALLOY STEELS ON THEIR STRUCTURE AND PROPERTIES

**V.A. Kostin, V.V. Zhukov, O.M. Berdnikova, V.V. Holovko and O.S. Kushnaryova**

E.O. Paton Electric Welding Institute of the NAS of Ukraine

11 Kazymyr Malevych Str., 03150, Kyiv, Ukraine. E-mail: [office@paton.kiev.ua](mailto:office@paton.kiev.ua)

The work studies the influence of modification of different compounds by dispersed particles on the structure, nonmetallic inclusions, their size and distribution, change of phase transformation temperatures and mechanical properties of weld metal joints of high-strength low-alloy steels. It is shown that the use of the temperature of maximum intensity of phase transformations allowed separating the influence of oxide, carbide and titanium-containing compounds on the structure and mechanical properties of weld metal of high-strength low-alloy steels. The use of powders of TiO<sub>2</sub>, ZrO<sub>2</sub> and MgO oxides promotes formation of a dispersed structure of acicular ferrite (from 30 to 90 %), which allows obtaining a favourable combination of high strength and impact toughness, especially at low extremely test temperatures (–40– –60 °C) in the weld metal. 11 Ref., 5 Tables, 9 Figures.

*Key words:* high-strength low-alloy steels, austenite decomposition diagram, phase transformations, critical transformation temperatures, automatic welding, weld metal, modification, microstructure, mechanical properties

High-strength low-alloy (HSLA) steels with a level of strength of 350–700 MPa and a high complex of toughness and ductility properties are now extensively used in construction, transport engineering, and ship-building in fabrication and repair of engineering welded structures of hoisting and transportation mechanisms, large-sized engineering constructions and frame structures [1–3].

Ever increasing requirements for improving the reliability and safety of welded structures, the level of operational loads, their fatigue life and cost-effectiveness make it necessary to use new HSLA steels. At present there is a problem of lowering the toughness values of weld metal in the welded joints at increase of strength values, in connection with development and application in industry of new HSLA steels with the strength level of 600–700 and even 800 MPa [4].

This problem can be solved by switching to the use of new HSLA steels with ferritic-bainitic or bainitic-martensitic structures in welded structures. This, on the one hand, requires application of new welding consumables, namely wires and fluxes, and on the other hand, more profound understanding of the processes of structure formation, influence of phase transformation kinetics and features of disperse phase formation on the structure and properties of HSLA steel welded joints.

Traditionally, the problem of improvement of weld metal strength to the level of 90–95 % of base metal

strength was solved by using higher alloyed welding wires, flux-cored wires of complex chemical composition or changing the welding mode [5].

At the same time, traditional approaches to increase of welded joint performance cannot always be applied, because of lowering of ductility, impact toughness, brittle fracture resistance and increase of cold cracking susceptibility of weld metal and HAZ [6]. This is related to the fact that the features of structure formation, kinetics of phase transformation development, mechanisms of the influence of dispersed exogenous phases on the structure and properties of welded joints of HSLA steels are not yet fully understood.

Determination of phase transformation temperatures in HSLA steels and their welded joints is a quite complex task that directly affects selection of welding, heat treatment modes and, consequently also the microstructure and mechanical properties of the weld metal.

In view of the above, the objective of the work consisted in studying the influence of different composition of modifier powders on structure formation processes, phase transformation temperatures, their distribution in the weld metal and establishing the influence of these parameters on the mechanical properties of weld metal of HSLA steels.

**Investigation materials.** The work presents the results of investigations of structural transformations in metal of welded joints on HSLA 14KhGNDTs

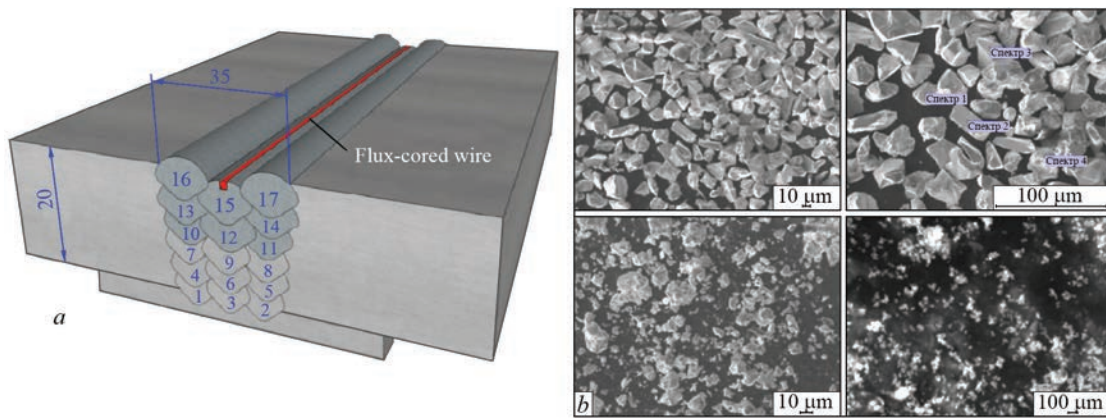


**Figure 1.** Scheme of filling the butt (a) and appearance of modifier powders (b): 1 – TiC; 2 – TiN; 3 – TiO<sub>2</sub>; 4 – ZrO<sub>2</sub>

steel, where modifier powders of different compounds, namely nitrides, carbides and oxides of different metals (TiC, TiN, SiC, VC, NbC, TiO<sub>2</sub>, Al<sub>2</sub>O<sub>3</sub>, MgO, ZrO<sub>2</sub>) were added. Liquid metal modification was performed by welding, using flux-cored welding wires, which included particles of the required composition. Welds Nos 1–9 were not modified, whereas welds Nos 10–18 were produced using modified flux-cored welding wires (Figure 1).

A feature of application of the proposed welding scheme for modifying the liquid metal is the need to protect the added powders from direct influence of the welding arc, in order to prevent their complete melting or evaporation. In this connection, we used the technology of adding flux-cored welding wires to the relatively «cold» part of the weld pool with pool temperature close to 1600–1800 °C, which was lower than the melting temperature of most of the particles.

Butt welded joints of 14KhGNDTs steel plates 20 mm thick were produced at reverse polarity direct current. Welding was performed in Ar + 18 % CO<sub>2</sub> shielding gas atmosphere, using Sv-08 flux-

cored wire of 1.6 mm diameter, filling factor being 18 %. Total content of TiC, TiN, SiC, VC, NbC, TiO<sub>2</sub>, Al<sub>2</sub>O<sub>3</sub>, MgO, ZrO<sub>2</sub> modifiers was 0.09 %. Welding was performed at reverse polarity direct current  $I = 240\text{--}250$  A, voltage  $U = 31\text{--}32$  V, welding speed of 10–12 m/h, heat input of 26–28 J/cm. Chemical composition and mechanical properties of test welds are shown in Table 1 and Table 2.

The nature of structural transformations in the metal of welds modified by powders was studied by the method of simulation of thermodeformational cycles of welding, using Gleeble 380 complex (DSI, USA), which was fitted with a high-speed dilatometer [7]. Samples were heated in a vacuum chamber up to the temperature of 1170 °C, and then were cooled by a thermal cycle characteristic for automatic submerged-arc welding at the speeds of 5; 10; 17; 30; 45 °C/s in the temperature range of 600–500 °C.

Weld microstructure was studied by light (NEOPHOT 32), scanning (JSM 840 (Jeol, Japan), transmission (JEM 200CX, Japan) and Auger-microprobe (JAMP 9500F, Japan) electron microscopy.

**Table 1.** Chemical composition of metal of the produced welded joints, wt.%

Type	C	Si	Mn	S	P	Cr	Ni	Mo	V	Cu	Al	Ti	Nb	Zr
Without mod.	0.042	0.34	1.19	0.021	0.02	0.106	2.13	0.282	–	0.72	0.028	0.029	0.004	–
FeTi	0.049	0.298	1.39	0.023	0.015	0.15	2.26	0.25	<0.02	0.44	0.039	0.008	0.006	–
TiN	0.035	0.317	1.4	0.019	0.009	0.14	2.29	0.26	<0.02	0.56	0.036	0.011	<0.002	–
SiC	0.053	0.321	1.2	0.02	0.025	0.22	2.42	0.26	<0.02	0.45	0.025	0.004	0.003	0.002
TiC	0.046	0.34	1.39	0.021	0.019	0.13	1.7	0.24	<0.02	0.54	0.033	0.011	0.007	–
VC	0.052	0.227	1.21	0.022	0.021	0.14	2.03	0.25	0.07	0.51	0.027	0.004	0.004	–
NbC	0.049	0.253	1.19	0.021	0.02	0.13	2.25	0.27	<0.02	0.55	0.029	0.003	0.075	–
ZrO <sub>2</sub>	0.041	0.288	1.32	0.021	0.024	0.12	1.36	0.25	<0.02	0.37	0.029	0.004	0.004	0.06
TiO <sub>2</sub>	0.035	0.405	1.24	0.016	0.021	0.11	1.97	0.27	0.009	0.68	0.031	0.017	0.002	–
Al <sub>2</sub> O <sub>3</sub>	0.023	0.424	1.4	0.017	0.023	0.11	2.15	0.29	0.007	0.77	0.032	0.015	0.002	–
MgO	0.031	0.227	1.11	0.025	0.024	0.14	1.85	0.29	–	0.6	0.023	0.03	–	–

**Table 2.** Mechanical properties of modified weld metal

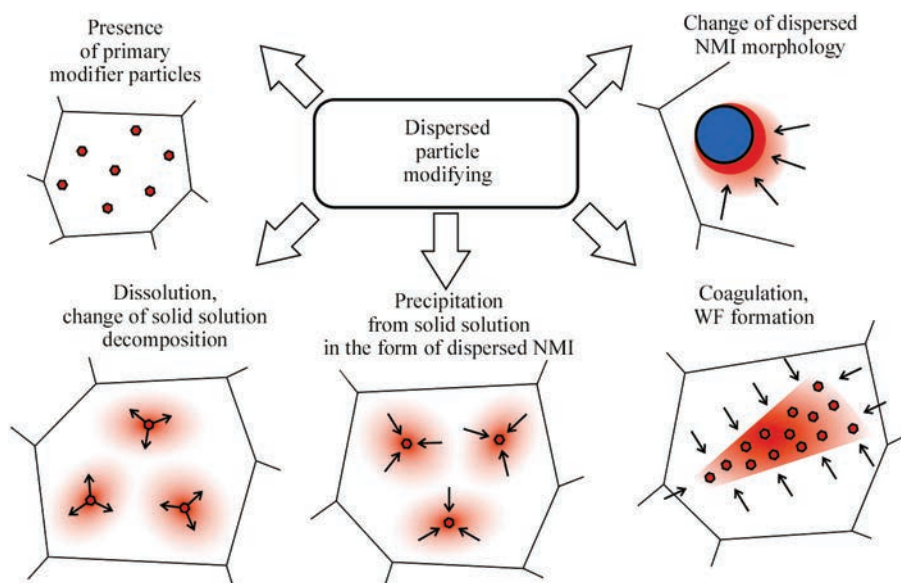
Modifier	$\sigma_t$	$\sigma_{0.2}$	$\delta$	$\psi$	KCV, J/cm <sup>2</sup> at T, °C			
	MPa		%		+20	0	-20	-40
Without modifying	693	605	14.5	48.4	97	87	75	53
FeTi	747	690	19	60	74	69	63	61
TiN	712	580	5.3	14.7	55	47	40	—
SiC	775	729	18	60	55	49	44	36
TiC	728	665	19	61	82	72	63	52
VC	780	706	14	56	57	55	52	—
NbC	594	594	3	5.75	44	35	24	—
ZrO <sub>2</sub>	645	556	21	60	116	96	98	82
TiO <sub>2</sub>	709	636	19	57	85	72	60	50
Al <sub>2</sub> O <sub>3</sub>	728	621	18	54	82	58	50	36
MgO	644	586	19	60	103	—	69	60

**Investigation results.** The process of the influence of liquid weld metal modification on improvement of its mechanical properties is quite complicated and ambiguous. Modifiers added to the liquid metal pool, can react with additives in the metal to form nonmetallic inclusions. Modification can also lead to decomposition of the existing nonmetallic inclusions and formation of new ones. Atoms of modifier compounds can also join the existing nonmetallic inclusions, forming more complex nonmetallic inclusions. Modifier particles can also dissolve, and, as a result, change the solid solution composition [8]. At liquid metal solidification modifiers can affect the primary dendrite structure of weld metal, parameters and nature of the dendrite structure of the weld [9]. At the same time, however, the nonmetallic inclusions formed as

a result of modification can influence the processes of secondary crystallization and structure formation during overcooled austenite transformation [10].

Change of the weld metal chemical composition and particles of refractory compounds will also have an impact on the kinetics of solid-state transformations, transformation temperature and forming microstructure. The microstructure will be also influenced by the composition, distribution and size of the modifying and secondary phases [10, 11].

Addition of powderlike material to the liquid metal pool (Figure 2) may have the following result: weld metal can contain the initial modifier particles; particles can dissolve, changing the solid solution composition; particles can precipitate in the form of dispersed nonmetallic inclusions; coagulation and sticking to-


**Figure 2.** Influence of weld metal modifying on the nature of dispersed particle transformations

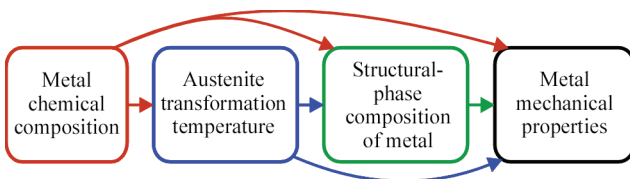


**Figure 3.** Mutual influence of chemical composition, austenite transformation temperature, structural-phase composition on mechanical properties of weld metal

gether of modifier particles with further formation of extended phase precipitates can take place. Dissolved particles can also change the morphology and composition of the already existing nonmetallic inclusions.

That is, the chemical composition and parameters of the particles will influence the austenite transformation temperature and the structural-phase composition, as

well as mechanical properties of the metal. This mutual influence is conditionally presented in Figure 3.

Nonmetallic inclusions and phase precipitates can have a strong influence on formation of the metal structural-phase composition, they can be the centers of crystallization and recrystallization that may facilitate in terms of energy formation of a particular structural component, changing not only the temperature range of transformation, but also the kinetics of structural-phase transformation, structural-phase composition and mechanical properties of the metal.

Change of austenite transformation kinetics as a result of modifying cannot change the temperature of the start or end of transformation, but it will influence the nature of metal deformation, associated with crys-

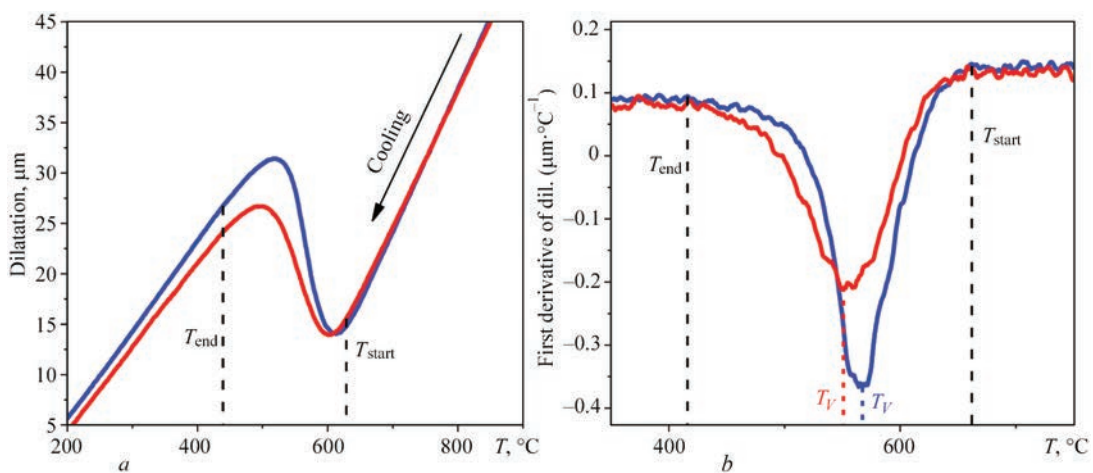


**Figure 4.** Influence of modifying on the change of phase transformation kinetics: *a* — dilatogram; *b* — first derivative of dilatation with respect to temperature

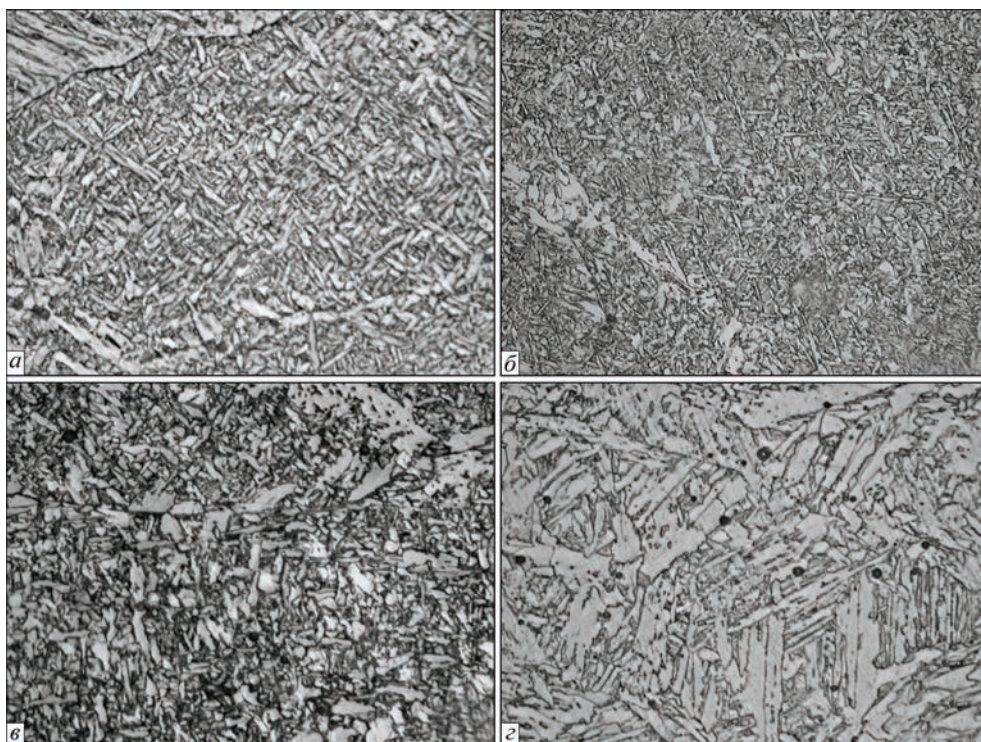


**Figure 5.** Microstructure ( $\times 1000$ ) of the metal of welds modified by powders: *a* — TiC; *b* — TiN; *c* — TiO<sub>2</sub>; *d* — ZrO<sub>2</sub>

**Table 3.** Structural composition of modified weld metal, %

Modifier type	AF	GBF	IGF	WF	B <sub>u</sub>	B <sub>l</sub>	MAC	Ferrite	Bainite
–	27	18	8	9	14	24	–	35	65
FeTi	55	18	13	11	–	–	3	42	55
TiN	52	16	18	8	–	–	6	42	52
TiC	30	16	3	6	20	25	–	25	75
SiC	17	15	3	4	11	43	7	22	71
VC	11	9	-	18	47	12	3	27	70
NbC	9	7	-	11	43	9	21	18	61
ZrO <sub>2</sub>	31	16	9	7	11	26	–	32	68
Al <sub>2</sub> O <sub>3</sub>	3	3	–	32	50	12	–	35	65
MgO	32	12	10	7	16	23	–	29	71
TiO <sub>2</sub>	60	12	20	–	–	8	–	32	68

talline lattice restructuring during transformation, i.e. with the transformation «speed» (Figure 4).

In connection with the above, the influence of modifying on weld metal microstructure, nonmetallic inclusion composition and distribution and phase transformation temperature was studied.

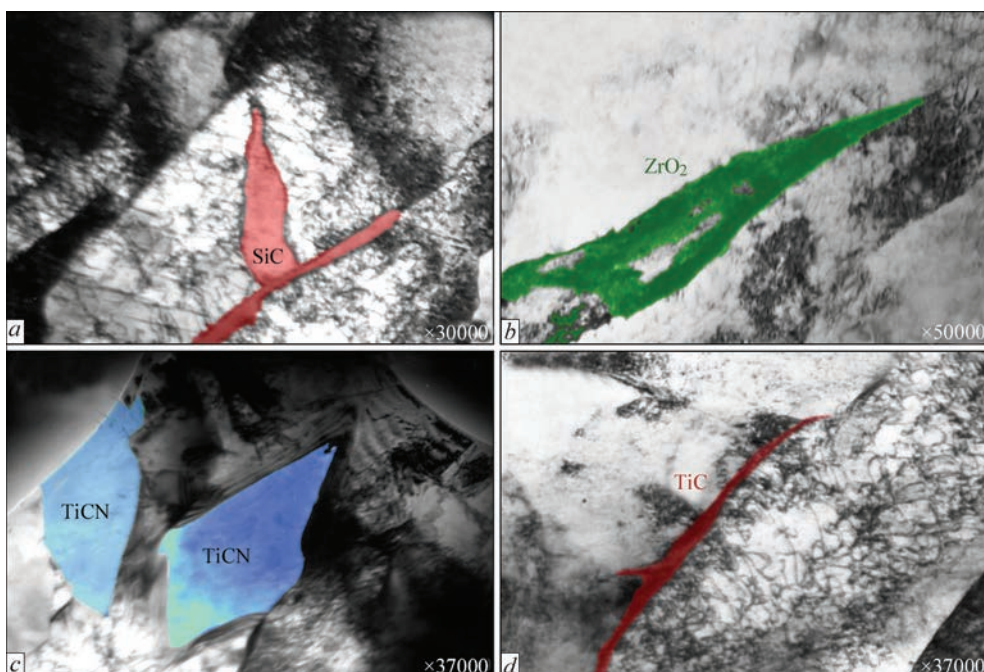
The results of studying the influence of modifying by dispersed particles the metal of HSLA steel weld on formation of the secondary crystalline structure are shown in Figure 5.

It was found that formation of different structural components is observed for all the studied samples of welded joint weld metal, such as upper bainite (B<sub>u</sub>), lower bainite (B<sub>l</sub>), Widmanstatten ferrite (WF), acicular ferrite (AF), grain-boundary ferrite (GBF), intragranular

ferrite (IGF), and martensite-austenite-carbide (MAC) precipitates. Quantitative metallography methods were used to determine the volume fraction of structural components, forming in modified welds (Table 3).

Electron transmission microscopy methods were used to conduct «transmission» analysis of the fine structure forming in the weld metal: substructure, lath parameters, distribution, dimensions and composition of phase precipitates, change of dislocation density of metal in modified welded joints, as well as for comparison with weld metal without modifying (Figure 6, Table 4).

It is found that nonmetallic inclusions based on titanium compounds form inside weld metal grains with dislocation density  $\rho = 10^{10} - 10^{11} \text{ cm}^{-2}$  around the inclusions, and increase the values of metal strength


**Figure 6.** Phase precipitates in the metal of welds modified by: *a* — SiC; *b* — ZrO<sub>2</sub>; *c* — TiN; *d* — TiC

**Table 4.** Parameters of fine structure of modified weld metal

Modifier type	$h_{\text{lath}}, \mu\text{m}$	$d_{\text{fr}}, \mu\text{m}$	$D_p, \mu\text{m}$	$\lambda_p, \mu\text{m}$	$\rho, \text{cm}^{-2}$
Without modifier	0.5–1.7	0.4–1.5	0.01–0.05*	0.05–0.17*	$(4-6) 10^{10}$
FeTi	0.7–2.3	0.4–1.6	0.03–0.05* 0.01–0.02**	0.06–0.15* 0.02–0.03*	$(4-6) 10^{10}$ $(1-2) 10^{11}$ **
TiN	0.4–1.2	0.3–1.0	0.02–0.08* 0.03–0.05**	0.08–0.15* 0.03–0.1**	$(4-6) 10^{10}$ $(2-3) 10^{11}$ **
SiC	0.7–1.5	0.4–0.8	0.03–0.1* 0.02–0.07**	0.03–0.15	$(4-8) 10^{10}$
ZrO <sub>2</sub>	0.4–1.4	0.2–1.0	0.017–0.08	0.05–0.13	$(6-8) 10^{10}$
TiC	0.5–1.5	0.2–1.2	0.013–0.07	0.04–0.1	$(4-8) 10^{10}$

*Note.* \* — in the grain volume; \*\* — on grain boundaries;  $h_{\text{lath}}$  — lath width;  $d_{\text{fr}}$  — fragment size,  $D_p$  — size of phase precipitate particles and distances between them ( $\lambda_p$ ),  $\rho$  — dislocation density.

and lower the crack resistance, while oxide nonmetallic inclusions form near the grain boundaries with dislocation density  $\rho = 10^8-10^9 \text{ cm}^{-2}$ .

Analysis of the influence of modifying on nonmetallic inclusion size distribution in the weld metal is shown in Figure 7, a.

It is found that modifying leads to coarsening of nonmetallic inclusions in the weld metal. The number of up to 0.3  $\mu\text{m}$  particles becomes smaller, due to increase of the fraction of particles of more than 0.5  $\mu\text{m}$  size. This is indicative of the fact that after dissolution the modifier particles, in addition to the possibility of formation of individual phase precipitates, similar in their composition to that of the modifiers, can coagulate with dispersed nonmetallic inclusions (of oxide type) present in the weld metal.

Determination of nonmetallic inclusion composition was conducted on microsections and fractures of samples after testing (Figure 7, b). Identification of the composition of nonmetallic inclusions by the method of X-ray spectrum microanalysis (RSMA), using Auger-microprobe JAMP-9500F showed that

practically all the analyzed inclusions are a composition of manganese, silicon, aluminium, titanium and sulphur oxides with different ratio of the components.

Analysis of the influence of modifying on temperature parameters of transformation of HSLA steel weld metal is given in Figure 8. Thermokinetic diagrams (TKD) of overcooled austenite decomposition were plotted, critical temperatures  $A_{c1}$  and  $A_{c3}$ , temperatures of the start and end of austenite decomposition, as well as the temperature of maximum transformation intensity  $T_V$  were determined (Table 5).

It is found that modifying by ZrO<sub>2</sub> and MgO particles leads to a certain increase of the temperatures of transformation start for cooling rates below 17 °C/s. Modifying by TiC, SiC, NbC, TiO<sub>2</sub>, Al<sub>2</sub>O<sub>3</sub> and TiN particles leads to lowering of critical transformation temperatures (see Table 5). Modifying by carbide modifiers and TiN leads to occurrence of a pronounced martensite phase at dilatometric and metallographic studies. The highest content of martensite and the highest values of metal microhardness were obtained for samples modified by TiN particles.

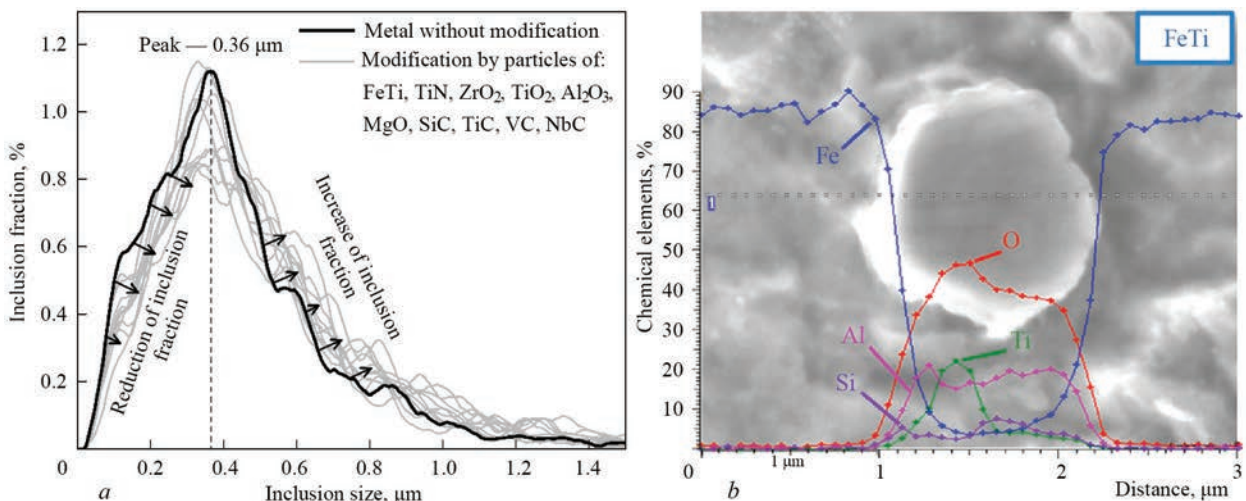


**Figure 7.** Influence of modification on the distribution of: a — inclusions by size; b — chemical elements in the inclusion in weld metal

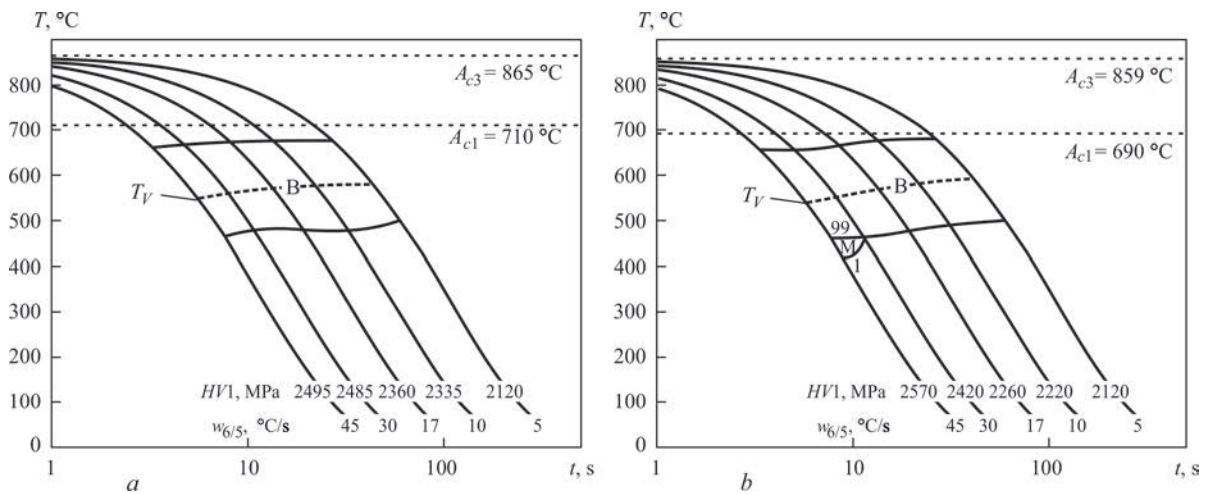


**Figure 8.** TKD of weld metal: *a* — without modification; *b* — modification by  $ZrO_2$

Dependence of transformation temperature on the cooling rate demonstrates a lowering of transformation temperature for all the studied samples. It should be noted that modifying by  $ZrO_2$  and MgO particles leads to increase of transformation temperature by 50–75 °C, and, on the whole, the values of transformation temperatures for MgO,  $ZrO_2$ ,  $TiO_2$ ,  $Al_2O_3$  oxide modifiers are located higher than those for SiC, VC, NbC carbide particles. The lowest values of transformation temperature are observed for a sample modified by TiN titanium nitride.

Analyzing the modifier influence on the structure and mechanical properties of HSLA steel weld metal it was established that application of titanium nitride TiN powders leads to increase of the fraction of intragranular and polygonal ferrite (up to 50 %) that has a negative effect on the value of impact toughness of the weld metal already at relatively high test temperature:  $KCV_{-20}$  40 J/cm<sup>2</sup>.

Application of  $TiO_2$ ,  $ZrO_2$ , MgO oxide powders promotes formation of a dispersed structure of acicular ferrite (from 30 to 90 %), which, as is known, allows obtaining a more favourable combination of high strength and impact toughness in the weld metal, particularly at extremely low test temperatures –40––60 °C (Figure 9).

Analysis of the obtained results shows that the strength values decrease with increase of transformation temperature (Figure 9, *a*), while impact toughness values (Figure 9, *b*) and ductility of metal in the

modified welds increase. Samples modified by niobium carbide NbC and titanium nitride TiN are an exception. Both the samples are characterized by lowering of the values of strength and ductility at relatively low value of the temperature of maximum intensity of austenite transformation.

It is found that for metal of modified welds the ratio of the structural components is almost linearly related to the temperature of maximum transformation intensity  $T_V$ .

Influence of structural composition on mechanical properties of modified weld metal showed that at increase of the ratio of ferrite phase quantity to that of bainite one, a lowering of strength characteristics and increase of ductility characteristics of weld metal is observed. Differences from the general dependence are demonstrated by samples of the metal of welds, modified by TiN and NbC that is attributable to formation of martensite phase, as a result of dissolution of carbide forming modifier elements.

Thus, it was found that the temperature of maximum transformation intensity  $T_V$  is the most significant value among the parameters, having the greatest influence on the mechanical properties of modified weld metal (chemical composition, nonmetallic and phase inclusions, transformation temperature, structural-phase composition, etc.). It is established that there is a clear dependence correlating the above-mentioned parameters for samples modified by oxide and carbide particles.

**Table 5.** Characteristic temperatures of modified weld transformation

$T$ , °C	Modifier particle type										
	Base	FeTi	TiN	$ZrO_2$	$TiO_2$	$Al_2O_3$	MgO	SiC	TiC	VC	NbC
$B_s$	677	654	600	678	652	651	684	647	653	645	647
$B_f$	470	472	422	492	478	466	486	440	476	460	458
$T_V$	576	573	505	579	575	564	587	535	573	559	545

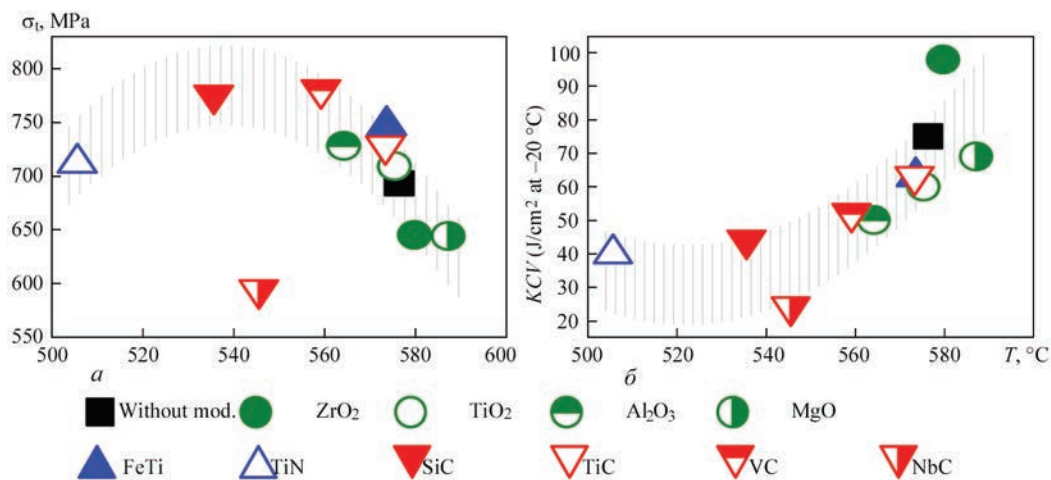


**Figure 9.** Influence of temperature of maximum transformation intensity  $T_v$  on structural-phase composition and mechanical properties of modified weld metal:  $a$  — ultimate strength;  $b$  — impact toughness  $KCV$

Dissolving in the metal of welds, carbide modifiers change the solid solution composition and thus affect the nature of structure formation. For welds modified by oxide and titanium compounds containing modifiers, a certain deviation of the values of kinetic transformation parameters is observed that confirms an essential influence of exogenous nonmetallic inclusions and phase precipitates and of the morphology of endogenous nonmetallic inclusions on the conditions of secondary structure formation and mechanical properties of HSLA steel welds.

## Conclusions

1. It is found that the composition of nonmetallic inclusions (oxide or based on titanium compounds), nature of their location relative to the grain boundaries (near the boundary or inside the grain) and the value of dislocation density gradient near the inclusion influence the kinetics of phase transformation and mechanical properties of HSLA steel welds.

2. Nonmetallic inclusions based on titanium carbide compounds form inside the metal grain with dislocation density of  $10^{10}$ – $10^{11}$  cm<sup>-2</sup> around the inclusions, increase the values of metal strength and lower the crack resistance, while oxide nonmetallic inclusions form near the metal grain boundaries with dislocation density of  $10^8$ – $10^9$  cm<sup>-2</sup>.

Application of powders of titanium nitride TiN leads to increase of the fraction of intragranular and polygonal ferrite (up to 50 %) that adversely affects the value of impact toughness of weld metal already at relatively high testing temperature  $KCV_{-20}$  40 J/cm<sup>2</sup>.

Use of powders of TiO<sub>2</sub>, ZrO<sub>2</sub>, MgO oxides promotes formation of a dispersed structure of acicular ferrite (from 30 to 90 %) that allows obtaining in the

weld metal a favourable combination of high strength and impact toughness, particularly at extremely low testing temperature (–40– –60 °C).

1. Grigorenko, G.M., Kostin, V.A., Golovko, V.V., Zhukov, V.V. (2016) Influence of modifier nanoparticles on kinetics of transformations in weld metal of high-strength low-alloy steels. *Dopovidi NANU*, **7**, 70–77 [in Russian].
2. (2018) *Science about materials, achievements, prospects*. Ed. by L.M. Lobanov. Kyiv, Akadempriodyka, Vol. 2 [in Ukrainian].
3. Poznyakov, V.D. (2017) Welding technologies for production and repair of metal structures from high-strength steels. *Bulletin of the National Academy of Sciences of Ukraine*, **1**, 65–73.
4. Rashid, M.S. (1980) High-strength, low-alloy steels. *Science*, **208**, 862–869.
5. Rees, G.I., Bhadeshia, H.K.D.H. (1994) Thermodynamics of acicular ferrite formation. *Mater. Sci. and Technology*, **10**(5), 353–358.
6. Yang, J.R., Bhadeshia, H.K.D.H. (1986) Thermodynamics of the acicular ferrite transformation in weld metals. Advances in welding science and technology. In: *Proc. of Int. Conf. on Trends in Welding Research (Gatlinburg, Tennessee, USA, May 18–22, 1986)*. ASM International, Materials Park, Ohio.
7. Kostin, V.A., Grigorenko, G.M., Golovko, V.V. et al. (2011) Physical modeling of structural transformations in heat-affected zone metal of pipe steels with ferritic-bainitic structures. *Zh. Nauk. Prats of Nats. Universytetu Korablebuduvannya*, **3**, 36–44 [in Russian].
8. Nejmark, V.E. (1977) *Modified steel ingot*. Moscow, Metallurgiya [in Russian].
9. Holovko, V.V., Yermolenko, D.Yu., Stepanyuk, S.M. et al. (2020) Influence of introduction of refractory particles into welding pool on structure and properties of weld metal. *The Paton Welding J.*, **8**, 8–14. DOI: <https://doi.org/10.37434/as2020.08.01>
10. Bhadeshia, H.K.D.H. (2001) *Bainite in steels — transformation, microstructure and properties*. 2<sup>nd</sup> Ed. London, Institute of Materials Communication Ltd.
11. Berdnikova, O., Hryhorenko, G., Holovko V. (2019) *Features of bainite structure in the low-alloy steel weld metal with dispersed inoculants modification*. Sumy, SumDU, 291–294.

Received 09.04.2021

# APPLICATION OF FRACTAL AND METALLOGRAPHIC ANALYSES FOR EVALUATION OF QUALITY OF WELD METAL

O.O. Shtofel<sup>1,2</sup>, V.V. Holovko<sup>1</sup> and T.G. Chyzhska<sup>2</sup>

<sup>1</sup>E.O. Paton Electric Welding Institute of the NAS of Ukraine

11 Kazymyr Malevych Str., 03150, Kyiv, Ukraine. E-mail: office@paton.kiev.ua

<sup>2</sup>National Technical University of Ukraine «Igor Sikorsky Kyiv Polytechnic Institute»

37 Peremohy Prosp., 03056, Kyiv, Ukraine

When analyzing the factors that determine the mechanical properties of welds, it is necessary to take into account both the size of individual components of the structure and their morphology. It is shown that the use of the method of fractal analysis makes it possible to numerically determine such parameters of weld metal microstructure, as the size of nonmetallic inclusions, and branching of grain boundaries, which was impossible at analysis of metallographic images. The results are obtained, which indicate the need to include in the multifractal analysis the characteristics that describe the morphological features of microstructural components, the distribution of nonmetallic inclusions by size, and the level of alloying of the solid solution. Research directions for the development of multifractal analysis of welded joints have been identified. 10 Ref., 2 Tables, 6 Figures.

*Key words:* metal of welded joints, fractal and metallographic analyses, structural parameters, mechanical characteristics

The general objective of metallographic analysis is investigation of the structure and defects, in particular, such as inclusions, base metal and deposited metal of the welded joint. Metallographic analysis includes investigations of metal macro- and microstructure. This list was recently complemented by fractal analysis method [1]. In works [2–5] the authors describe the cause for application of fractal analysis method, based on fractal concepts known in different scientific fields. The main purpose of fractal application in the materials science field is establishing a connection in the «structure–composition–fractal/multifractal dimension–properties» system. The above-described approaches were used to describe in work [6] one of the stages of searching for connections between the results of fractal analysis and the data of the reference scale of structural components in the metal of low-alloy steel welds. Existence of «fractal dimension–grain size» and «fractal dimension–structural parameters» connections was shown.

This work describes application of fractal analysis method for analysis of the structure of weld metal samples. Metallographic investigation can be used to establish the parameters, which affect the metal quality, in particular, to reveal certain metal defects, presence of oxides on the grain boundaries, «contamination» by nonmetallic inclusions, size of metal grains, chemical composition of weld metal, presence of microscopic cracks, pores and other structural de-

fects. In order to establish a connection between the structural composition of the metal and its mechanical properties, it is necessary to conduct quantitative description of the structural complex, i.e., perform its parametrization. At present, structure description in materials science is based on their approximate representation in the form of geometrical objects of certain dimensions. Here, parameters characterizing individual structural elements, and not the structure as a whole, are used. That is, the size of structural grains, blocks, and nonmetallic inclusions is assessed, but no answer is given on the influence of the sum of these characteristics on metal properties.

Metallographic analysis is one of the methods of welded joint testing. It is usually performed at final inspection of finished welded joints. The finished joint should completely meet the operation requirements. The total labour consumption of all the inspection operations is equal on average to 30 % of the total labour consumption of welded metal structure fabrication. Researchers know well that it is impossible to describe the impact of the structure on the mechanical properties of steel just on the base of determination of the geometrical features of the structure grains. Both the parameters of grain boundaries and of nonmetallic inclusions should be taken into account. Characteristics of grain structure, grain boundaries and nonmetallic inclusions can be combined in one analysis only using the methods of fractal parametrization and multifractal analysis of metal. In particular,

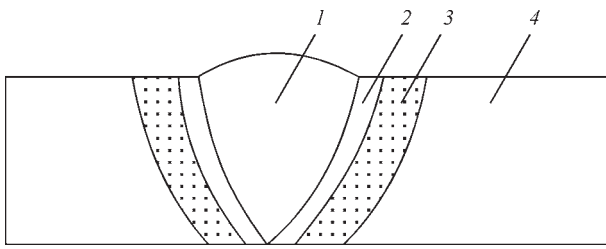


**Figure 1.** Scheme of weld metal structure: 1 — weld; 2 — fusion zone; 3 — heat-affected zone (HAZ); 4 — base metal

studies using fractal analysis of the influence of parameters of nonmetallic inclusions contained in the welds on the mechanical properties of the metal [7], allowed comparing the values of fractal dimension with the characteristics of destruction of weld metal structure [8].

The scheme of weld metal structure (Figure 1) consists of four main zones. The first zone is base metal (4), the structure of which was formed during rolled sheet production and was not exposed to thermal impact.

On the boundary of contact of weld pool molten metal (2) with the base metal an abrupt temperature gradient and overcooling phenomenon develop in a thin layer of metal along the fusion line that leads to formation of a large number of crystallization centers resulting in the fine-grained structure of the layer. Base metal zone (3), which was exposed to thermal impact from the weld pool and welding arc, is the columnar crystal zone. In the weld metal proper (1) the conditions of heat removal and degree of overcooling of steel change over time. As a result, the weld metal structure contains both columnar crystals and equiaxed crystals. The welded joint metal belongs to materials, exposed to energy impact during manufacture or treatment. Presence of connections between the elements in an open system, determines formation of a collective response to the external impact of the welding arc. As a result of such a reaction, a structure forms in the weld metal, which corresponds to a certain spatial, time or space-time self-organization that, in its turn, causes changes in the metal properties as a whole (Figure 2).

The structure of weld metal is traditionally described using the methods of optical and electron

metallography. Such approaches are insufficient at description of systems with a complex and heterogeneous structure, which weld metal structures are, as they do not allow for one of the most important properties of the system — its integrity. One of the promising ways to solve the problem of quantitative description of material structures is their parameterization, based on application of fractal theory.

Investigations of the parameters of welded joint metal structure by fractal analysis method provide a certain set of data as regards the fractal dimension for zones 1, 2, 3 and 4. These values add up to one general concept of a multifractal, which, in its turn, is an inhomogeneous fractal, and, therefore, each of the multifractal components has its own specific weight.

In order to study the connection between the fractal parameters of the structure and mechanical properties of weld metal, investigations were conducted on samples of the metal of welds on low-alloy high-strength steel. During the experiment, the metal impact toughness at different temperatures (from 20 to  $-40\text{ }^{\circ}\text{C}$ ) was studied on samples of welds, produced at welding of butt welded joints of 09G2 steel by Sv-08GNMA wire in M21 shielding gas atmosphere. During the experiments the impact of weld pool modification on weld metal structure and properties was studied. Weld pool modification was performed by a procedure, presented in work [9]. Results of spectral analysis of weld metal given in Table 1, are indicative of the fact that by its chemical composition the weld metal corresponds to steel strength category K60. Samples for metallographic investigation were cut out of welds from welded joint zones 1–4, which are shown in Figure 1. At metallographic investigations parameters of nonmetallic inclusions and structural components were determined. Results of metallographic analysis of the samples in NEOPHOT-32 microscope at  $\times 1000$  and  $\times 320$  magnifications were recorded using a digital photcamera (Figure 3).

To confirm the stochasticity of fractal functions which describe the influence of the dimensions of structural components, images of the structure at dif-

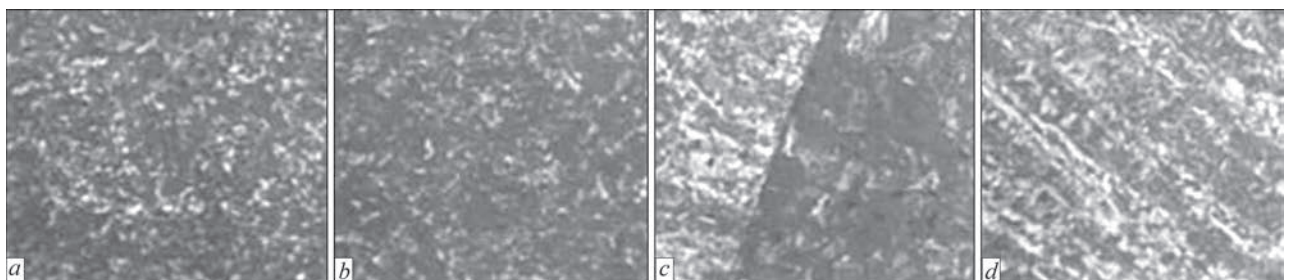


**Figure 2.** Scheme of the structure of low-alloy steel welded joint: a — base metal; b — overheated zone; c — on the fusion line; d — weld metal

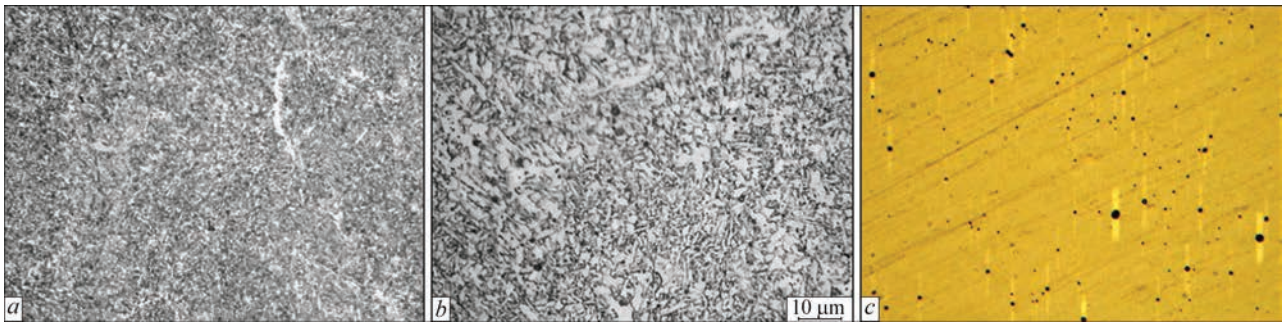


**Figure 3.** Typical microstructures of welds: *a* —  $\times 320$ ; *b* —  $\times 1000$ ; *c* — nonmetallic inclusions,  $\times 1000$

**Table 1.** Chemical composition of metal of the studied welds (deposited metal), wt.%

Weld number	C	Si	Mn	S	P	Cr	Ni	Mo	Al	Ti	Modifier
W1	0.054	0.263	1.28	0.025	0.011	0.13	2.22	0.26	0.035	0.009	TiC
W2	0.035	0.317	1.40	0.019	0.009	0.14	2.29	0.26	0.036	0.011	TiN
W3	0.066	0.270	0.92	0.016	0.024	0.14	1.72	0.23	0.021	0.005	SiC
W4	0.035	0.405	1.24	0.016	0.021	0.11	1.97	0.27	0.031	0.027	TiO <sub>2</sub>
W5	0.034	0.324	1.12	0.017	0.023	0.12	2.15	0.29	0.032	0.025	Al <sub>2</sub> O <sub>3</sub>

**Table 2.** Results of mechanical testing of weld metal of the studied samples and results obtained by fractal analysis method

Weld number	$D_{inc}$	$D_{320}$	$D_{1000}/D_{inc}$	$D_{1000}$	KCV, J/cm <sup>2</sup> at $T$ , °C			
					20	0	-20	-40
W1	0.928	1.902	0.488	1.877	112	93	85	73
W2	0.91	1.938	0.469	1.939	55	47	40	33
W3	0.907	1.941	0.467	1.932	85	72	65	61
W4	0.920	1.907	0.483	1.815	85	72	60	50
W5	0.919	1.897	0.485	1.825	82	58	50	36

ferent magnifications were used at assessment of the values of weld mechanical properties.

Fractal analysis of the structural components was performed on the base of a procedure, given in work [10]. Used as the data base were the results of digital processing of images, obtained at metallographic analysis of samples in NEOPHOT-32 optical microscope. Fractal index of nonmetallic inclusions in the weld metal in images with  $\times 1000$  magnification ( $D_{inc}$ ), as well as branching of grain boundaries at  $\times 320$  ( $D_{320}$ ) and  $\times 1000$  ( $D_{1000}$ ) magnification, were determined. In addition, Table 2 gives the results of determination of  $D_{1000}/D_{inc}$  ratio, as an example of multifractal analysis. Results of fractal analysis and impact toughness of weld metal at testing in the temperature range from 20 to  $-40$  °C are given in Table 2.

From the data given in Table 2, the closeness of indices  $D_{320}$  and  $D_{1000}$  (less than 10 % difference) should be noted first of all that is indicative of the stochasticity of fractal dependence and possibility of its application for assessment of weld metal structure as a whole.

For visualization of the applicability of individual indices of fractal dimension (in the form of relative

units) for assessment of the metal mechanical properties, graphs of interrelation of impact toughness and fractal dimension of the inclusions (Figure 4) and dependence of impact toughness and fractal dimension of grain boundaries in weld metal microstructure (Figure 5) were plotted by the results of impact toughness testing.

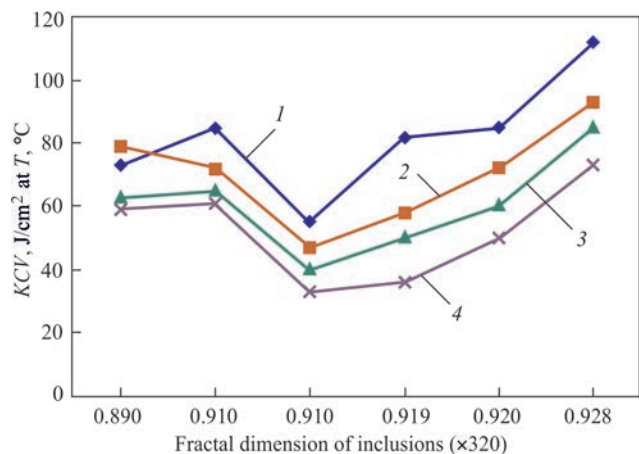


**Figure 4.** Interrelation of impact toughness and fractal dimension of inclusion size in the weld metal at the following temperature: 1 — 20; 2 — 0; 3 —  $-20$ ; 4 —  $-40$  °C

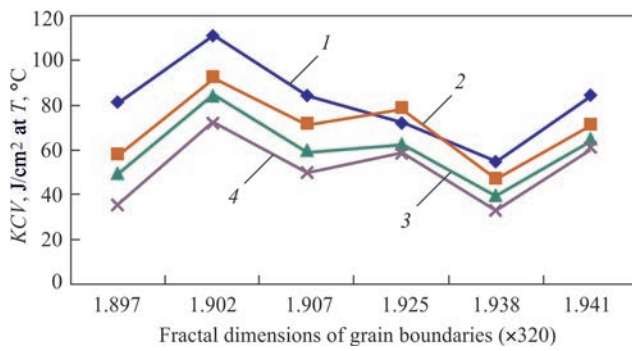


**Figure 5.** Interrelation of impact toughness and fractal dimensions of grain boundaries in weld metal microstructure at the following temperature: 1 — 20; 2 — 0; 3 — -20; 4 — -40 °C

**Discussion of the results.** Application of fractal analysis method enables numerical determination of such parameters of weld metal microstructure as the size of nonmetallic inclusions and branching of the grain boundaries that was impossible at analysis of metallographic images (Figure 3).

Level of impact toughness is an accumulating index, which is influenced not only by the volume fraction of nonmetallic inclusions in the metal, but also by their size distribution and level of homogeneity in the structure. At analysis of the factors, determining the mechanical properties of welds, it is necessary to take into account both the size of individual components of the structure, and their morphology. Obtained results show that the level of metal impact toughness increases with increase of fractal dimension of the nonmetallic inclusions (i.e. with reduction of the inclusion size) (Figure 4). Reduction of branching of intergranular boundaries influences the decrease of this index, despite the presence of rather fine inclusions in the structure (Figure 5).

Dependencies given in Figures 4–6, as well as the results of initial multifractal calculation (Figure 6), give a very general idea about the influence of both nonmetallic inclusions and grain boundaries on mechanical properties of weld metal. These results are indicative of the need to involve in the multifractal analysis the indices which describe the morphological features of the microstructural components, size distribution of nonmetallic inclusions, and level of solid solution alloying.

The outlined directions are the main objectives for development of computerization of metallographic investigations based on multifractal analysis.

**Conclusions**

The stochastic nature of fractal analysis of weld metal microstructure is shown. Examples are given of determination of the indices of fractality of the size of non-

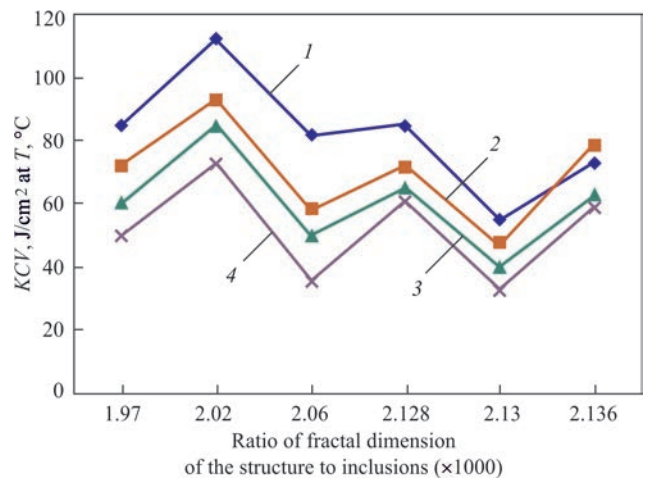


**Figure 6.** Interrelation of impact toughness and ratio of fractal dimension of grain boundaries and inclusion size in weld metal microstructure at the following temperature: 1 — 20; 2 — 0; 3 — -20; 4 — -40 °C

metallic inclusions and grain boundaries in the weld metal structure. The need to apply multifractal analysis to describe the influence of structural parameters on mechanical properties of welds was established. Investigation directions for development of multifractal analysis of welded joints were defined.

- Shtofel, O., Golovko, V., Chyzhska, T. (2021) *Fractal and metallographic analyses as an innovation in ensuring the quality of metal products. Innovative «Approaches to Ensuring the Quality of Education, Scientific Research and Technological Processes»*. Wydawnictwo Wyższej Szkoły Technicznej w Katowicach, 1013–1018. (ISBN 978-83-957298-6-7).
- Kirichenko, L.O., Radivilova, T.A. (2019) *Fractal analysis of self-similar and multifractal hour series*. Kharkiv, KhNURE [in Ukrainian].
- Haken, G. (1980) *Synergetics*. Moscow, Mir [in Russian].
- Nikolis, G., Prigozhin, I. (1979) *Self-organization in nonequilibrium systems. From dissipative structures to order through fluctuation*. Moscow, Mir [in Russian].
- Mandelbrot, B. (2009) *Fractals and chaos. Mandelbrot set and other wonders*. Benoit Mandelbrot. Izhevsk, RDC «Regular and chaotic dynamics [in Russian].
- Shtofel, O.O. (2019) Application of fractal analysis method to study the metal structure. *Metalozn. Obrobka Met.*, 91(3), 40–46 [in Ukrainian].
- Shtofel, O.O., Chizhskaya, T.G., Kulieznova, S.S. (2020) Metallographic studies of vessel steel samples: DS, 35G/40G and steel 20 by fractal analysis. *J. of Multidisciplinary Engineering Sci. Studies (JMESS)*, 6, 2. ISSN: 2458-925X.
- Shtofel, O.O., Rabkina, L.M. (2019) Application of fractal analysis method to study the change of metal properties. *Visnyk KPI, Seriya Pryladobuduvanniya*, 58(2) [in Ukrainian]. ISSN (Online) 2663-3450, ISSN (Print) 0321-2211.
- Holovko, V.V., Kuznetsov, V.D., Fomichov, S.K., Loboda, P.I. (2016) *Nanotechnologies in welding of low-alloy high-strength steels*. Kyiv, Politekhnik [in Ukrainian].
- Poyarkova, E.V. (2019) *Fractal analysis in diagnostics of the structures of materials: Procedural recommendations*. Orenburg, Orenb. State University [in Russian].

Received 30.03.2021